

UNIVERSIDADE FEDERAL DE MINAS GERAIS

Programa de Pós-Graduação em Engenharia Metalúrgica, Materiais e de Minas

“Bioacessibilidade de arsênio em amostras de solo em região de mineração de ouro”

“Bioaccessibility of arsenic in soil samples from a gold mining region”

Autora: Daphne Chiara Antônio

Orientadora: Prof<sup>a</sup> Virgínia S. T. Ciminelli

Co-orientadora: Cláudia Lima Caldeira

Março/2017

Daphne Chiara Antônio

Bioacessibilidade de arsênio em amostras de solo em região de mineração de  
ouro

Dissertação apresentada ao Programa de Pós-Graduação em Engenharia Metalúrgica, Materiais e de Minas da Escola de Engenharia da Universidade Federal de Minas Gerais como requisito parcial para a obtenção do título de Mestre em Engenharia Metalúrgica.

Área de Concentração: Tecnologia Mineral  
Orientadora: Profª Virgínia S. T. Ciminelli  
Co-orientadora: Cláudia Lima Caldeira

Belo Horizonte  
Escola de Engenharia da UFMG  
2017

A635b	<p>Antônio, Daphne Chiara. Bioacessibilidade de arsênio em amostras de solo em região de mineração de ouro [recurso eletrônico] / Daphne Chiara Antônio. - 2017. 1 recurso online (xii, 105 f. : il., color.) : pdf.</p> <p>Orientadora: Virgínia Sampaio Teixeira Ciminelli. Coorientadora: Cláudia Lima Caldeira.</p> <p>Dissertação (mestrado) - Universidade Federal de Minas Gerais, Escola de Engenharia.</p> <p>Apêndices: f. 80-105.</p> <p>Bibliografia: f. 70-89. Exigências do sistema: Adobe Acrobat Reader.</p> <p>1. Engenharia de minas - Teses. 2. Tecnologia mineral - Teses. 3. Bioacessibilidade - Teses. 4. Arsênio - Teses. 5. Avaliação de riscos de saúde - Teses. I. Ciminelli, V. S. T. (Virgínia Sampaio Teixeira). II. Caldeira, Cláudia Lima. III. Universidade Federal de Minas Gerais. Escola de Engenharia. IV. Título.</p> <p style="text-align: right;">CDU: 622 (043)</p>
-------	---



UNIVERSIDADE FEDERAL DE MINAS GERAIS  
ESCOLA DE ENGENHARIA  
Programa de Pós-Graduação em Engenharia  
Metalúrgica, Materiais e de Minas



Dissertação intitulada "**Bioacessibilidade de Arsênio em Amostras de Solo em Região de Mineração de Ouro**", área de concentração: Tecnologia Mineral, apresentada pela candidata **Daphne Chiara Antônio**, para obtenção do grau de Mestre em Engenharia Metalúrgica, Materiais e de Minas, aprovada pela comissão examinadora constituída pelos seguintes membros:

Profª Virginia Sampaio Teixeira Ciminelli  
Orientadora - PhD (UFMG)

Cláudia Lima Caldeira  
Co-orientadora - Drª (UFMG)

Prof. Júlio César José da Silva  
Dr. (UFJF)

Marcus Manoel Fernandes  
Dr. (SENAI-FIEMG)

Prof. Rodrigo Lambert Oréfice  
Coordenador do Programa de Pós-Graduação em Engenharia  
Metalúrgica, Materiais e de Minas/UFMG

Belo Horizonte, 06 de março de 2017

## AGRADECIMENTOS

Agradeço aos meus amigos e à minha família, em especial à Desireé e ao Silas, pelo amor, exemplo e dedicação.

Agradeço à professora Virgínia Ciminelli e à Dra. Cláudia Caldeira pela orientação, suporte, incentivo e por todo conhecimento transmitido ao longo deste trabalho.

Agradeço à Ilda Batista e à Isabel Carvalho por me apoiarem incondicionalmente durante esses dois anos, por me oferecerem palavras de incentivo, conforto e compreensão e, acima de tudo, me acolherem como parte da família.

To Prof. K. Osseo-Asare for inspiring me with your greatness and kindness. Thank you, Professor, to teach to have faith above all things.

Agradeço ao Marcus Manoel pela coleta das amostras, ao Alberto Afonso do Departamento de Engenharia de Minas da UFMG pelo auxílio na preparação das amostras de solo, à Ilda Batista pelas análises de área superficial específica, à engenheira Isabel Carvalho pelas análises de difração e fluorescência de raios-X; à Guilhermina Oliveira e à Patrícia Lopes do Laboratório de Análises Químicas pelas análises químicas, pelo companheirismo e valiosas contribuições na discussão dos resultados. Agradeço à Dra. Profa. Maria Sylvia S. Dantas pelas análises de espectroscopia Raman, ao Dr. Itamar Delbem pelas análises de MLA e SEM, ao pesquisador Érico Freitas pelas análises de TEM, tratamento e auxílio na discussão dos resultados, ao Centro de Microscopia da UFMG pela excelente infraestrutura.

I would like to thank Prof. Massimo Gasparon at Queensland University for his critical evaluation and contributions to this work.

Agradeço à Christina Salvador pelo carinho, atenção e disponibilidade em me ajudar sempre. Agradeço aos colegas do Laboratório de Processamento Aquoso de Minerais e Materiais, Alexandre, Daiany, Glastone, Rafael, Renata, Tássio, Nathália e Nelson, por todos os bons momentos e ótimo convívio diário.

Agradeço a todos os funcionários do DEMET e PPGEEM pela colaboração e convivência prazerosa, em especial à Maria Aparecida Pacheco e ao Nelson A. Azevedo da Secretaria

de Pós-Graduação por demonstrarem disponibilidade e atenção para resolver os vários pedidos dos alunos.

Agradeço ao Conselho Nacional de Desenvolvimento Científico e Tecnológico (CNPq) e ao INCT-ACQUA (Instituto Nacional de Ciência e Tecnologia em Recursos Minerais, Água e Biodiversidade), pelo suporte financeiro e infraestrutura.

Finalmente, a todos que contribuíram para o sucesso deste trabalho, meu muito obrigada.

## OUTLINE

<b>LIST OF FIGURES .....</b>	<b>viii</b>
<b>LIST OF TABLES.....</b>	<b>x</b>
<b>ABSTRACT .....</b>	<b>xi</b>
<b>RESUMO.....</b>	<b>xii</b>
<b>1. INTRODUCTION .....</b>	<b>1</b>
<b>2. LITERATURE REVIEW .....</b>	<b>4</b>
2.1 <i>Arsenic in the environment</i> .....	4
2.2 <i>Oral bioaccessibility</i> .....	5
2.3 <i>Characterization techniques</i> .....	13
2.3.1 <i>Mineral Liberation Analyzer</i> .....	13
2.3.2 <i>Transmission electron microscopy</i> .....	17
<b>3 HIGH ARSENIC CONCENTRATIONS AND LOW BIOACCESSIBILITY IN SOILS FROM A GOLD MINING REGION .....</b>	<b>20</b>
3.1 <i>Introduction</i> .....	20
3.2 <i>Experimental</i> .....	22
3.2.1 <i>Sampling and sample preparation</i> .....	22
3.2.2 <i>Physical and chemical characterization</i> .....	22
3.2.2.1 <i>Mineralogical characterization</i> .....	22
3.2.2.2 <i>Specific surface area</i> .....	23
3.2.3 <i>Chemical composition by the Method 3051a (USEPA 2007)</i> .....	24
3.2.4 <i>Energy Dispersive X-ray Fluorescence (EDXRF)</i> .....	25
3.2.5 <i>Total sulfur (S-total) and total carbon (C-total)</i> .....	26
3.2.6 <i>Oral bioaccessibility</i> .....	26
3.2.7 <i>Electron microscopy analyses</i> .....	27
3.3 <i>Results and discussion</i> .....	29
3.3.1 <i>Soil characterization</i> .....	29
3.3.1.1 <i>X-ray diffraction (XRD)</i> .....	29
3.3.1.2 <i>Specific surface area (SSA)</i> .....	29
3.3.1.3 <i>EDXRF analyses</i> .....	32
3.3.1.4 <i>Raman analyses</i> .....	32
3.3.2 <i>Chemical analyses</i> .....	36
3.3.3 <i>Oral bioaccessibility test</i> .....	39
3.3.4 <i>Arsenic-bearing phases</i> .....	41

3.4 Conclusions.....	43
<b>4 LOW ARSENIC BIOACCESSIBILITY BY FIXATION IN NANOSTRUCTURED IRON(HYDR)-OXIDES QUANTITATIVE IDENTIFICATION OF AS-BEARING PHASES.</b>	<b>44</b>
4.1 Introduction .....	44
4.1.2 Description of the sampling site.....	47
4.2 Experimental .....	48
4.2.1 Sampling and sample preparation .....	48
4.2.2 Chemical concentrations using Method 3051a (USEPA 2007) .....	48
4.2.3 Oral bioaccessibility.....	51
4.2.4 Electron Microscopy analyses .....	52
4.3 Results and discussion.....	54
4.3.1 Bioaccessible Arsenic in the soil samples.....	54
4.3. 2 Arsenic-bearing phases.....	58
4.3.3 HRA and Environmental Implications .....	65
4.4 Conclusions.....	67
<b>5. CONCLUSIONS .....</b>	<b>69</b>
<b>6. REFERENCES .....</b>	<b>70</b>



## LIST OF FIGURES

Figure 2.1: Main inorganic and organic arsenic compounds (Adapted from Campbell and Nordstrom, 2014).....	6
Figure 2.2: Conceptual exposure pathways of As and its proportional risks (Ng et al., 2014). .....	7
Figure 2.3: Scheme of the influence of speciation, particle size and morphology on As bioavailability (Ruby et al., 1999). .....	9
Figure 2.4. MLA analysis of a composite particle (Gasparon et al., 2016). .....	16
Figure 2.5: A schematic of a transmission electron microscope where the main components are indicated (Adapted from Williams and Carter, 2009). .....	18
Figure 3.2. Correlation between aluminum soluble content and specific surface area.....	31
Figure 3.3. Raman spectra for Fe-(hydr)oxides in soil samples and reference Raman spectra for synthesized (syn) goethite and hematite. Gt - Band attributed to presence of goethite; Hm – bands attributed of hematite; *Indication of goethite to hematite transformation.....	35
Figure 3.4. SEM micrograph of sample K23 (> 2 mm) showing muscovite lamellae (1) within goethite (2) matrix (1.7% As) .....	42
Figure 3.5. (a) Bright Field TEM image of sample K21 (< 2 mm) showing nanoparticle aggregates of goethite and its correspondent SAD pattern (inset); (b) HRTEM image of the are inside the white square in (a) and its correspondent Fast Fourier Transform (FFT); (c) EDS maps of oxygen, iron, aluminum and arsenic.....	42
Figure 4.1. Sampling location, Paracatu, MG, Brazil, showing the complete set of samples and the selected samples (*) for this study. Santa Rita (SR) and Rico creek (RC) watersheds are also shown.....	49
Figure 4.2. Concentrations (expressed in mg kg <sup>-1</sup> ) of chemical As in the three fractions of the high arsenic samples. Square dots (in red) represent the median; circle dots represent the outliers, the box indicates the range 25–75% of the distribution and the whiskers represent minimum and maximum. Analyses carried out in duplicate for the >2 mm fraction and in triplicate for the others.....	56
Figure 4.3 SEM micrographs of typical soil samples .....	63
(a) (1) Hematite (66.5% Fe, 30.6% O, 1.5% Al, 1.4% As), (2) Quartz, (3) Muscovite; (highlighted by the arrow); (b) (4) Muscovite within the Fe-(hydr)oxide matrix (1.8% As) and (5) Goethite (62.4% Fe, 34.2% O, 1.5% Al, 1.0% As, 0.1% Si, 0.8% P); (c) (3) Muscovite, (4) Fe-(hydr)oxide matrix (1.1% As); (6) Botryoidal goethite (62.9% Fe, 31.9%	

O, 2.3% Al, 2.9% As); (d) (5) Goethite (62.9% Fe, 31.9% O, 2.4% Al, 2.9% As) and (7) Botryoidal hematite (67.0% Fe, 27.8% O, 1.5% Al, 0.6% As, 0.4% Si).....	63
Figure 4.4 (a) Bright Field TEM image of an oriented aggregate of goethite nanoparticles in sample K21 (< 2mm) and the selected area electron diffraction pattern (inset); (b) HRTEM image of the area inside the white square in (a) with the Fast Fourier transform (FFT) of goethite; (c-f) EDS maps of oxygen, iron, aluminum and arsenic of the goethite particle shown in (a); (g) Bright Field TEM image of sample K48 (> 2mm) showing oriented aggregates of hematite nanoparticles pointed by the arrow; (h) HRTEM image of the area inside the white square in (g) with FFT; (i and j) EDS spectra of the goethite and hematite, respectively pointed in the insets (a) and (g). Copper signal originated from the sample grid. ....	64

## LIST OF TABLES

Table II.1. Bioaccessibility tests .....	11
Table III.1: Microwave digestion conditions.....	24
Table III.2: Instrumental conditions (ICP-OES).....	25
Table III.3: Instrumental conditions (HG-ICP-OES).....	27
Table III.4. Specific surface area (SSA) BET for N <sub>2</sub> adsorption using degasification temperature of 120°C for 12 hours (n=1, < 2 mm).....	30
Table III.5. Mean, minimum and maximum of major elements expressed as oxides by EDXRF (%) in different size fractions of the select soil samples and quality control figures .....	33
Table III.6. Chemical concentrations by ICP-OES (n = 3, < 2 mm) and by LECO (S and C, n = 2, < 2 mm) (Mean±SD) .....	38
Table III.7. Bioaccessible arsenic in the < 250 µm fraction of the soil samples and in the certified material (Mean±SD, n=3) .....	40
Table IV.1: Microwave digestion conditions. ....	49
Table IV.2: Instrumental conditions (ICP-OES) .....	50
Table IV.3. Instrumental conditions (HG-ICP-OES).....	52
Table IV.4. SEM/MLA mainly instrumental parameters .....	53
Table IV.5. Median, mean and range of chemical As concentration (mg kg <sup>-1</sup> ) in different size fractions of the select soil samples and quality control results. For each sample, analyses were carried out in triplicate. ....	54
Table IV.6. Chemical As content in different particle sizes of the soil samples (mean±SD, n=3).....	55
Table IV.7. Bioaccessible arsenic in the < 250 µm soil samples and in the certified material (Mean±SD; n=4). ....	59
Table IV.8. Major mineral phases (wt%) in soil samples .....	60
Table IV.9. Number of particles for selected phases .....	60
Table IV.10. Arsenic intake from soil, water and food ingestion and predicted cancer risk	65

**ABSTRACT**

High levels of arsenic (As) (up to approx. 6354 mg kg<sup>-1</sup>) associated with a geologic anomaly are found in soil samples collected in a gold mining region in Minas Gerais state, Brazil. The samples were collected and prepared for different analyses: chemical analyses, energy dispersive X-ray fluorescence (EDXRF), Mineral liberation analysis (MLA), Scanning and Transmission electron microscopy (SEM and TEM) and micro Raman spectroscopy. Bioaccessibility tests were carried out in order to evaluate risk assessment. The results indicated that silicates (quartz and muscovite) are the main mineral constituents; iron (hydr)oxides (goethite and hematite) and gibbsite are also identified in some samples. Among the minor elements, only As showed concentrations significantly higher (median of 748.0 mg kg<sup>-1</sup>) than the National guideline values established for As concentration in soils. According the chemical analysis, an As-enrichment in the coarse fractions is associated to Fe-enrichment. Nevertheless, bioaccessible fraction was very low. The mean bioaccessible As is 7.0 mg kg<sup>-1</sup>, with a median value of 4.4 mg kg<sup>-1</sup>; percent As bioaccessible has a mean value of 1.3% and a median of 0.7%. Quantitative, single particle identification of As-bearing phases showed that arsenic is mainly found in iron (hydr)oxides–phyllosilicates mixture. Few arsenopyrite (e.g. 7 out of approx. 74,000 particles) and scorodite particles (e.g, 9 out of approx. 74,000) were identified. Arsenic was shown to be trapped in oriented aggregates of crystalline Fe-(hydr)oxides nanoparticles. The unambiguously and precise identification of As association with crystalline nanoparticles of Fe-(hydr)oxides supports the low As bioaccessibility reported here. Furthermore, the intergrowth of the Fe-(hydr)oxides with the phyllosilicates adds additional constraint to arsenic release/mobilization in the environment, thus minimizing the health risks.

## RESUMO

Elevados níveis de arsênio (As) (concentrações até 6354 mg kg<sup>-1</sup>), associados a uma anomalia geológica, são encontrados em amostras de solo coletadas em uma região de mineração de ouro no estado de Minas Gerais. As amostras foram preparadas para diferentes análises: análise química, difração de raios-X (XRD), fluorescência de raios-X por dispersão de energia (EDXRF), análise de liberação mineral (MLA), microscopia eletrônica de varredura e transmissão (MEV e MET) e micro Espectroscopia Raman. Ensaio de bioacessibilidade foram realizados para a avaliação de risco à saúde humana. Os silicatos (quartzo e muscovita) são os principais constituintes minerais; óxi-hidróxidos de ferro (goethita e hematita) também são identificados em algumas amostras. Entre os elementos minoritários, apenas As apresentou concentrações significativamente maiores (mediana de 748,0 mg kg<sup>-1</sup>) do que os valores de diretrizes nacionais estabelecidos para a concentração deste elemento em solos. De acordo com a análise química, concentrações majoritárias de arsênio nas frações grosseiras foram associadas à altas concentrações de ferro nessas frações. No entanto, a concentração de As bioacessível foi muito baixa. A dose média de bioacessibilidade é de 7,0 mg kg<sup>-1</sup>, com uma mediana de 4,4 mg kg<sup>-1</sup>; a porcentagem de As bioacessível apresentou um valor médio de 1,3% e uma mediana de 0,7%. A identificação quantitativa individual de partículas mostrou que o arsênio é encontrado principalmente na mistura de óxihidróxidos de ferro associados à filossilicatos. Foram identificadas poucas partículas de arsenopirita (aprox. 7 em 74 000) e de escorodita (aprox. 9 em 74000). O arsênio se mostrou fortemente associado aos agregados cristalinos orientados de nanopartículas de óxihidróxidos de ferro. A identificação inequívoca e precisa da associação de As com nanopartículas cristalinas de óxihidróxidos de ferro suporta a baixa bioacessibilidade relatada aqui. Além disso, o intercrescimento dos óxi-hidróxidos de ferro com os filossilicatos acrescenta restrição adicional à liberação / mobilização de arsênio no ambiente, minimizando assim os riscos à saúde.

## 1. INTRODUCTION

The city of Paracatu is located in the northwest of Minas Gerais state, approx. 500 km from the state capital, Belo Horizonte. Housing more than 90,000 people, the local economy is based on agriculture and mining activities (e.g. gold, zinc and lead). With companies such as Kinross Brasil Mineração, Nexa Resources, and Monsanto, the city won notoriety by housing the largest open-pit gold mine of the world. Mining is considered the main employer in Paracatu (Kinross, 2017; Monsanto, 2017; Paracatu-MG, 2017; VMetais, 2017).

Metal extraction activities can release contaminants to the environment, which may have an impact on human health, especially when the mine is adjacent to residential properties, such as in Paracatu (Rezende et al., 2015; Ng et al., 2014; Ono et al., 2012). Gold extraction often involves the treatment of ores containing arsenic-bearing minerals, which are exposed during ore beneficiation and disposed of in nearby areas (Matschullat, 2000).

Arsenic (As) is a chemical element with similar properties to metals and nonmetals, so it is classified as a metalloid. The main As minerals are arsenopyrite ( $\text{FeAsS}$ ), scorodite ( $\text{FeAsO}_4 \cdot 2\text{H}_2\text{O}$ ), orpiment ( $\text{As}_2\text{S}_3$ ) and realgar ( $\text{AsS}$ ) (Mandal and Suzuki, 2002; Nordstrom, 2002; Smedley and Kinniburgh, 2002).

The human contamination by As can cause health effects by long-term exposure (e.g., skin cancer of skin, bladder and lungs, neurotoxicity and skin lesions) in addition to the symptoms related to acute poisoning (e.g., vomiting, abdominal pain, numbness and diarrhea) (Flanagan et al., 2012; Ng et al., 2003; Nordstrom, 2002). The toxicity depends on speciation. For drinking water, for example, the lethal dose ranges from 1.5 mg (arsenic trioxide,  $\text{As}_2\text{O}_3$ ) to 500 mg (dimethylarsinic acid, DMA) per kg of body weight (WHO, 2011).

Although several investigations studied environmental samples from Paracatu region (e.g. water, sediments, soil, dust and food), only a few had investigated the relation between the total amount of As with the mobile and bioavailable portions, very relevant in terms of human and environmental risk assessment (Ng et al., 2014; Ono et al., 2012). This information is essential for a more precise assessment (Silvetti et al., 2014; Ng et al., 2014; Ono et al., 2012; Varejão et al., 2011; Bradham et al., 2011). None of these studies comprise a number of samples that represent the geological units and soil types present in the region.

Bioaccessibility tests can be used to estimate the bioavailability of an element and to relate the chemical nature of the compounds to their interaction with the human organism. The oral bioaccessibility tests aim to estimate the soluble element's fraction in a gastrointestinal environment (Ruby et al., 1999).

Combining bioaccessibility tests with characterization techniques, this work aims to assess As bioaccessibility in twenty (20) soil samples of Paracatu thus contributing to improve the protocols for health risk assessment in this and in other mining areas with important arsenic anomalies. From the 20 samples, fourteen (14) were analyzed at the Universidade Federal de Minas Gerais (UFMG), Belo Horizonte, Brazil, and seven (7) samples at the University of Queensland, Australia.

A careful investigation of selected soil samples with a detailed study of chemical composition, bioaccessibility evaluation and mineral characterization will help to elucidate the nature of arsenic extremely high concentrations in samples of Paracatu region and their effects on environmental and health risks assessment. Therefore, the main objective of this work is to determine the oral bioaccessibility of arsenic in enriched As-soils samples from Paracatu-MG. The specific objectives of the present dissertation are:

- i. To determine the mineral composition (using powder X-ray diffraction (XRD), energy dispersive X-ray fluorescence (EDXRF), Mineral liberation analysis (MLA), Scanning and Transmission electron microscopy (SEM and TEM) and micro Raman spectroscopy) as well as specific surface area (SSA) of the soil samples aiming the correlation of these parameters with the bioavailability of arsenic.
- ii. To determine the chemical composition of soil fractions above 2 mm (> 2 mm), below 2 mm (<2 mm) and below 250  $\mu\text{m}$  (<250  $\mu\text{m}$ ) as indicated in national and international soil standards.
- iii. To determine the bioaccessible fraction of arsenic in the soil fraction <250  $\mu\text{m}$ .

The document is organized in 5 chapters and 5 appendices.

Chapter 1 provides an introduction to the theme of this investigation.

A literature review of arsenic in the environment is presented in Chapter 2. In this chapter, a critical review on oral bioaccessibility tests, a summary of important works found in the

literature and briefly review on the principal characterization techniques used in this work, are presented.

In Chapter 3, the results obtained in this work are presented and discussed as follows: mineral phases identified by XRD, SSA values, major oxides percentage provided by energy dispersive X-ray fluorescence (EDXRF) spectrometer, and chemical composition obtained by microwave digestion and inductively coupled plasma optical emission spectrometer (ICP-OES) quantification.

In the Chapter 4, Arsenic concentrations in the three soil fractions ( $> 2\text{mm}$ ,  $< 2\text{ mm}$ ,  $<250\ \mu\text{m}$ ), the quantitative mineral characterization focus on arsenic-bearing phases, arsenic bioaccessibility and healthy risk assessment are presented.

Finally, Chapter 5 brings the main conclusions of the work.



## 2. LITERATURE REVIEW

### 2.1 Arsenic in the environment

Arsenic is a trace element that has been the subject of several investigations around the world since health problems related to its presence in groundwater were reported in Bangladesh and in India in the early 1980's (Nickson et al., 1998; Kumar, 1997; Bagla and Kaiser, 1996) Nordstrom, 2002; Smedley and Kinniburgh, 2002). Arsenic toxicity and other physico-chemical features depend on chemical speciation (*i.e.*, the chemical forms in which arsenic exists in the environment) and its concentration in the system. Speciation affects As solubility, solid-phase associations, physiological effects and it is also critical to designing remediation strategies, species transformation and understanding human exposure routes (Campbell and Nordstrom, 2014; Nordstrom, 2002; Smedley and Kinniburgh, 2002; Cullen and William, 1989).

Different As compounds are shown in Figure 2.1. Arsenic is stable in five (5) oxidation states (-III, -I, 0, III, V) being that As(III) and As(V) are the most common oxidation states in the environment, as in the inorganic species of arsenites and arsenates, respectively. Inorganic arsenic species (iAs) are more toxic than organic As species (e.g., dimethylarsinic acid - DMAs<sup>V</sup>, monomethylarsonic acid-MMA<sup>V</sup>, tetramethylarsonium ion-TMAs, trimethylarsine oxide-TMAO) wherein As(III) is around 60 times more toxic than As(V). Organic arsenic species such as arsenobetaine (AsB), arsenocholine (AsC) and arsenic sugars show low toxicity (Campbell and Nordstrom 2014; Nordstrom, 2002; Mandal and Suzuki, 2002; Cullen and William, 1989). Therefore, to assess the environmental and human health risks posed by arsenic, it is necessary to evaluate speciation, potential mobility in the environment and availability to be absorbed by the human body.

Through its toxicity, inorganic As compounds such as arsine (AsH<sub>3</sub>), arsenic and arsenious acid (H<sub>3</sub>AsO<sub>4</sub> and H<sub>3</sub>AsO<sub>3</sub>) are classified as carcinogenic to humans in Group 1 by the International Agency for Research on Cancer (IARC). Group 1 is a category which the agent presents sufficient evidence for carcinogenicity in humans and limited evidence for carcinogenicity in animals (WHO, 2011; IARC, 1987).

The As compounds represented among others are distributed in environmental samples as sediments, soils, groundwater and plants which may be released to the surrounding

society due to anthropogenic and natural activities (WHO, 2011; Nordstrom, 2002; Matschullat, 2000; Cullen and William, 1989).

Volcanic emissions, geothermal waters, and biological activity are considered the main natural pathways of As compounds. The primary anthropogenic sources of As species are mineral extraction and processing wastes, fossil fuel combustion and the use of arsenic herbicides, fungicides, and insecticides (Nordstrom, 2002; Smedley and Kinniburgh, 2002; Cullen and William, 1989).

In conclusion, an accurate evaluation of arsenic speciation and potential bioavailability in soils from a region of well-established As anomaly is crucial for risk assessment and for developing suitable remediation strategies, when needed.

## **2.2 Oral bioaccessibility**

Drinking water and food are the primary exposure routes to arsenic for humans. Nevertheless, incidental soil ingestion is also a relevant pathway contributing to human health risks, especially for children, because of activities that involve frequent hand-to-mouth behavior and its subsequent ingestion (Meunier et al., 2010; Ruby et al., 1999). Relative to the health risk assessment, the exposure to As by dermal absorption and inhalation are considered negligible compared to ingestion (Ng et al., 2014; Silvetti et al., 2014; De Miguel et al., 2012). The primary exposure pathways of arsenic are shown in Figure 2.2.

Oral toxicity doses for As (oral reference value and cancer slope factors) is based on studies of human populations exposed to the metalloid in an aqueous solution (USEPA, 2012b; Bradham et al., 2011; Wester et al., 2004; Ruby et al., 1999). In other words, the dissolved fraction of As is considered. In the case of soil samples, As can be found in mineral phases encapsulated or not in other phases, adsorbed or complexed with soil constituents and therefore, not readily available to be absorbed by the organism after ingestion. Based on this understanding, bioaccessibility (BAC) and bioavailability (BA), rather than total content, are increasingly used as a key indicators of the risks contaminants can provoke to the environment and to human health (Ng et al., 2015; Bradham et al., 2011; Meunier et al., 2010; Koch et al., 2007; Navarro et al., 2006; Ruby et al., 1999).

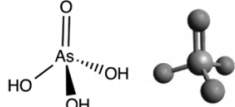
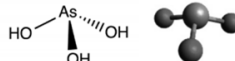
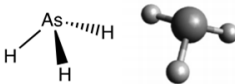
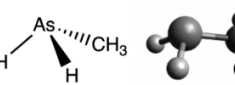
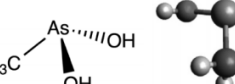
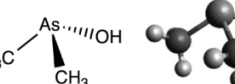
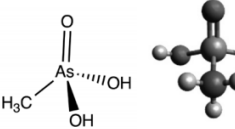
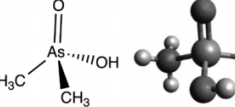
Name	Chemical & Structural Formula
arsenic acid, hydrolytic anions	$H_3AsO_4, H_2AsO_4^-, HAsO_4^{2-}, AsO_4^{3-}$ 
arsenous acid (arsenious acid), hydrolytic anions	$H_3AsO_3, H_2AsO_3^-, HAsO_3^{2-}, AsO_3^{3-}$ 
arsine	$AsH_3$ 
methylated arsines	$CH_3AsH_2, (CH_3)_2AsH, (CH_3)_3As$ 
monomethylarsonous acid [MMAs(III)]	$CH_3As(OH)_2$ 
dimethylarsenous acid [DMAs(III)]	$(CH_3)_2AsOH$ 
monomethylarsonic acid [MMAs(V)]	$CH_3AsO(OH)_2$ 
dimethylarsinic acid [DMAs(V), cacodylic acid]	$(CH_3)_2AsO(OH)$ 

Figure 2.1: Main inorganic and organic arsenic compounds (Adapted from Campbell and Nordstrom, 2014).

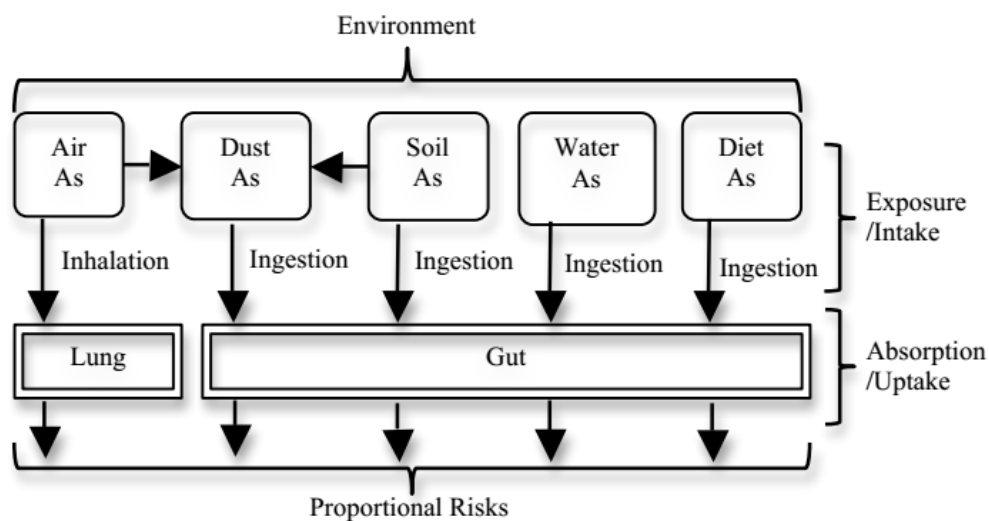


Figure 2.2: Conceptual exposure pathways of As and its proportional risks (Ng et al., 2014).

The most precise approaches for risk assessment are the bioavailability tests. However, those analyses require longer and costly procedures, which include the approval by an Ethics Committee for animal experimentations, hence limiting the application of these models to the largest assays (USEPA, 2012b; Bradham et al., 2011; Ruby et al., 1999). Therefore, the development of accurate, faster and more economical procedure, which is capable to estimate the bioavailability, became necessary. One of the alternatives that have been frequently applied is the *in vitro* bioaccessibility test (USEPA, 2012a,b; Meunier et al., 2010; Ruby et al., 1999).

Oral bioaccessibility (BAC) is the fraction of total contaminant mass in the sample, which is soluble in the gastrointestinal environment and may be available for absorption into the body (*in vitro* tests) (Silvetti et al., 2014; Ng et al., 2015; USEPA, 2012a; Meunier et al., 2010; Koch et al., 2007; Ruby et al., 1999). Once that fraction is absorbed, it becomes bioavailable and is incorporated into the metabolism. Oral bioavailability (BA) refers to the fraction that is soluble in the gastrointestinal tract and is available for absorption by blood stream (*in vivo* tests) (Ng et al., 2015; Meunier et al., 2010; Navarro et al., 2006).

Another related term is the relative bioavailability (RBA). Relative bioavailability (RBA) is the ratio of the absolute oral BA of a contaminant present in some samples (e.g., soil, sediment, water, food) to the absolute oral BA of that same contaminant in another matrix. The RBA allows us to compare a portion bioavailable in different forms of an analyte or for

a different exposure media containing the analyte (Ng et al., 2015; USEPA, 2012a; Bradham et al., 2011; Ruby et al., 1999). Arsenic dissolution from soil samples and, consequently, its bioavailability and bioaccessibility is controlled by mineralogy (*i.e.*, mineral phases, occurrence, interaction and distribution of the metalloid among these different phases), particle size distribution (Ng et al., 2015; Bradham et al., 2011; Navarro et al., 2006; Ruby et al., 1999), among other factors (e.g. temperature, solid/liquid ratio) related to the dissolution conditions.

The *in vitro* tests (*i.e.*, BAC tests) consist, basically, in extraction at corporal temperature employing a biochemical solution that simulates the conditions in the gastric and/or gastrointestinal environment. The amount of analyte extracted from the sample is quantified and has been used to estimate the BAC of the contaminant in the sample (e.g., soil, sediments, food and water) (USEPA, 2012a,b; Bradham et al., 2011; Meunier et al., 2010; Navarro et al., 2006; Ruby et al., 1999).

For the oral bioaccessibility, generally, two extraction types are used: a solution that simulates the gastric-phase solution (*i.e.*, the acidic biochemical stomach environment) and a solution that simulates the intestinal-phase (*i.e.*, the biochemical environment of the small intestine) (USEPA, 2012a,b).

The extraction procedure consists basically in a biochemical compound (amino acids, enzymes or proteins) mixture at different pH and under heating. The extractions are dependent of the temperature and the solution's pH. The temperature is generally set at 37°C to simulate the body temperature in which the biochemical compounds are considered stables. The pH, on the other hand, varies with the biological system studied (e.g., gastric, intestinal and respiratory system); the compound will have different behavior in each of the solutions. At acid solutions (pH < 7.0), the compounds generally deprotonate and seem not to interfere in the bioaccessible portion because of the dissolution is promoted by the stronger acid present. At neutral solution (pH ~ 7.0), the amino acid and enzymes, for example, may interact or not with the analyte depending on the molecular structure and physicochemical properties (Lehninger et al., 1995). Metal precipitation should also be considered at neutral pH conditions.

The most common biochemical compounds applied to BAC protocols are the glycine and pepsin, an amino acid and an enzyme, respectively. An acid solution is capable of to extract a major portion of the analyte. For that reason, a single stage using the gastric

solution is commonly applied. Also, the *in vitro* test for As in soil and sediment was validated comparing the portion bioaccessible in an acid glycine solution with *in vivo* data from monkey and swine studies (USEPA, 2012b). Results showed correlation of *in vitro* with the *in vivo* data. The best correlations were at pH 1.5 in 0.4 mol L<sup>-1</sup> glycine solutions for monkeys ( $R^2= 0.87$ ) and at pH 7.0 for swine ( $R^2= 0.85$ ) in a 0.4 mol L<sup>-1</sup> glycine and 0.05 mol L<sup>-1</sup> phosphate solution. Results of analysis suggest that the *in vitro* methods can be applied as an alternative to the *in vivo* BA tests. The standard procedure adopted by the United States Environmental Protection Agency (USEPA) is an extraction with a 0.4 mol L<sup>-1</sup> glycine solution adjusted to pH 1.5 with hydrochloric acid (HCl), which is considered representative of the analyte's BAC (USEPA, 2012 a,b). RBA is the relative bioavailability and IVBA is the *in vitro* BAC. Ruby and co-workers (1999) are responsible for one of the pioneer BAC studies. The authors summarize the mineral and soil factors (e.g., particle size, mineral phase, grain encapsulation), which influence arsenic and lead (Pb) bioavailability. In a critical review perspective, the authors highlighted the importance of the aspects shown in Figure 2.3 in the control of an element's dissolution.

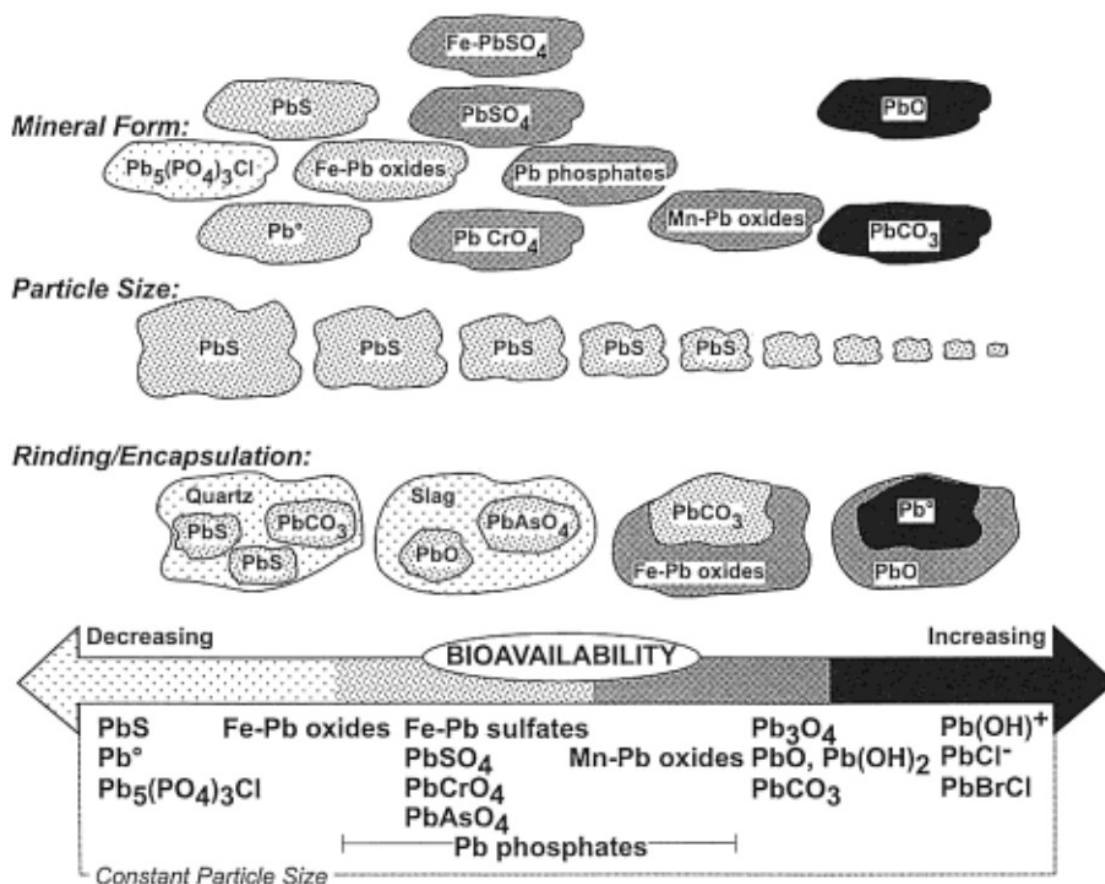


Figure 2.3: Scheme of the influence of speciation, particle size and morphology on As bioavailability (Ruby et al., 1999).

Many researchers applied the BAC tests to estimate the portion of As bioaccessible in sediments, soils and mine wastes. The procedures are summarized in [Table II.1](#) and will be discussed in the following paragraphs. [Navarro and co-workers \(2006\)](#) evaluated the bioavailability of Pb, Cd and As in soils and waste material from an old mining site located near La Unión (Spain). The authors studied the extent to which BAC is influenced by the mineralogy. The BAC test was performed with two extractants solutions: a gastric phase and an intestinal phase according to the SOP developed by the SBRC ([SBRC, 2001](#); [Ruby et al., 1999](#)). For all the analytes, the major portion was leached in the gastric solution due to the low pH. The analyte extraction order was discussed based on the distinct solubility of each analyte, in chemical speciation and the binding capacity to different soil and sediment materials.

[Bradham and researchers \(2011\)](#) correlated the *in vivo* and *in vitro* (SBRC/EPA) assays (As) with physicochemical characterization of soils from sites affected by mining and smelter activities. The results showed a great correlation between the *in vivo* and *in vitro* analyses ( $R^2=0.92$ ), hence the authors suggested that both methods can be used to estimate the potential risks associated with exposure to As contaminated soils.

With a different approach, [Silvetti and co-workers \(2014\)](#) applied BAC tests to measure the *in situ* remediation effectiveness. Two As contaminated soils were submitted to the SBRC method for As and Pb bioaccessibility. The results showed that the bioaccessibility is affected by various soil amendments such as soil conditions and the origin of contamination.

Investigating the association between the soil geochemistry and the bioaccessibility of trace elements, [De Miguel and co-workers \(2012\)](#) studied surficial soil samples from 16 playground areas in Madrid (Spain). The samples were submitted to the *in vitro* procedure with three extractant solutions: an artificial saliva solution that simulates the gastric-intestinal environment (RVIM method) and two acid solutions, the gastric environment, a  $0.4 \text{ mol L}^{-1}$  glycine solution at pH 1.5 (SBET according to the author, but in fact is the SBRC/EPA method) and a  $0.07 \text{ mol L}^{-1}$  HCl solution at pH 1.5 (HCl). Arsenic and metal extractions were similar in both acidic media (SBET and HCl). The researchers pointed to the need to determine and understand the samples mineralogical composition in order to provide reliable results of bioaccessibility among different elements and different matrices.

Table II.1. Bioaccessibility tests

References	Sample size fraction	Extraction solutions	pH
<b>SBRC/EPA SOP</b>			
Navarro et al., 2006; Bradham et al., 2011.; Silvetti et al., 2014	<250 $\mu\text{m}$	<i>Gastric phase:</i> 0.4 mol L <sup>-1</sup> <b>Glycine</b>	1.50±0.05/ <b>HCl</b> .
Meunier et al., 2010.	<150 $\mu\text{m}$	<i>Gastric phase:</i> PBET solution: mixture of 1.25 g L <sup>-1</sup> <b>pepsin</b> , 0.5 g L <sup>-1</sup> <b>sodium citrate</b> , 0.5 g L <sup>-1</sup> <b>malic acid</b> , 1 ml L <sup>-1</sup> <b>glacial acetic acid</b> and 0.15 mol L <sup>-1</sup> <b>NaCl</b> .  <i>Gastrointestinal phase:</i> same <b>PBET</b> solution.	<i>Gastric phase:</i> 1.80/ <b>HCl</b> . <i>Gastrointestinal phase:</i> 7.0/ saturated <b>Na<sub>2</sub>CO<sub>3</sub></b> solution
Ono et al., 2012: protocol proposed by Rodriguez et al., 1999	<150 $\mu\text{m}$	<i>Gastric phase:</i> a mixture of 1 g with 150 mL of a gastric solution consisting of 1% <b>pepsin</b> in 0.15 mol L <sup>-1</sup> <b>NaCl</b> .  <i>Intestinal phase:</i> same <b>gastric solution</b> + 0.525 g of a <b>porcine bile</b> extract and 0.053 g of <b>pancreatin</b> .	<i>Gastric phase:</i> 1.80±0.05/ <b>HCl</b>  <i>Intestinal phase:</i> 5.5±0.1 / <b>NaHCO<sub>3</sub></b>
De Miguel et al., 2012	<100 $\mu\text{m}$	1) RIVM method: <b>artificial saliva</b> + <b>gastric juice</b> + <b>intestinal juices</b> . 2) SBET/SBRC/EPA: 0.4 mol L <sup>-1</sup> <b>glycine</b> 3) HCl: 0.07 mol L <sup>-1</sup> <b>HCl</b>	1) RIVM method: 7.0 2)SBET/SBRC/EPA: 1.5/ <b>HCl</b> 3) HCl: 1.5/ <b>HCl</b>
Ng et al., 2014	<250 $\mu\text{m}$ .	PBET (Ng et al., 2015) <i>Gastric phase:</i> 1.25 g L <sup>-1</sup> <b>pepsin</b> , 0.5g L <sup>-1</sup> <b>sodium malate</b> , 0.5 g L <sup>-1</sup> <b>sodium citrate</b> , 420 $\mu\text{l}$ L <sup>-1</sup> <b>lactic acid</b> , 500 $\mu\text{l}$ L <sup>-1</sup> <b>acetic acid</b> . <i>Gastrointestinal phase:</i> 1.75 g L <sup>-1</sup> <b>bile</b> , 0.5 g L <sup>-1</sup> <b>pancreatin</b> .	<i>Gastric phase:</i> 1.5; 2.5 and 4.0/ <b>HCl</b> .  <i>Gastrointestinal phase:</i> 7.0.

\*All the authors adopted the temperature as 37°C.



With the aim to study the As bioaccessibility in samples of tailings collected in Nova Scotia (Canada), [Meunier and co-workers \(2010\)](#) applied the *in vitro* physiologically based on extraction test (PBET) and investigated the influence of the pH of the simulated solution, the liquid-to-solid ratio and sample particle size. The PBET consisted in a two extraction solutions: an acid solution with 1.25 g L<sup>-1</sup> pepsin, 0.5 g L<sup>-1</sup> sodium citrate, 0.5 g L<sup>-1</sup> malic acid, 1 ml L<sup>-1</sup> glacial acetic acid and 0.15 mol L<sup>-1</sup> NaCl at pH 1.80 which simulates a gastric phase and a gastric-intestinal phase with the same solution, although adjusted to pH 7.0 with a saturated Na<sub>2</sub>CO<sub>3</sub> solution neutral solution. The authors observed that the highest As BAC (up to 49%) was associated with the calcium-iron arsenate phase. Samples containing As predominantly as arsenopyrite (FeAsS) or scorodite (FeAsO<sub>4</sub>) had the lowest bioaccessibility (<1%). The percentage of As bioaccessible was lower in the samples with higher As concentrations. It could indicate solution saturation or the influence of the insoluble mineral phases, however only the first hypothesis was investigated by the authors. Meunier et al. (2010) also investigated the liquid-to-solid ratios (100:1, 250:1, 500:1, 1000:1, 2000:1, and 5000:1) on 13 samples representing a range of As concentrations. The results showed that the percent of As bioaccessible was insensitive to different liquid-to-solid ratios and the 100:1 ratio was adopted. In relation to the particle size distribution, the results indicated no statistically significant differences in BAC between the three particle size fractions (<45 µm, <150 µm and <250 µm) and the <150 µm particle size fraction selected.

[Ono and co-workers \(2012\)](#) studied samples of soil, substrates and tailings from Paracatu, MG, Brazil. The authors evaluated As BAC employing a gastro intestinal (IVG) solution based on the protocol proposed by Rodriguez et al. (1999), which consists of two sequential phases: an acid solution with 1% pepsin in 0.15 mol L<sup>-1</sup> NaCl at pH 1.80 and an intestinal phase using the gastric solution at pH 5.5 was adjusted with NaHCO<sub>3</sub> followed by adding 0.525 g of a porcine bile extract and 0.053 g of pancreatin.

The *in vitro* results showed very low average values of bioaccessible As for both extractants (4.8 to 79 mg kg<sup>-1</sup> which corresponds to 1.2 to 4.2%). The method described by Ono et al. (2012) involves a gastric solution (mix of pepsin and NaCl at a pH of 1.8) similar but simpler than that from the original PBET protocol while the intestinal phase is completely different from the PBET protocol.

[Ng and co-workers \(2014\)](#) carried out a three-year research with water, surface dust and soil samples of the Paracatu region aiming to evaluate all relevant possible exposure pathways for the health risk assessment of As, and to address the public health concern.

The As BAC was calculated employing the PBET test (gastric solutions: pH 1.5, 2.5 and 4.0; intestinal phase: pH 7.0). The mean of As bioaccessible in the surface dust samples was 2.9% and therefore similar to that reported by Ono et al. (2012) for samples from the same region (As BAC% of 1.2 to 4.2%). In addition, the authors point out the relevance of BAC studies and the consideration of all exposure pathways to provide an accurate risk assessment.

The aforementioned review shows that the bioaccessible fraction varies with the samples' properties, the biochemical extraction solution and the interaction between the analytes and the matrix constituents. The SBRC/EPA method is a product of an extensive and systematic work to identify the optimal conditions for the BAC tests. The procedure offers a single extraction step using a simple extraction fluid, based on a validated *in vivo-in vitro* correlation, reliable and reproducible alternative for an *in vitro* study refers. Therefore, the SBRC/EPA procedure was chosen for this study.

## **2.3 Characterization techniques**

Electron microscopy analyses were applied to identify and quantify the mineral phases present in the soil, ore and other samples. A brief review on these techniques is presented in the next sections.

### **2.3.1 Mineral Liberation Analyzer**

Mineral Liberation Analyzer (MLA) is an automated mineralogical system that combines image analysis with chemistry data using a scanning electron microscope (SEM) with an energy dispersive spectrometer (EDS) (Gu, 2003). Although the system was originally developed for support mineral processing, environmental applications are growing due to their ability to characterize a variety of samples including fine-grained materials such as tailings, soil and contaminated sediments (Jamieson et al., 2015; Sylvester, 2012; Gu, 2003).

The technique is based on backscattered electron (BSE) image analysis for determining grain boundaries of the mineral phases in each particle. These are then distinguished based on homogeneous grey levels. After the particles segmentation, an EDS spectra is collected for each phase in the sample to obtain the chemical composition data (Gu, 2003).

Each spectrum acquired is then compared with a user-generated or a standard mineral spectra library. The creation of the user library is the most important part of the analysis and is created before analysis which each mineral phase is characterized by carefully collection of high quality X-ray spectra (Fandrich et al., 2006). The construction of a standard library directly from the sample ensures that analysis conditions are reflected in the standards (Fandrich et al., 2006; Gu, 2003). Finally, the mineral phases are classified based on user-defined criteria and assigned a false color to each mineral phase/composition to produce a mineral map of the particles. X-rays data that do not match any minerals are classified as “unknown” and can be relocated and classified with user input (Gu, 2003). Figure 2.4 presents MLA classification system.

As mentioned, MLA is used in several different research fields. The following works will concentrate on its environmental application, the focus of the present work. In a previous study from the group, Gasparon and co-workers (2016) developed a new method for characterizing atmospheric particulates. The samples were collected in Paracatu area, Minas Gerais, Brazil, and analyzed using MLA. The results showed arsenopyrite phase and helped to propose the source of phases.

The relation of silicate minerals and As was observed by Alam and co-workers (2014). The authors used a SEM-EDX with FEI-MLA to determine the mineral composition of a till sample collected in Avondale, Canada. Quartz ( $\text{SiO}_2$ , 42.8 wt %), albite ( $\text{NaAlSi}_3\text{O}_8$ , 38.7 wt %) and potassium feldspar ( $\text{KAISi}_3\text{O}_8$ , 9.3 wt%) were the major minerals (wt >5 %) identified and the presence of Fe-rich clays and Fe-(hydr)oxides were also observed. No arsenic minerals and no arsenic were detected in any of the samples. Therefore the authors suggested that the main As reservoir was silicate minerals containing 75 % of As whereas Fe–Mn-(hydr)oxides the second largest As reservoir (16 % of As).

Besides the identification and quantification of mineral phases, Redwan et al. (2012) applied MLA to elucidate the mineralogical transformation of mine tailings samples in Freiberg, Germany. Major phase's silicate, carbonate and heavy-mineral were identified. The results also showed a large decrease of the 2D pore area, from 43% in the unoxidized layer compared to 10.5% in the hardpan layer, which was attributed to the precipitation of amorphous gels and secondary phases.

Veen et al. (2016) used a FEI Quanta 600 SEM-MLA microscope to characterize sulfidic mine wastes of a mine waste repository site in Cornwall, U.K. In the mine waste (MW) samples, the majority of silicates and iron oxides and a few sulfide grains were observed. In the oxidized samples As was mainly associated with Fe, O, Si and Al. Due this association is suggest that As is immobilized in Fe-(hydr)oxides and alumino silicates (clays), most probable ferro-saponite, because of its cation exchange characteristics and ability to insert molecules in its structure.

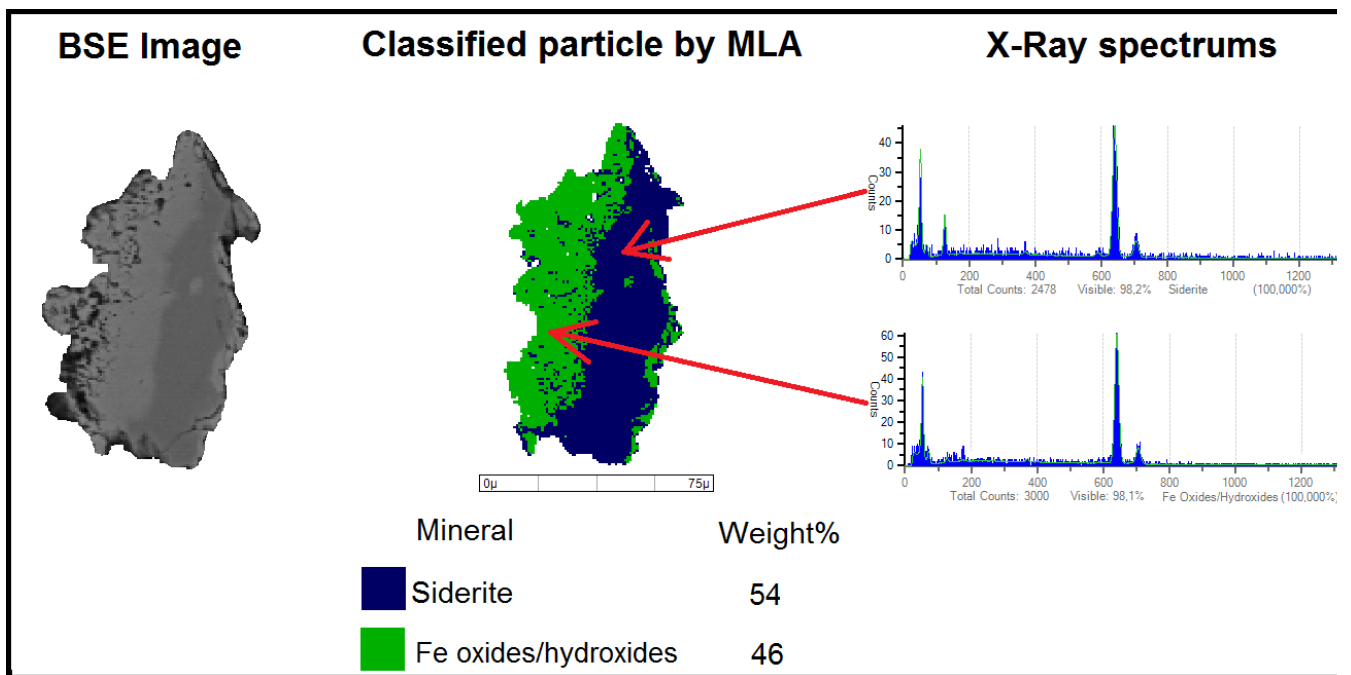


Figure 2.4. MLA analysis of a composite particle (Gasparon et al., 2016).

### 2.3.2 Transmission electron microscopy

The transmission electron microscopy (TEM) is a technique broadly used for the characterization of a large variety of materials (e.g., biological materials, environmental samples, carbon nanotubes and electronic components) and offers very useful and precise information on crystal structure, atom position, strain, and chemical composition. It can achieve a resolution in the order of picometer (pm:  $10^{-12}$  m) and a magnification up to 10 million times ( $10^6$  x) (Williams and Carter, 2009).

Figure 2.5 shows a schematic of a TEM microscope and illustrates the positions of the components. A transmission electron microscope consists basically of an electron source, an electron column, electromagnetic lenses and apertures for transmitting the electron beam through the instrument, a detector, a specimen chamber for samples, a fluorescent screen (CCD camera) to capture and record the images and vacuum pumps which ensures that the electrons will transmit through the column without scattering and also keeps contaminations from accumulating on the sample surface, which is detrimental to the quality of the image. A range of detectors can be used according the analysis propose such as CCD (Charge-coupled device) cameras for regular imaging to EDX (Energy dispersive X-ray) detectors for chemical composition (Williams and Carter, 2009).

In a transmission electron microscope, a broad beam is emitted from the electron source and the condenser lens accelerated towards a thin sample (*i.e.*, electron transparent) with thickness  $<100$  nm. After interaction some electrons pass through and some are scattered at certain angles these are named backscattered electrons (BSE). These signals are then focused at different points in the back-focal plane (BFP) of the objective lens and hereby all the signals are collected in the image plane to produce an image. Once the image is formed, a set of electromagnetic lenses is used to magnify it. The result can be viewed on a fluorescent screen and recorded by a CCD camera (Williams and Carter, 2009).

In the present work, TEM analysis were used to identified and characterize mineral phases related directly or indirectly to the presence of As in the soil samples, hence the following works aim similar interests.

To assess the potential risk of coal cleaning rejects (CCRs), Vallejulelo and co-workers (2017) investigated coal residues of abandoned mines in four regions in Santa Catarina state, Brazil.

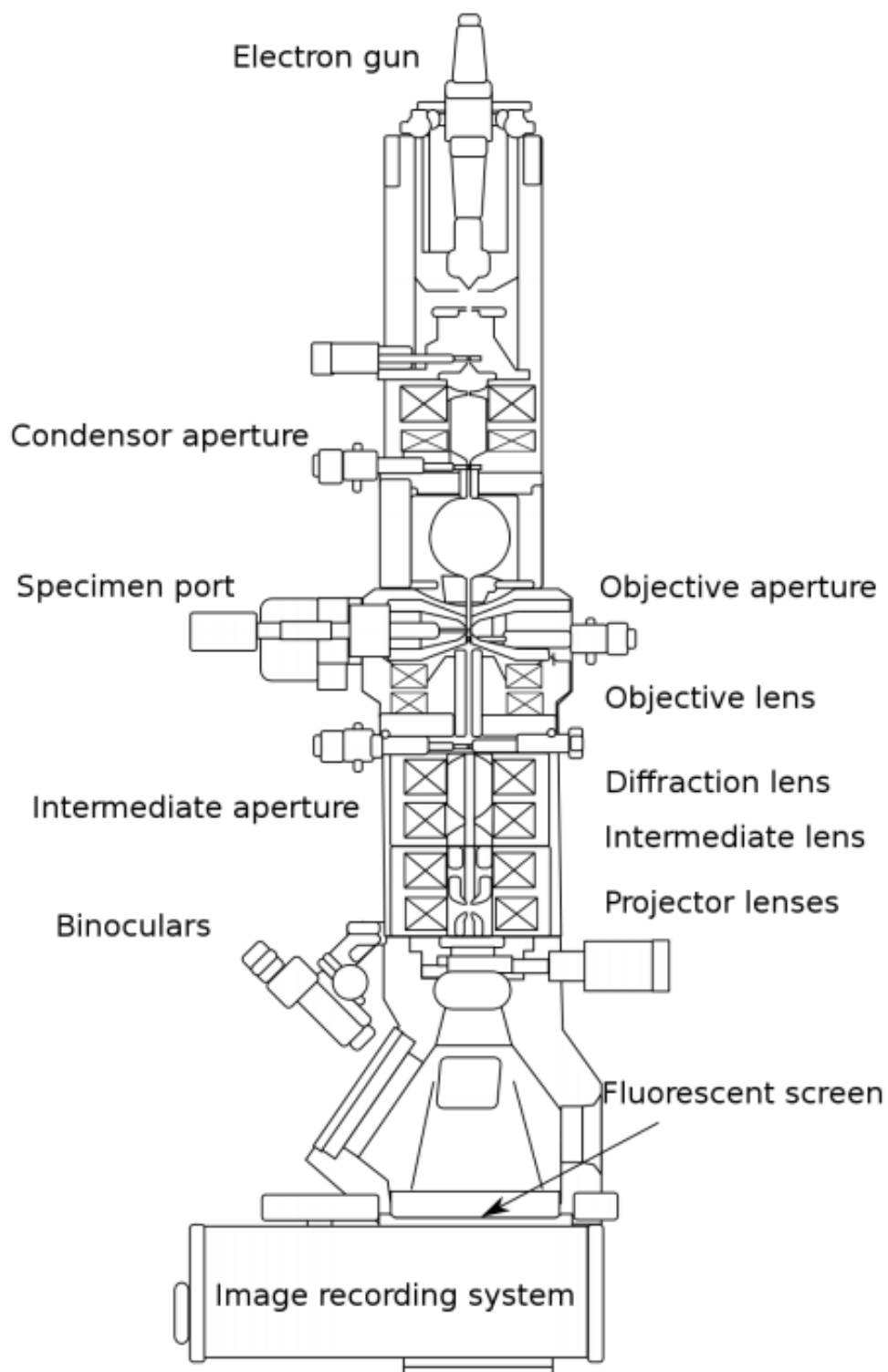


Figure 2.5: A schematic of a transmission electron microscope where the main components are indicated (Adapted from [Williams and Carter, 2009](#)).

XRD, FE-SEM, and HR-TEM were used to determine the mineralogy and nano-mineralogy whereas Inductively Coupled Plasma Mass Spectrometry (ICP-MS) was applied to quantify As, Cd, Cr, Cu, Ni, Pb, and Zn. FE-SEM and HR-TEM/EDS/SAED images of ultra-fine and nano-minerals mixed identified spherical hematite ( $\text{Fe}_2\text{O}_3$ ), angular goethite ( $\text{FeOOH}$ ), pseudomorph jarosite ( $\text{KFe}_3(\text{OH})_6(\text{SO}_4)_2$ ), amorphous clays, gibbsite ( $\text{Al}(\text{OH})_3$ ), ferrihydrite ( $\text{Fe}_2\text{O}_3$ ), and schwertmannite ( $\text{Fe}_8\text{O}_8(\text{OH})_6(\text{SO}_4)$ ). Distribution maps for Al, As and Fe indicate that the surface structures of illite-smectite (clay mineral), kaolinite ( $\text{Al}_2\text{Si}_2\text{O}_5(\text{OH})_4$ ), and associated (amorphous phases) Al-(hydr)-oxides are enriched in Fe and As.

Wang et al. (2014) collected TEM and high-resolution TEM (HRTEM) images to investigate the morphologies and structures of synthesized Al-substituted  $\alpha$ -FeOOH samples. XRD, field emission scanning electron microscope (FESEM), Fourier-transform IR spectroscopy (FTIR), selected area electron diffraction (SAED) and nitrogen adsorption isotherms were also used to characterize the materials. The results showed that Al incorporation into the crystal structure of goethite occurs via isomorphous ionic substitution of Al for Fe.

Serrano and co-workers (2015) studied dispersible colloid fractions (DCFs) (10–1000 nm) of an As-rich mine waste pile and its adjacent sediments and soils of an abandoned smelting factory in Madrid, Spain. The authors combined asymmetrical-flow field-flow fractionation (AsFIFFF)/inductively-coupled plasma–mass spectrometry (ICP–MS), TEM and X-ray absorption (XAS) spectroscopy to determine samples composition and As and Fe speciation. The results of TEM/EDS and XAS analysis revealed the presence of Fe nanoparticle in all samples downstream of the waste pile and scorodite ( $\text{FeAsO}_4$ ) nanoparticle in one DCF sample.

The As sorption onto iron biominerals was studied by Sowers et al. (2017). The authors determined the extent of As sorption onto synthetic and natural iron biominerals, i.e., bacteriogenic Fe minerals which are poorly ordered, present low crystallinity and high surface area. The environmental samples were collected Rocky Branch Creek, North Carolina, USA. To characterize the morphology, phase, and surface properties of Fe(III) minerals; XRD, surface area analyzer, Fe K-edge X-ray absorption spectroscopy (XAS) and TEM were used. The micrographs (TEM) of environmental and synthetic Fe-(hydr)-oxides showed differences in the morphology. The environmental Fe-(hydr)-oxide presented particles sizes ranging from approx. 50 to 200 nm whereas the synthetic iron compound appears to be comprised of regular aggregates of small ball-like masses.



### 3 HIGH ARSENIC CONCENTRATIONS AND LOW BIOACCESSIBILITY IN SOILS FROM A GOLD MINING REGION<sup>1</sup>

#### 3.1 Introduction

There is an increasing concern on the stability of As-containing materials in the environment in view of sound evidences for the carcinogenicity of inorganic arsenic to humans following long-term exposure to trace amounts of the element, especially in drinking water (IARC, 2012). Arsenic is relatively abundant in geological materials, such as gold, base metals ores and coal (Smedley and Kinniburgh, 2002). Gold mining in the state of Minas Gerais goes back to the 17<sup>th</sup> century and gold is often found in association with arsenopyrite and other sulfide minerals. Large amounts of mining wastes containing arsenic have been produced and disposed of over the centuries. High concentrations of arsenic (up to 3,000 mg kg<sup>-1</sup>) have been reported in soils and sediments in mining areas (Rezende et al., 2015; de Vicq et al.; 2015; Mello et al., 2006; Deschamps et al., 2002), including Paracatu, a city in northwest Minas Gerais state (Figure 3.1).

These concentrations, which create legitimate concern in local population and authorities, leads to the question on how can rigorously assess the potential, long-lasting risks associated to natural enriched-As materials or wastes generated by anthropogenic activities. In addition to the traditional tests for the classification of residues for disposal other tools are needed and increasingly used. Assessment of bioavailability (BA) and of bioaccessibility (BAC) (i.e. the fraction of contaminants that are bio soluble and potentially available to be absorbed by the human body) helps to better evaluate the risks that a given material poses to human health. Advanced analytical techniques allow one to understand at a nanoscale or molecular level the mechanisms involved in chemical species fixation in the environment. Our work will demonstrate how the combination of various analytical tools has improved our understanding of the stability of arsenic in the soils of Paracatu. We will also demonstrate that despite the very high, natural As concentration in the soil samples in this municipality, naturally-occurring processes responsible for the uptake and fixation of As in Fe-Al-(hydr)oxides also take place. And at the end, arsenic becomes immobile and will remain as such, as long as environmental conditions allow the stability of the host mineral phases. Advances in the understanding of As fixation under natural

---

<sup>1</sup> Erico T.F. Freitas (UFMG), Marcus M. Fernandes (Center for Innovation and Technology SENAI – CETEC), Massimo Gasparon (The University of Queensland).

<sup>2</sup> This chapter was published by Journal of Hazardous Materials in march 2018. Authors: Virginia S.T. Ciminelli, Daphne C. Antônio, Claudia L. Caldeira, Erico T.F. Freitas, Itamar Daniel Delbem, Marcus M.

conditions are expected to drive the development of improved long-term storage or disposal options and to assist stakeholders in a mature debate on environmental and health risks.



Figure 3.1. Map of Brazil showing the state of Minas Gerais. The square indicates the selected area for this study. Square highlights Paracatu city area.

## 3.2 Experimental

### 3.2.1 Sampling and sample preparation

The soil sampling (June-July of 2014) was undertaken according to the procedure adopted by the State Program Soils of Minas (Solos de Minas) following the State Environmental Agency-FEAM (2013), and in agreement with international practice (USEPA, 1992). Four classes of soils occurring on Santa Rita and Rico Creek watersheds and comprising areas of gold mineralization and areas representing the region's background were selected (Figure 3.1). In both cases, the samples (in a total of forty-nine) were collected in areas with no evidences of anthropogenic activity. The collection was carried out with an excavator and a stainless-steel sampler to make composite samples. The surface soil samples (0-20 cm) were transferred to clean polypropylene bags, identified and stored at room temperature until further processing. Fourteen samples with the As concentrations above  $100 \text{ mg kg}^{-1}$  were selected for this work.

The bulk samples were oven-dried at  $40^\circ\text{C}$  for 12 hours until they reached a constant weight, then disaggregated, split into sub-samples and sieved at 2 mm. The size fraction cutoff was chosen based on the USEPA methods (2007) and National guidelines (Anonymous, 2009) for soil classification ( $< 2 \text{ mm}$ ). Some fractions were fine-ground to ( $< 44 \mu\text{m}$ ) prior to chemical analyses and soil characterization by powder X-ray diffraction (XRD), Energy Dispersive X-ray Fluorescence (EDXRF) and transmission electron microscopy (TEM). Using an Agate mortar, some fractions were fine-ground ( $< 250 \mu\text{m}$ ) for particle characterization by SEM-MLA. The electron microscopy analyses were performed in the Center of Microscopy at the Universidade Federal de Minas Gerais (UFMG), Belo Horizonte, Brazil, and at the Center for Microscopy and Microanalysis of the University of Queensland, Australia.

### 3.2.2 Physical and chemical characterization

#### 3.2.2.1 Mineralogical characterization

The mineralogical composition of the soils samples was identified combining powder X-ray diffraction (XRD) and energy dispersive X-ray fluorescence (EDXRF). Powder X-ray diffraction was recorded on a Philips (PANalytical) diffractometer with Cu K $\alpha$  radiation (1.54

Å, 25 mA and 40 kV). The scan ranged from 3° to 80° 2θ with a step size of 0.05, with a scan rate of 1s/step. The diffractograms were compared to the database PDF-2 provided by the ICDD (International Center for Diffraction Data) and the software X'PertHigh Score. Selected samples were analyzed by Raman spectroscopy, in order to identify trace arsenic, iron and aluminum phases not found by the XRD. Raman spectra were obtained with a LabRam-HR 800 (Horiba/ JobinYvon) spectrograph equipped with a 633 nm He-Ne laser, 20 mV of power, attached to an Olympus BX-41 microscope provided with objectives lens of 10, 50 and 100X. To avoid sample degradation, the laser power was always kept below 0.12 mW at the sample with the help of filters. The sample was targeted by the laser beam through a high-aperture microscope objective (Olympus 100x, 0.9 NA), and the scattered light was collected through the same objective in a back-scattering configuration. The entrance slits to the spectrograph were 100 μm with a correspondent resolution of 2.0 cm<sup>-1</sup>. Holographic grating was of 600 g/mm. Frequency calibration was achieved using the 520 cm<sup>-1</sup> line of silicon. A small quantity of sample was placed on a glass slide on the microscope stage. After each spectrum had been recorded, a careful visual inspection was performed using white light illumination on the XY microscope stage to detect any change that could have been caused by the laser.

### 3.2.2.2 Specific surface area

The specific surface area (SSA) was determined by single- and multipoint Brunauer, Emmett and Teller (BET) surface area method (Quantachrome – NOVA 1200e), using nitrogen gas (N<sub>2</sub>) adsorption in relative pressures ( $P/P_0$ ) within a range of 0.05–0.3 and an automatic cell calibration with helium gas. The surface cleaning procedure was a vacuum degassing for 12 hours at 120°C. The surface area was calculated from the basic BET equation, Equation III. 1, (Lowell et al., 2004):

$$\frac{1}{W[P/P_0 - 1]} = \frac{1}{W_m C} + \frac{C-1}{W_m C} \left( \frac{P}{P_0} \right) \quad (1)$$

Where  $W_m$  is the weight of N<sub>2</sub> adsorbed in a monolayer,  $P$  stands for the pressure of adsorbate gas,  $P_0$  is the saturation pressure of adsorbate gas and  $C$  is the dimensionless constant.

### 3.2.3 Chemical composition by the Method 3051a (USEPA 2007)

The concentrations of trace and major elements of soil samples and BAC samples were determined following digestion with *Aqua regia* using a microwave-assisted (Ethos, Milestone, USA) digestion procedure (USEPA, 2007). An amount of  $200 \pm 0.1$  mg of ground  $< 44 \mu\text{m}$  samples (in triplicate), 3 mL of  $\text{HNO}_3$  (65%P.A., Química Moderna, São Paulo, Brazil) and 9 mL HCl (37%, ACS P.A., Química Moderna, São Paulo, Brazil) were weighed into Teflon digestion vessels (50 mL) and digested as described in Table III.1.

Table III.1: Microwave digestion conditions.

Step	Time (min)	Temperature (°C)	Power (W)
Ramp	5.5	RT <sup>1</sup> – 175	1500
Hold	4.5	175	1500
Cooling	30	175 – 80	-
Total run	40	-	-

Pressure:  $9.2 \times 10^5 \text{ N/m}^2$  - 1. RT: room temperature

On the following day and after reaching room temperature ( $\sim 25^\circ\text{C}$ ), in a fume hood, the extracted solutions were transferred to Falcon<sup>TM</sup> tubes and made up to 50 mL with deionized (Milli-Q Integral 5) water. The vessels were washed at least three times with deionized water to ensure the complete recovery of the extracted solution. The resultant solutions were stored at  $4^\circ\text{C}$  until further analysis. Arsenic, Al, Cd, Co, Cr, Cu, Fe, Ni, Pb and Zn were analyzed by a Perkin Elmer (Norwalk, Connecticut, USA model Optima 7300DV) inductively coupled plasma optical emission spectrometry (ICP-OES), according to the conditions indicated in Table III.2.

Detection and quantification limits (DL and QL) were evaluated by blanks measures ( $n = 10$ ) and using the International Union of Pure and Applied Chemistry (IUPAC) recommendations, Equation III. 2.

$$X_L = \bar{X}_{bi} + k S_i \quad (2)$$

Where  $X_L$  is the calculated limit,  $X_{bi}$  is the mean of the blank measures,  $S_i$  is the standard deviation of the blank measures, and  $k$  is a numerical factor chosen according to the confidence level desired, three for detection limit and ten for quantification limit (IUPAC, 2014). As quality assurance and quality control, two standard reference materials (SRM NIST 2710a and CANMET Till- 3) were analyzed for each batch of 10 samples at the microwave oven. Internal standard (Lu, 1 mg L<sup>-1</sup>) and analytical blanks were analyzed as well. The certified material used for quality control was selected based on the As level and matrix similarities with the samples, the data are presented in Table A.I.1.

Table III.2: Instrumental conditions (ICP-OES)

<i>Parameter</i>	<i>Condition</i>
Radiofrequency (W)	1300
Internal Standard	Lu 1 mg L <sup>-1</sup>
Nebulizer	Gemcone high flow at 0.60 L min <sup>-1</sup>
Alumina injector (mm)	2.0
Plasma flow (L min <sup>-1</sup> )	15
Auxiliary gas (L min <sup>-1</sup> )	0.2
Sample flux (mL min <sup>-1</sup> )	1.30
Wash between samples (s)	30
$\lambda$ (nm)	As 193.696r, Al, 396.153r; Cd, 214.440r; Co, 228.616a; Cr, 267.717a; Cu, 327.393a; Fe, 259.959r; Ni, 231.604a; Pb 220.353r; Zn, 213.859r

### 3.2.4 Energy Dispersive X-ray Fluorescence (EDXRF)

Energy Dispersive X-ray Fluorescence was carried out in a Shimadzu EDX-7000 energy-dispersive X-ray fluorescence spectrometer. The soil samples were placed in XRF sample cups of polyethylene (24.5 mm of aperture and 10 mL of capacity) (SPEX SamplePrep, Metuchen, NJ, USA) with a polypropylene thin-film (5  $\mu$ m) (SPEX SamplePrep, Metuchen, NJ, USA) sample support. The cell was inverted and a sample was introduced through the top open end and presented for analysis of the major elements. The current was set at 100  $\mu$ A for all the elements and two voltage values were used: 50 kV for Ti and Fe and 15 kV for the others. The following measurement times were applied: 300 seconds for the Na and Mg and 100 seconds for the other elements. The filters were applied as follow: filter #2

(K, Ca and Ti); and filter #3 (Fe). The other elements were quantified without using any filter. All experiments were performed in helium atmosphere and at room temperature (~25°C). The standard reference material NIST SRM 2710a was analyzed among with the samples as quality control.

### 3.2.5 Total sulfur (S-total) and total carbon (C-total)

Subsamples of  $0.15 \pm 0.01$ g of the pulverized material were mixed with  $0.30 \pm 0.01$ g of COM-CAT™ and analyzed in duplicate for total sulfur (S-total) and total carbon (C-total) using a LECO SC632 furnace instrument. Six reference materials (LECO – ore standards (502-320 411B, 502-318/1009, 502-319/ 1014), CANMET- RTS-3a, kzk-1 and MP-1b) were analyzed as quality assurance and quality control and the recoveries ranged from 98 to 109% for further data see [Table A.1.2](#).

### 3.2.6 Oral bioaccessibility

Bioaccessibility tests were performed according to the USEPA protocol ([USEPA, 2012](#)), which consists of a simple extraction with a glycine solution in an acid environment to simulate the gastric phase. Prior to the analysis, the <2 mm soil samples were sieved to <250 µm. This fraction is recommended for the bioaccessibility test, as the upper bound of particle size that likely adheres to the adult/children's hands and can be incidentally ingested.

In summary, a  $0.4 \text{ mol L}^{-1}$  glycine (99%, Sigma-Aldrich, Missouri, USA) solution was prepared and acidified with HCl (37%, Química Moderna, São Paulo, Brazil) to reach  $\text{pH } 1.50 \pm 0.05$  simulating a gastric intestinal solution ("stomach phase") and heated to 37°C. A 30 mL aliquot of this solution was added to an amount of 0.3 g of soil sample placed in a 120 mL high-density polypropylene (HDPE) vials (Fisherbrand, USA) and left under constant horizontal agitation ( $200 \pm 2 \text{ rpm}$ ) at  $37 \pm 2 \text{ °C}$  (Innova 44 incubator, New Brunswick scientific) for one hour. At the end of 1 h, the HDPE vials were removed from the incubator and the pH of the suspension measured. After confirming that both the pH ( $1.5 \pm 0.5$ ) and the time criteria (total elapsed time less than 1 hour and 30 minutes) where met, the extract was centrifuged (Rotofix 32A, Hettich, Germany) at 3,000 rpm for 10 min. Aliquots of supernatant fluid (20 mL) were then filtered (using a 25 mL syringe) on a  $0.45 \text{ µm}$  cellulose acetate membrane with Swinnex™ holder filter (25 mm diameter). The extraction phases were stored at  $4 \pm 2 \text{ °C}$  for one week until analysis by hydride

generation inductively coupled plasma optical emission spectroscopy (HG-ICP-OES, Optima 7300DV, Perkin-Elmer, USA). Pre-reductant solution (1 mL 5% w v<sup>-1</sup> KI / 5% w v<sup>-1</sup> ascorbic acid and 2 mL 50% v v<sup>-1</sup> HCl) was added to the samples, and made up to 10mL with deionized water. After 45 minutes of reaction time (~25 °C), the samples were analyzed. In a flow-injection mode, reductant (0.65% w v<sup>-1</sup> NaBH<sub>4</sub>- 0.2 mol L<sup>-1</sup> NaOH) and extracts were mixed in a sample valve. Arsine and hydrogen gases (H<sub>2</sub>) were separated with a gas/liquid separator and the As compound was carried away by high-purity argon gas to the spectrometer. The calibration curve ranged from 2.5 to 50 µg L<sup>-1</sup>; blank and a synthetic sample of 10 µg L<sup>-1</sup> As were analysed every ten samples for quality control. The recovery of the synthetic samples (n=20) lied within 95 ± 11%. Table III.3 shows more detailed information for hydride generator components and the instrumental conditions selected for the analysis. A batch of extraction was composed by samples performed in triplicate, a blank consisting of a glycine solution at pH 1.5 and a reference material of soil (NIST 2710a).

Table III.3: Instrumental conditions (HG-ICP-OES)

<i>Parameter</i>	<i>Condition</i>
Radiofrequency (W)	1450
Nebulizer	Gemcone high flow at 0.80 L min <sup>-1</sup>
Alumina injector (mm)	2.0
Plasma flow (L min <sup>-1</sup> )	17
Auxiliary gas (L min <sup>-1</sup> )	0.3
Pump flow (mL min <sup>-1</sup> )	1.00
Wash between samples (s)	30
Reductant (NaBH <sub>4</sub> /NaOH)	0.65% (w v <sup>-1</sup> )-0.2 mol L <sup>-1</sup>
Reaction time (min)	45 at room temperature
λ (nm)	As 193.7 radial
DL (µg kg <sup>-1</sup> , n=7)	1.5
QL (µg kg <sup>-1</sup> , n=7)	5.6

### 3.2.7 Electron microscopy analyses

Six samples representing different soil classes were selected for arsenic-bearing phases characterization and quantitative mineralogy based on single particle using a FEI Quanta



650 field emission gun scanning electron microscope (FEG-SEM) equipped with two Bruker Quantax X-Flash 5010 EDS detectors and FEI's MLA suite 3.1.1.283 for data acquisition and process. In this study, the grain-based X-ray mapping (GXMAP) measurement mode was applied for identification of materials. Prior to the analyses the selected samples (< 2 mm and > 2 mm) were ground in an agate mortar with pestle and sieved through a 250 µm screen to create a uniform particle size material. Two of these samples, identified as K03 and K06, were already below 250 µm. The polished sections were prepared in a 25 x 25 mm polypropylene mounting cup by mixing the epoxy resin, the catalyzer and material particles in relative weight proportions of 7:1.75:1.5. The mounting set was then submitted to vacuum in a vacuum chamber to remove any air bubble formed during the mixing step. After assembling and hardening, the mountings were roughed and polished using a grinder/polisher (MiniMet 1000, Buehler, USA) system. The roughing stage was carried out with sandpaper in a size sequence of 240, 320, 400 and 600 µm, at 25 rpm for 6 minutes. This was followed by a six-step diamond paste sequence (15, 9, 6, 3, 1 and 0.25 µm). Finally, a thin carbon film was deposited on the sections to create a conducting layer necessary to the SEM analyses.

For the TEM analyses, each powder sample was dispersed in Milli-Q water in Eppendorf tubes and sonicated in ultrasound bath for three minutes. A drop of each suspension was placed on carbon coated Cu-TEM grids (300 mesh) and left drying in a desiccator for at least 1 day prior TEM analysis. The analyses were performed using High Resolution Transmission Electron Microscopy (HRTEM), Scanning TEM (STEM), Energy Dispersive X-Ray Spectroscopy (EDS) and Electron Energy-Loss Spectroscopy (EELS) using a FEI TEM-LaB6 Tecnai G2-20 (200 kV) and a FEI F20 FEG-STEM (200kV). The achieved energy resolution of in EELS was 1.5eV and energy dispersion of 0.25 eV/pixel. The electron microscopy analyses were performed in the Center of Microscopy at the Universidade Federal de Minas Gerais (UFMG), Belo Horizonte, Brazil, and at the Center for Microscopy and Microanalysis of the University of Queensland, Australia.

### 3.3 Results and discussion

#### 3.3.1 Soil characterization

##### 3.3.1.1 X-ray diffraction (XRD)

The predominant mineral phases identified by XRD in the soil fraction (<2 mm) were quartz ( $\text{SiO}_2$ ), muscovite  $(\text{K,Na})(\text{Al,Mg,Fe})_2(\text{Si}_{3.1}\text{Al}_{0.9})\text{O}_{10}(\text{OH})_2$ , feldspar  $(\text{Na,Ca})\text{Al}(\text{Si,Al})_3\text{O}_8$ , pyroxene  $(\text{Mg}_{0.944}\text{Fe}_{0.056})(\text{Ca}_{0.844}\text{Na}_{0.156}\text{Fe}_{0.014})(\text{Si}_2\text{O}_6)$  and kaolinite  $(\text{Al}_2\text{Si}_2\text{O}_5(\text{OH})_4)$  (diffractograms see Appendix A.II). Quartz and muscovite appear as the main soil constituents in all the samples. Hematite ( $\text{Fe}_2\text{O}_3$ ) and goethite ( $\text{FeOOH}$ ) were identified by XRD in two samples (K22 and K23). The detection limit of this technique is approximately 1% (Norton and Suryanarayana, 1998). Gibbsite ( $\text{Al}(\text{OH})_3$ ) was detected in two samples (K40 and K43). No arsenic minerals, such as scorodite ( $\text{FeAsO}_4 \cdot 2\text{H}_2\text{O}$ ), realgar ( $\text{AsS}$ ) and arsenopyrite ( $\text{FeAsS}$ ), were detected. These findings are in agreement with other mineralogical data from Paracatu region (Andrade et al., 2012; Mello et al., 2006).

##### 3.3.1.2 Specific surface area (SSA)

Table III. 4 shows the specific surface areas (SSA - SBET) of the undersize soil fraction (< 2 mm) by BET-methods. The results obtained by the multi and single-point methods showed a very small difference and so a good linearity. The global relative error ranged from 0.05 to 3%. The SSA values ranged from 3.28 (K21) to 26.15 (K43)  $\text{m}^2 \text{g}^{-1}$ . The highest value for the K43 sample may be related to its high Al content (Tab. III.6). A good correlation (86%) was observed between SSA and %Al by chemical analyses (Figure 3. 2). The increase of Al content in the Fe-(hydr)oxides has been related to an increase in SSA (Silva et al., 2010).

Table III.4. Specific surface area (SSA) BET for N<sub>2</sub> adsorption using degasification temperature of 120°C for 12 hours (n=1, < 2 mm)

Sample (<2mm)	Specific surface area (m <sup>2</sup> g <sup>-1</sup> )		Constant C (BET)	Relative error (%)
	Multi Point BET	Single point BET		
K03	15.60	15.21	137	2%
K06	26.07	25.51	163	1%
K09	10.23	9.97	120	2%
K21	3.28	3.20	128	2%
K22	17.26	16.91	247	1%
K23	12.81	12.60	4682	0.05%
K36	11.76	11.47	171	1%
K37	5.60	5.44	121	2%
K40	12.55	12.16	96	2%
K43	26.15	25.46	108	2%
K44	9.71	9.42	88	3%
K47	4.47	4.37	191	1%
K48	8.40	8.18	129	2%
K49	8.88	8.66	132	2%
<i>Range</i>	3.28 – 26.15	3.20 – 25.51	88 - 4682	0.05 - 3
<i>Global average</i>	12.34	12.04		2

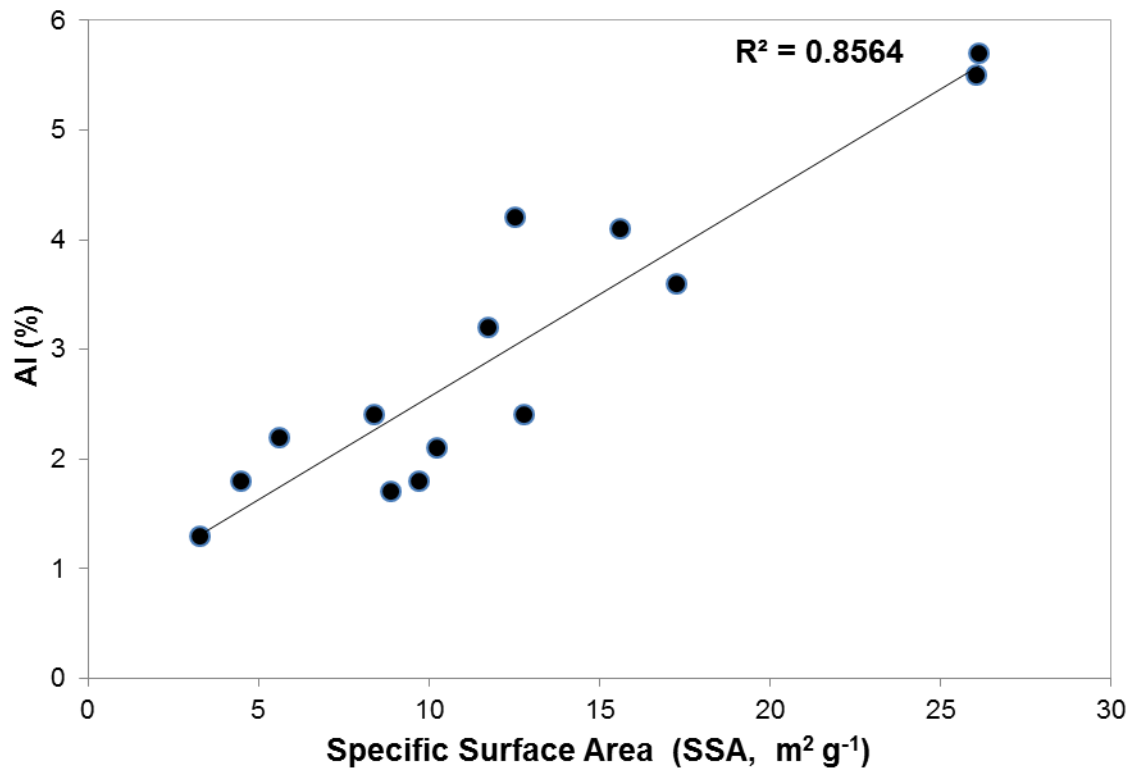


Figure 3.2. Correlation between aluminum soluble content and specific surface area.

### 3.3.1.3 EDXRF analyses

Table III.5 shows the mean, minimum and maximum concentration of the major elements by EDXRF in three size fractions ( $> 2$  mm,  $< 2$  mm and  $< 250$   $\mu\text{m}$ ) of the soil samples, (see complete data Appendix III). The major elements in all the size fractions were  $\text{SiO}_2$ ,  $\text{Al}_2\text{O}_3$ , and  $\text{Fe}_2\text{O}_3$ . The results of NIST SRM 2710a (Tab.III.5) showed recoveries ranging from 73% ( $\text{K}_2\text{O}$ ) to 142% ( $\text{CaO}$ ), which is acceptable for a semi-quantitative technique.

The high  $\text{SiO}_2$  content is in agreement with the predominance of silicates (quartz, muscovite, kaolinite, feldspar and pyroxene) identified by XRD (Appendix II). The  $\text{SiO}_2$  content ranged from 33.7% (K23) to 68.3% (K36) for the oversize fraction ( $> 2$ mm) and from 45.9% (K23) to 65.5% (K09) for the fraction  $< 2$  mm. The fraction below 250  $\mu\text{m}$  showed  $\text{SiO}_2$  ranging from 46.8% (K23) to 69.9% (K09), in similar values of the fraction  $< 2$  mm.

The  $\text{Al}_2\text{O}_3$  (present in the aluminosilicates and in gibbsite) was the second main constituent in the fine fractions ( $< 2$  mm and  $< 250$   $\mu\text{m}$ ) and the third main element constituent in the coarse fraction ( $> 2$  mm), followed by  $\text{SiO}_2$  and  $\text{Fe}_2\text{O}_3$ . The  $\text{Al}_2\text{O}_3$  content ranged from 11.1% (K23) to 22.1% (K47) in the oversize ( $> 2$  mm) fraction and from 12.6% (K23) to 30.6% (K43) in the fraction  $< 2$  mm. The similarity between the fractions  $< 2$  mm and  $< 250$   $\mu\text{m}$  was also observed for aluminum.

The  $\text{Fe}_2\text{O}_3$  was the only element whose concentration increases significantly with the particle size (Tab. III.5), with the highest values being detected in the oversize ( $> 2$  mm) fraction - 9.9% (K21) to 46.2% (K22) - and the lowest values in the  $< 250$   $\mu\text{m}$  fraction - 3.5% (K47) to 31.1% (K23).

### 3.3.1.4 Raman analyses

The Raman is a nondestructive, very specific, and structure-sensitive technique commonly used for the identification of chemical compounds and mineral phases in ores, environmental samples, and construction materials (Das & Hendry, 2011; Müller et al., 2010; Faria et al., 1997).

Table III.5. Mean, minimum and maximum of major elements expressed as oxides by EDXRF (%) in different size fractions of the select soil samples and quality control figures

	Na <sub>2</sub> O	MgO	Al <sub>2</sub> O <sub>3</sub>	SiO <sub>2</sub>	K <sub>2</sub> O	CaO	TiO <sub>2</sub>	Fe <sub>2</sub> O <sub>3</sub>
	%							
<b>&gt; 2 mm</b>								
Mean	0.2	0.5	15.8	52.0	3.5	0.1	0.6	26.5
Min.	0.0	0.3	11.1	33.7	1.4	0.1	0.4	9.9
Max.	0.7	0.8	22.1	68.3	6.4	0.2	0.9	46.2
<b>&lt; 2 mm</b>								
Mean	0.2	0.6	23.0	56.2	5.0	0.2	1.8	12.8
Min.	0.0	0.4	12.6	45.9	2.3	0.1	1.3	4.5
Max.	0.6	0.8	30.6	65.5	8.5	0.5	3.7	36.0
<b>&lt; 250 μm</b>								
Mean	0.2	0.6	23.2	58.2	5.1	0.2	2.5	9.8
Min.	0.0	0.4	12.2	46.8	2.0	0.1	1.5	3.5
Max.	0.7	0.8	31.0	69.9	8.7	0.6	6.6	31.1
SRM NIST 2710a								
Measured	1.0	1.0	14.4	68.7	3.8	1.9	0.7	8.1
Certified value	1.2	1.2	11.2	66.5	5.2	1.4	0.5	6.2
Recovery (%)	83	85	128	103	73	142	140	131

Figure 3.3 shows Raman spectra of the soil samples and synthesized goethite and hematite (Müller et al., 2010). Quartz, mica, amorphous carbon, rutile, ilmenite, goethite and hematite were identified (some of them not shown). The Fe-(hydr)oxides, usual As-bearing phases, were the focus of the analyses. Despite small differences in peaks positions ( $\pm 5 \text{ cm}^{-1}$ ), hematite ( $\text{Fe}_2\text{O}_3$ ) and goethite ( $\text{FeOOH}$ ) were identified in the samples with a good agreement with reported literature spectra. Hematite spectrum usually presents nine peaks (225, 247, 293, 299, 412, 498, 613, 660 and  $1,319 \text{ cm}^{-1}$ ) and goethite spectrum as well (96, 243, 299, 385, 479, 550, 685 and  $993 \text{ cm}^{-1}$ ). The intensity of the peaks and their position may be influenced by temperature, sample crystallinity, and atoms substitution (Liu et al., 2013; Faria et al., 1997).

The goethite and hematite spectra (Fig. 3.3) exhibit broad bands and shifted peak position compared to synthesized goethite and hematite spectra. It suggests the presence of contaminants/substitution atoms (Liu et al., 2013) or a low crystallinity of the goethite phase (Das & Hendry, 2011). Liu and co-workers (2013) noticed that the band features of goethite shifted to high wavenumbers after Fe substitution for Al in the mineral structure. Aluminum was identified in goethite particles by SEM/EDS analyses in this work, as shown

further in this document. The Fe substitution for Al may affect physicochemical properties such as density, adsorption capacity, and XRD pattern. The Al substitution for Fe was shown to improve the adsorption of Co, Zn, Ca, and As on goethite and to decrease their mobilization in the environment (Liu et al., 2013; Das & Hendry, 2011). The overlap of the hematite and goethite peaks is also showed in Fig. 3.3 and suggests the phase transformation of goethite to hematite. This transformation involves the loss of water (dehydroxylation) followed by a rearrangement in goethite's structure (Gialanella et al., 2010). Comparison hematite and synthesized spectra shows an increasing in the band intensity around  $660\text{ cm}^{-1}$ . It can be attributed to Fe substitution on the structure for other elements (Massey et al., 1990).

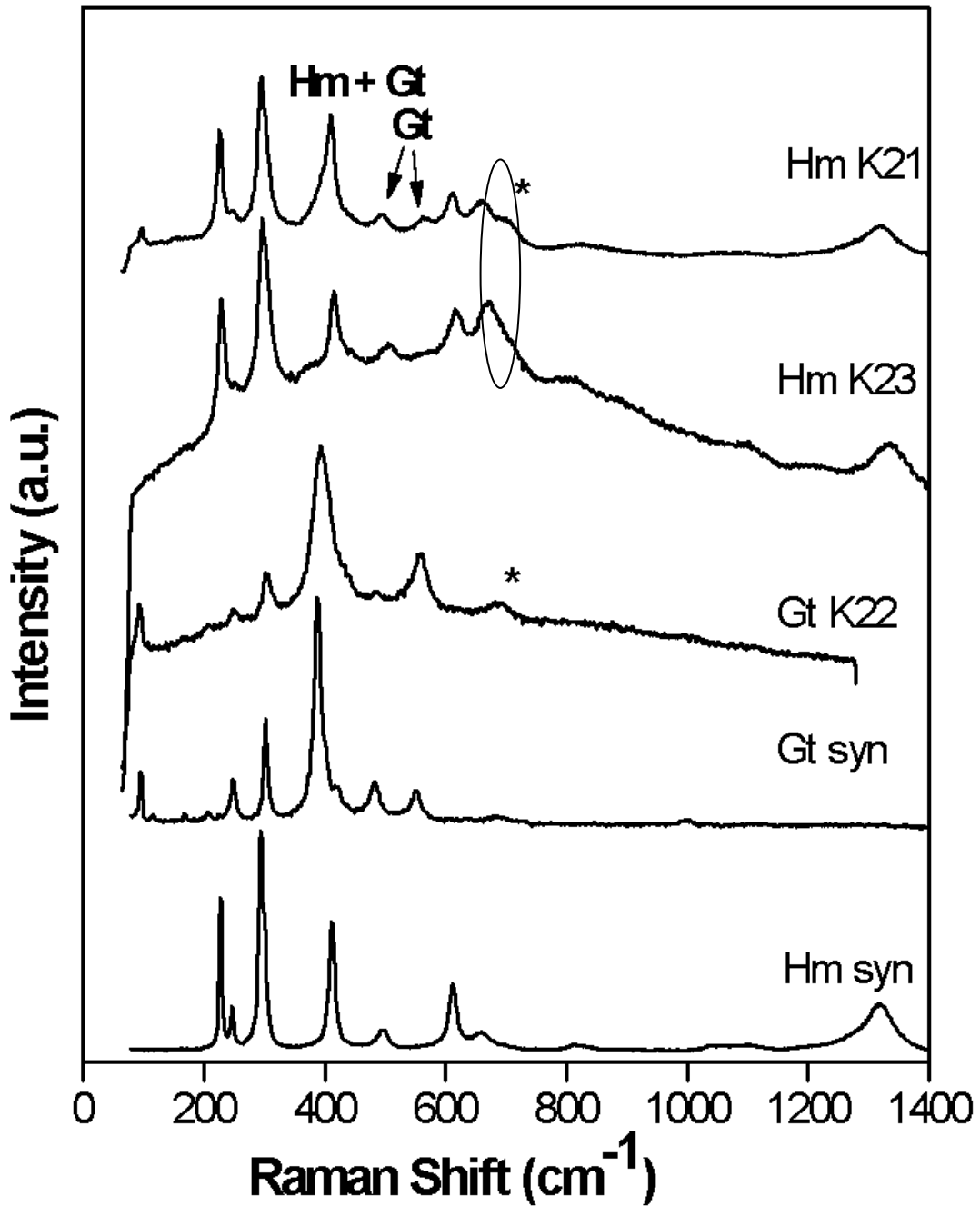


Figure 3.3. Raman spectra for Fe-(hydr)oxides in soil samples and reference Raman spectra for synthesized (syn) goethite and hematite. Gt - Band attributed to presence of goethite; Hm – bands attributed of hematite; \*Indication of goethite to hematite transformation.



### 3.3.2 Chemical analyses

Table III.6 shows the chemical concentrations of Al, Fe, As, Cd, Co, Cu, Ni, Pb and Zn by ICP-OES from *Aqua regia* digestion (USEPA, 2007) for the soil fraction below 2 mm. Appendix IV presents the concentrations of these elements for the other soil fractions (> 2 mm and < 250  $\mu\text{m}$ ). The method is applied to elemental quantification in environmental samples, where partial digestion allows the dissolution of the main elements (base metal, As, Sb, e others), and some compounds (e.g. quartz, silicates, titanium dioxide) are kept insoluble. The results show good recoveries for the SRM 2710a analytes ranging from 82 to 114%, except for Al. The low Al recovery (26%) may be related to the partial digestion of silicates minerals and is similar that value presented in data sheet for SRM2710a (17%). Among major constituents of the extracted phase, Al concentration ranges from 1.3% (K21) to 5.7% (K43) and the Fe concentration from 1.8% (K47) to 20.6% (K23). The S and C vary from < 0.01 to 0.029%, and from 0.38 to 6.14%, respectively. This low bulk sulfur concentration agrees with the lack of sulfide phases identified by Raman and XRD. The C content may be ascribed to organic matter since no carbon phase was observed by XRD and only amorphous carbon was identified by Raman (not shown). These results are in agreement with the one reported by the Center for Innovation and Technology (SENAI/FIEMG, 2014). Arsenic concentrations varied from 112 (K36) to 6,354 (K23)  $\text{mg kg}^{-1}$ , median of 748  $\text{mg kg}^{-1}$ . Sample K23 presented the highest As concentration and was classified as an outlier according the Grubbs' Test (G-test), (ISO 5725, 1994), as it lies in an abnormal distance (> 25%) of the mean. Sample K36 is also classified as an outlier by G-test but presented the lowest As concentration (112  $\text{mg kg}^{-1}$ ). The median values have been used to represent the central tendency of data since it is less affected by the outliers than the mean. The other analytes (Cd, Co, Cr, Cu, Ni, Pb and Zn) showed relatively low concentrations.

The high As concentrations (Tab. III.6) are not unusual for soil samples collected in mining regions in Minas Gerais (Ono et al., 2012 - 35 to 426  $\text{mg kg}^{-1}$ ; Mello et al., 2006 - 30 to 910  $\text{mg kg}^{-1}$ ) and in other parts of the world, such as Australia (Juhász et al., 2015 -81 to 2,270  $\text{mg kg}^{-1}$ ), England (Palumbo-Roe et al., 2015 - 3.8 to 848  $\text{mg kg}^{-1}$ ), United States (Gonzales et al., 2014 - 10 to 3,500  $\text{mg kg}^{-1}$ ) and China (Kim et al., 2014 - 3.6 to 700  $\text{mg kg}^{-1}$ ; Yin et al., 2016 - 75.2–1,470  $\text{mg kg}^{-1}$ ). WHO (2000) reports As concentration for non-mineralized soils in a range of 0.2 to 40  $\text{mg kg}^{-1}$ . There are no federal regulations limiting soil As levels in the USA. However, the US Environmental Protection Agencies (EPA)

superfund risk model gives a value of  $0.43 \text{ mg kg}^{-1}$  total soil As for a cancer risk of 1 in  $10^6$  for exposure by soil ingestion (WHO, 2000).

Table III.6 also shows the National criteria and guideline values (known as CONAMA 420/2009) for soil quality relative to the presence of chemical substances, and the guidelines for environmental management of contaminated areas, as result of anthropogenic activities (Anonymous, 2009). It can be observed that arsenic concentrations are significantly greater than the investigation values (IV) established by CONAMA 420/2009 for agriculture ( $35 \text{ mg kg}^{-1}$ ), residential ( $55 \text{ mg kg}^{-1}$ ) and industrial ( $150 \text{ mg kg}^{-1}$ ) areas.

Table III.6. Chemical concentrations by ICP-OES (n = 3, &lt; 2 mm) and by LECO (S and C, n = 2, &lt; 2 mm) (Mean±SD)

Samples (< 2 mm)	Al	Fe	S	C	As	Cd	Co	Cr	Cu	Ni	Pb	Zn	
	(%)				(mg kg <sup>-1</sup> )								
K03	4.1±0.4	5.3±0.2	0.024±0.001	2.91±0.04	411±62	1.1 ±0.2	12 ±2	64 ±6	38 ±4	19.7 ±4.7	36 ±2	52 ±6	
K06	5.5±0.9	6.3±0.1	0.020±0.002	1.95±0.01	392±45	1.5 ±0.2	14±3	62 ±5	50 ±3	26.5 ±3.8	38 ±1	74 ±3	
K09	2.1±0.3	4.5±0.2	<0.01	1.63±0.03	250±8	1.1 ±0.1	20±5	89 ±3	33 ±4	18.0 ±3.4	26 ±12	77 ±8	
K21	1.3±0.9	3.2±0.2	0.01±0.03	0.83±0.01	1560±204	0.6 ±0.3	5 ±1	105 ±14	38 ±3	5.2 ±0.3	159 ±8	16 ±2	
K22	3.6±0.6	14.4±0.1	0.0175±0.0002	2.58±0.04	1738±102	3.6 ±0.4	15 ±3	104 ±22	41 ±3	26.6 ±3.5	50 ±4	78±6	
K23	2.4±0.2	20.6±1.2	0.019±0.003	0.38±0.04	6354±468	5.2 ±0.3	10 ±3	198 ±27	65 ±7	15.2 ±3.4	95±12	57 ±8	
K36	3.2±0.1	7.6±0.7	<0.01	1.95±0.01	112 ±15	1.9 ±0.3	49 ±4	129 ±17	67 ±2	21.4 ±2.4	150 ±4	65±2	
K37	2.2±0.7	3.0±0.3	<0.01	1.02±0.02	930 ±109	0.4 ±0.2	5 ±2	82 ±8	29 ±5	12.0±4.3	108±9	30 ±5	
K40	4.2±0.3	2.8±0.2	0.0288±0.0004	6.14±0.01	690 ±30	0.5 ±0.3	4 ±1	188 ±8	16 ±2	9.6 ±0.5	37 ±2	26 ±1	
K43	5.7±0.6	6.5±0.4	0.010±0.005	3.46±0.02	262 ±25	1.3 ±0.1	7±2	60 ±6	31 ±2	10.0 ±2.5	33 ±3	86 ±13	
K44	1.8±0.4	5.8±0.3	<0.01	2.43±0.02	614 ±42	1.1 ±0.3	16 ±4	43 ±10	34 ±2	13.5 ±3.4	45 ±3	70 ±11	
K47	1.8±0.8	1.8±0.1	0.012±0.002	0.74±0.03	916 ±200	0.3 ±0.2	7 ±1	68 ±17	41 ±9	4.5 ±0.4	65 ±13	11±5	
K48	2.4±0.2	5.8±0.3	0.014±0.003	1.85±0.03	1355 ±161	1.3 ±0.5	5 ±2	91 ±7	52 ±1	7.8 ±0.4	28 ±4	36±1	
K49	1.7±0.3	5.2±0.2	<0.01	2.05±0.02	806 ±115	2.0 ±1.6	11 ±2	63 ±10	44.7 ±5.1	9.9 ±0.1	16±2	76 ±15	
Min.	1.3	1.8	<0.01	0.38	112	0.3	4	43	16	16	16	11	
Max.	5.7	20.6	0.0288	6.14	6354	5.2	49	198	67	67	159	86	
Mean	3.0	6.6		2.1	1171	1.6	13	96	41	14	63	54	
Median	2.4	5.6		2.0	748	1.2	10	86	39	13	41	61	
<b>Prevention values by CONAMA 420/2009</b>													
	--	---	--	--	--	15	1.3	25	75	60	30	72	300
<b>Investigation values by CONAMA 420/2009</b>													
Agricultural APMax <sup>1</sup>	--	---	--	--	--	35	3	35	150	200	70	180	450
Residential	--	---	--	--	--	55	8	65	300	400	100	300	1000
Industrial	--	---	--	--	--	150	20	90	400	600	130	900	2000

<sup>1</sup>maximum protection agricultural.

In general, the elements Co, Cu, Ni and Zn show concentrations below the prevention values established by CONAMA 420/2009 with exception of the sample K36 for Co and samples K23 and K36 for Cu. Prevention value (PV) is the maximum allowed concentration for a given substance in the soil without affecting its main functions (Anonymous, 2009). The elements Cd, Cr and Pb show concentrations below the investigation values for agricultural areas established by CONAMA 420/2009, with exception of samples K22 and K23 for Cd and samples K23 and K40 for Cr. Investigation values (IV) are the concentrations of a substance in soil or in groundwater water above which there are potential risks, direct or indirect, to human health, considering a standard exposure (Anonymous, 2009).

*Fluvisols* are mineral soils formed by overlapping layers of recent alluvial sediments without pedogenetic relationships, *i.e.* without involving a soil formation relation, between them due to their low pedogenetic development. Generally they have a much diversified thickness and granulometry, along the soil profile, due to the diversity and the forms of deposition of the originating material. Most of them have low potential for agricultural activity due to the need for acidity correction, drainage and fertilization. The *Leptosols*, on the other hand, consist of shallow soils, with a maximum depth of 50 cm, being usually associated with more sloping reliefs. Shallow depth is a limitation for root growth, the use of machines and increases the risk of erosion. The *Ferralsols* have a marked red color, due to the higher contents and the nature of the iron oxides present in the material and characteristics of uniform color, texture and structure in depth. This type of soil occurs predominantly in flat and smooth undulating areas favoring agricultural activity (FEAM, 2013).

### 3.3.3 Oral bioaccessibility test

The bioaccessible As concentrations (As BAC) for the soils samples and the NIST SRM 2710a are shown in Table III.7. In agreement with the presented by Koch et al. (2005), the control sample of NIST SRM 2710 soil showed a percent BAC of  $30 \pm 5\%$  BAC which was within the range of the control limits ( $28 \pm 17\%$ ). The bioaccessible As concentrations (As BAC) varied from 0.2 to 22.2 mg kg<sup>-1</sup> with a mean of 7.0 mg kg<sup>-1</sup> and a median value of 4.4 mg kg<sup>-1</sup>. The percent As BAC ranged from 0.3% to 5.0%, with a mean of 1.3% and a median of 0.7%. The sample with the lowest As BAC concentration (K36) has also the lowest As content whereas the sample with the lowest As BAC percent (K23) is an outlier, as discussed earlier (Tab. III.6). The relationship between the magnitude of bioaccessible

As concentration (BAC) in the different soil samples and percent As BAC is not straightforward, due to the differences in the total As concentration in the original sample. For example, the As concentration extracted in the gastric phase solution are similar for samples K21 and K40, whereas the percent As BAC is twice higher for the sample K40 (5.0%). The low As BAC (mean of 1.3%) found here is consistent with the conclusions of other studies (Ono et al., 2012 and Ng et al., 2014) (mean of 2.2% and 3.4%, respectively), all showing low % As BAC ( $\leq 5.0\%$ ). Arsenic concentrations in the soil samples are significantly higher than the investigation values (Tab.III.6) established by legislation. Nevertheless, the As BAC lies within the guidelines, regardless the different sources and the different bioaccessible test conditions (*i.e.*, the biochemical extraction, pH, particle size) used in this and other works (Ng. et al., 2014; Ono et al., 2012). The low As BAC values are consistent with the association of arsenic with the Fe-(hydr)oxides described in the following paragraphs.

Table III.7. Bioaccessible arsenic in the  $< 250 \mu\text{m}$  fraction of the soil samples and in the certified material (Mean $\pm$ SD, n=3)

Samples ( $<250 \mu\text{m}$ )	As ( $\text{mg kg}^{-1}$ )	BAC ( $\text{mg kg}^{-1}$ )	% BAC
K03	464 $\pm$ 64	1.9 $\pm$ 0.1	0.41 $\pm$ 0.03
K06	405 $\pm$ 3	1.21 $\pm$ 0.01	0.30 $\pm$ 0.00
K09	325 $\pm$ 5	1.8 $\pm$ 0.1	0.57 $\pm$ 0.03
K21	841 $\pm$ 28	19.47 $\pm$ 0.03	2.31 $\pm$ 0.00
K22	575 $\pm$ 83	1.9 $\pm$ 0.4	0.33 $\pm$ 0.10
K23	4304 $\pm$ 286	17 $\pm$ 1	0.39 $\pm$ 0.03
K36	40 $\pm$ 6	0.218 $\pm$ 0.003	0.55 $\pm$ 0.01
K37	494 $\pm$ 6	8 $\pm$ 1	1.67 $\pm$ 0.10
K40	443 $\pm$ 14	22 $\pm$ 4	5.01 $\pm$ 1.00
K43	211 $\pm$ 39	0.86 $\pm$ 0.04	0.41 $\pm$ 0.02
K44	459 $\pm$ 15	4 $\pm$ 1	0.94 $\pm$ 0.20
K47	379 $\pm$ 33	9 $\pm$ 3	2.45 $\pm$ 0.80
K48	324 $\pm$ 29	4.6 $\pm$ 0.1	1.42 $\pm$ 0.05
K49	332 $\pm$ 36	5 $\pm$ 1	1.62 $\pm$ 0.40
Mean	685	7.0	1.3
Median	424	4.4	0.7
Min. <sup>1</sup>	40	0.2	0.3
Max. <sup>2</sup>	4304	22.2	5.0
SRM NIST 2710a			
Certified values	1540	-	28 $\pm$ 17
Measured (n=4)	1461 $\pm$ 41	440 $\pm$ 74	30 $\pm$ 5

<sup>1</sup>Min.: minimum <sup>2</sup> Max.: maximum. Samples K23 and K36 are classified as outlier by G-test.

### 3.3.4 Arsenic-bearing phases

Figure 3.4 shows a typical backscattered electron image of the soil samples and the chemical composition provided by EDS. One can notice the intergrowth of small phyllosilicate lamellae with Fe-(hydr)oxides, which appears as the main As reservoir in the soil samples. No As mineral phase was identified by XRD, Raman or semi-quantitative electron microscopy. The low As BAC (Tab. III.7) shown by the soil samples is consistent with the observed association of Fe-(hydr)oxides and the silicate minerals, as both phases are not soluble under the BAC extraction conditions and stable under a wide range of environmental conditions.

Figure 3.5 shows TEM micrograph of As-bearing Fe-(hydr)oxides phases. A nanometer resolution for chemical composition and the spatial distribution of Al, Fe, O and As are provided by STEM-EDS. The EDS maps of Fe-(hydr)oxide aggregate show that Al, O, Fe and As are homogeneously dispersed within the structure of the Fe-(hydr)oxides, Figure 3.5c. The distribution of As suggested that the metalloid is incorporated in the oriented aggregate of Fe-(hydr)oxides, in a microscopic pattern also observed by Freitas and co-workers (2015) in a previous work of our group.

The aggregate shown in Fig. 3.5 was further identified as goethite (Fig. 3.5) by selected area electron diffraction (SAD) and HRTEM analyses. The interplanar distances ( $d$ ) were measured from both SAD pattern (inset of Fig. 3.5a) and the Fast Fourier Transform (FFT) of the HRTEM image (inset of Fig. 3.5b). Other aggregates (not shown here) were identified as hematite.

The identification of As in association with oriented aggregates of crystalline nanoparticles of Fe-(hydr)oxides supports the low As BAC reported here. Furthermore, the intergrowth of the Fe-(hydr)oxides with the phyllosilicates adds additional constrain to arsenic release as these mineral phases are not soluble under the extraction (BAC) conditions.

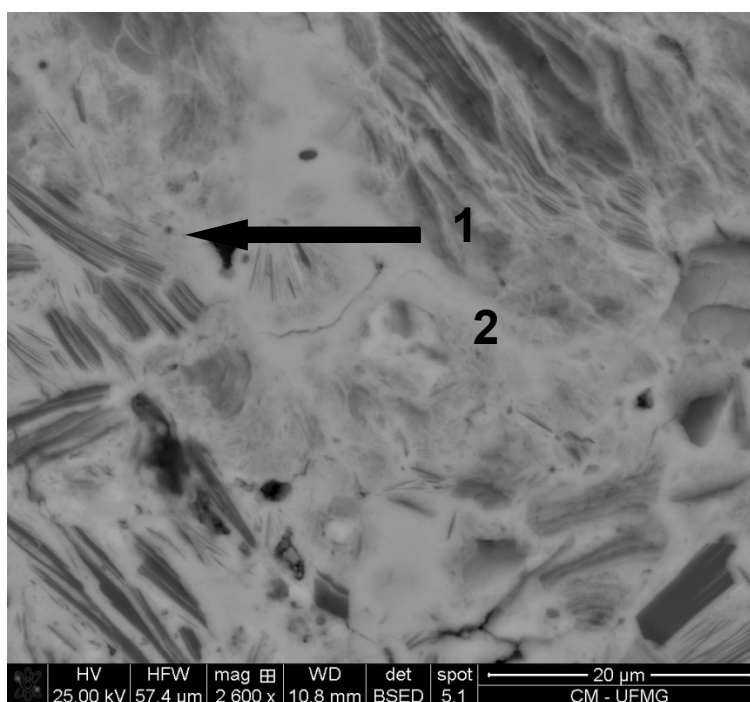


Figure 3.4. SEM micrograph of sample K23 (> 2 mm) showing muscovite lamellae (1) within goethite (2) matrix (1.7% As)

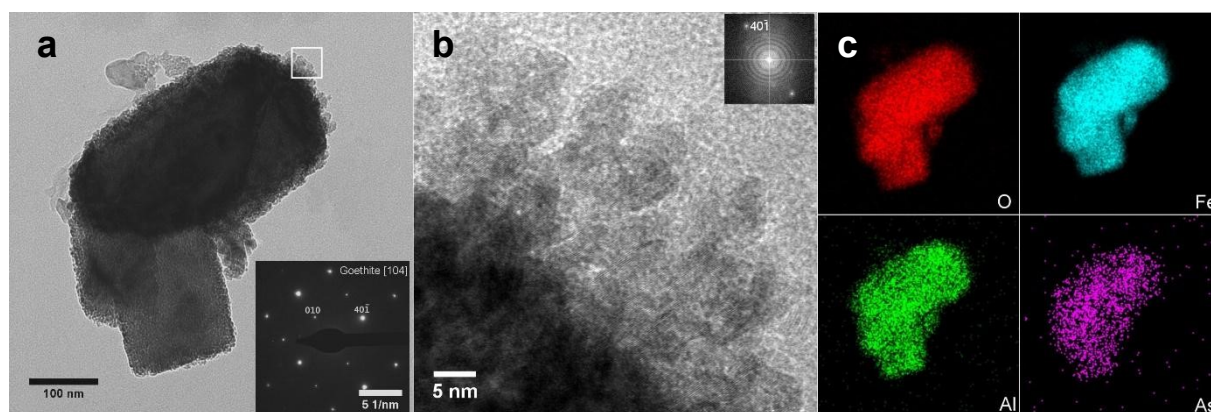


Figure 3.5. (a) Bright Field TEM image of sample K21 (< 2 mm) showing nanoparticle aggregates of goethite and its correspondent SAD pattern (inset); (b) HRTEM image of the area inside the white square in (a) and its correspondent Fast Fourier Transform (FFT); (c) EDS maps of oxygen, iron, aluminum and arsenic

### 3.4 Conclusions

Soil samples with high levels of arsenic (As) (up to approx. 6354 mg kg<sup>-1</sup>) were investigated. The samples constituents are mainly silicates (quartz and muscovite) according to XRD and EDXRF analyses. The increase in specific surface areas showed a good correlation with the aluminum soluble in *Aqua regia*. Hematite and goethite are the Fe-(hydr)oxides identified by XRD and Raman analyses. The Raman spectra of these minerals presented features suggesting the presence of contaminant/substitution species or a less crystalline phase. The phase transformation of goethite to hematite is also indicated. Among the minor constituents of environmental concern, only As showed concentrations significantly higher (median of 748.0 mg kg<sup>-1</sup>) than the guideline values established by the local legislation for As concentration in soils for agriculture (35 mg kg<sup>-1</sup>), residential (55 mg kg<sup>-1</sup>), and industrial use (150 mg kg<sup>-1</sup>). The non-conformities values for Cd, Co, Cr and Cu were observed degree and in few samples. The mean bioaccessible As was 7.0 mg kg<sup>-1</sup>, with a median value of 4.4 mg kg<sup>-1</sup>; % As BAC showed a mean value of 1.3% and a median of 0.7%. Arsenic was shown to be trapped in oriented aggregates of crystalline Fe-(hydr)oxides nanoparticles, in a pattern that supports the large difference between As concentration and the bioaccessible arsenic as shown by HRTEM/EDS analyses. Furthermore, the observed intergrowth of the Fe-(hydr)oxides with mica (muscovite mainly) adds additional constrain to As release/mobilization, as both group of minerals are insoluble in the extraction solution and stable under broad environmental conditions.



## 4 LOW ARSENIC BIOACCESSIBILITY BY FIXATION IN NANOSTRUCTURED IRON(HYDR)-OXIDES QUANTITATIVE IDENTIFICATION OF AS-BEARING PHASES<sup>2</sup>

### 4.1 Introduction

The stability of As-containing materials in the environment is a concern due to evidence that inorganic arsenic is a human carcinogen (IARC, 2012). Nonetheless, investigations associating the stability of this element in soil particles and its effect on human health are still scarce, especially in areas influenced by mining activities. Moreover, it remains difficult to establish a clear correlation between the results of extraction tests and the actual stability of As-bearing phases present in soil, and therefore arsenic bioaccessibility.

The main source of arsenic in soils is geogenic and therefore related to the parent rock. Background concentrations in natural soil can range from as low as 0.2 mg kg<sup>-1</sup> to as high as 40 mg kg<sup>-1</sup> (WHO, 2000), with baseline values generally in the 5–10 mg kg<sup>-1</sup> range. Nevertheless, arsenic concentrations much higher than the baseline values are found in some mineralized areas and where additional inputs are linked to anthropogenic activities, including mining activities, smelting, fossil-fuel combustion products, pesticides and phosphate fertilizers (Smedley and Kinniburgh, 2002). In soils affected by mining activities, the high concentrations are due to the presence of primary sulfide mineral phases, as well as secondary iron arsenates and iron oxides formed by oxidation of the ore constituents.

The long-term stability of arsenic compounds is a function of several parameters, including site characteristics, particle size and crystallinity, presence/absence of oxygen, complexing agents, (Riveros et al., 2001), and on the nature of the As-bearing phases. Dissolution of sulfide phases, such as arsenopyrite (FeAsS), is favored under acidic, aerated conditions in reactions catalyzed by microbial reactions or under alkaline conditions where chemical reactions predominate. The remobilization of arsenic associated with iron (hydr)oxides precipitates or as ferric arsenates is expected to occur under strong alkaline conditions, due to the formation of soluble iron and arsenate species. Under reducing conditions, the ferric (hydr)oxides also undergo reduction and dissolution, with the subsequent release of arsenic (Ciminelli, 2014).

---

<sup>2</sup> This chapter was published by Journal of Hazardous Materials in march 2018. Authors: Virginia S.T. Ciminelli, Daphne C. Antônio, Claudia L. Caldeira, Erico T.F. Freitas, Itamar Daniel Delbem, Marcus M. Fernandes, Massimo Gasparon, Jack C. Ng. doi: <https://doi.org/10.1016/j.jhazmat.2018.03.037>

The bioavailable and bioaccessible arsenic may be significantly lower than the total concentration in a solid matrix, as it represents only the As that is soluble in the body fluids and hence the amount that can be absorbed by the organism. *In vivo* and *in vitro* bioavailability and bioaccessibility tests are increasingly used as the main indicators of potential risks that chemicals pose to the environment and human health, and have therefore become useful tools to determine As exposure from soil ingestion (Ng et al., 2015). Arsenic bioavailability can vary markedly with As speciation. Oxidized Arsenic(V) and As(III) compounds (e.g., Ca ferric arsenate; arsenolite; claudetite; amorphous ferric arsenates) are generally more toxic than arsenic in sulfide minerals (e.g., arsenical pyrite ( $\text{FeS}_2$ ) and arsenopyrite ( $\text{FeAsS}$ )) (Brown et al., 1999). Toujaguez et al. (2013) reported bioaccessible As values in mining tailings of up to 35,372 mg  $\text{kg}^{-1}$  ranging from 0.65 to 40.5% of the total As content. The maximum As bioaccessibility was ascribed to the presence of goethite and amorphous Fe arsenate, and the low bioaccessibility to arsenic in arsenopyrite and scorodite.

Soil properties such as pH, ageing, the presence of oxides of other elements and total organic carbon (TOC) have been shown to influence bioaccessibility (Xia et al., 2016; 2017). Further, Smith et al. (2009) showed an increase in arsenic bioaccessibility with decreasing particle size, thus highlighting the importance of this parameter in assessing risks in contaminated environments. These are typical parameters affecting dissolution of solids in aqueous systems in general. Caetano et al. (2009) showed that the amount of arsenic released from synthesized scorodite ( $\text{FeAsO}_4 \cdot 2\text{H}_2\text{O}$ ) decreased from 13.6 mg  $\text{L}^{-1}$  to 0.1 mg  $\text{L}^{-1}$  with aging of the solid phase. In addition, round-shaped scorodite particles showed an arsenic leachability higher than that of plate-like shaped scorodite for particles with the same specific surface area. Therefore, a morphological characterization of As-bearing phases is also relevant for understanding As dissolution behavior from the various environmental matrices.

Precise, single particle characterization of As-bearing phases in environmental samples by traditional analytical techniques is not trivial. Bulk X-ray absorption spectroscopy has helped identify the molecular environment of As in various matrices for more than a decade (Foster et al., 1998, Ladeira et al, 2001, Toujaguez et al., 2013). The combination of synchrotron-based techniques with theoretical modeling and other spectroscopic techniques has improved the understanding of the mechanisms of arsenic fixation in typical substrates found in the environment (Duarte et al, 2012). Micro-X-ray fluorescence ( $\mu\text{-XRF}$ ) combined with microfocused-X-ray absorption spectroscopy ( $\mu\text{-XAS}$ ) has enabled

*in situ* characterization of As in soil samples (e.g., oxidation state, association, and coordination) with spatial resolution usually down to the micrometer level (Ono et al., 2015). In this study and in the literature in general, arsenic association with the solid phases (collected *in situ* or synthesized) is generally explained by models involving inner sphere complexation (i.e., specifically adsorbed As), metal arsenates formation or association with amorphous or crystalline metal (hydr)oxides (mostly iron). It should be noted that the identification of the molecular environment of As by synchrotron-based techniques depends on the selection of standards for linear combination fitting to the experimental spectra by approximations. Moreover, these methods do not provide the spatial resolution necessary to investigate highly heterogeneous nanoscale phases in soil samples, down to a few nanometres, or allow statistically sound quantification of As-bearing phases. To overcome these limitations, we will combine high-resolution transmission electron microscopy with scanning electron microscopy and automated image analysis.

This investigation was conducted in a region where elevated arsenic levels associated with gold mineralization are well documented (Ono et al., 2012; Mello et al., 2006). Gold extraction by artisanal mining dates back to 1734, while industrial mining was established in 1987. There are concerns that the communities living in this mineral-rich region may be exposed to elevated concentrations of As, derived either from the natural weathering and erosion of rocks, and from soils and water, or from mine wastes accumulated over centuries of mining activities. As a result, this mining region has attracted significant attention from the local and international media over recent years. Within this context, As exposure from soils in this As-enriched environment together with a precise, statistically sound identification of As sources and association is needed to address the legitimate concerns of the local population.

Soil samples were collected and analyzed for bioaccessibility using synthetic gastrointestinal fluids. The bioaccessible As concentrations were used to estimate the daily total As intake from unintentional soil ingestion and then in the assessment of As exposure and the associated risks. Quantitative, single particle identification of As-bearing phases, as well as their partition and association with other soil constituents, was made possible by using Mineral Liberation Analyzer (MLA), a scanning electron microscopy (SEM)-based automated image analysis system (Gu, 2003). Nanoscale investigation of As association with the soil constituents was done by Transmission Electron Microscopy (TEM) (Freitas et al., 2015).

The primary aim of this investigation was to develop an analytical protocol for the identification of arsenic in soil samples and for the assessment of its potential risk to human health. It will be demonstrated that the analytical procedure developed by combining statistically sound SEM with automated image analysis with the precise identification of As association by HR-TEM allows the identification of As-bearing nanoparticles in As-rich soils, the form of As association with the soil constituents, and how this association determines As bioaccessibility and potential risks to human health.

#### 4.1.2 Description of the sampling site

The study area is located in the northwestern of Minas Gerais State, Brazil, in a typical “cerrado” (tropical savanna ecoregion characterized by a rich and unique floral and faunal diversity). The climate is influenced by a regional tropical system in the mid-latitudes with well-defined dry (April to September) and rainy seasons (October to March). The main economic activities of the region include agriculture, cattle grazing, charcoal production and mining. Elevated arsenic levels associated with gold mineralization in the region are well documented (Rezende et al., 2015; Mello et al., 2006). Gold, discovered in the late 18<sup>th</sup> century, attracted artisanal mining and the early European settlers to this and other regions of the state. At the end of the 1980s, these activities declined. Large-scale, open-pit industrial gold mining has been in operation since 1987. The mine is located immediately to the north of Paracatu city, with some residential dwellings situated less than 1 km from the open pit. Gold is found in association with geogenic arsenic anomalies, mainly scorodite ( $\text{FeAsO}_4 \cdot 2\text{H}_2\text{O}$ ) and arsenopyrite ( $\text{FeAsS}$ ) (Ciminelli et al., 2017).

The main geological units (Canastra, Vazante, Canastra/Morro do Ouro member, Alluvium/colluvium) and watersheds (Santa Rita and Rico Creek) are shown in Figure 4.1. Four classes of soils are found in areas under the influence of gold mineralization and areas that represent the region’s background. *Leptosols*, which are typically shallow soils over bedrock and thus indicating little influence of pedogenetic process or soil forming processes, occur in the Canastra and Vazante Groups. Ferralsols, which are soils in the advanced state of weathering, are also found in these geological units. Spots of *Fluvisols* are found in the Alluvium / Colluvium areas (Figure 4.1). Chemical analyses of the soil samples (data not shown) indicate high values of exchangeable aluminum and low values of exchangeable calcium and magnesium. Medium and high levels of organic matter ( $7 - 31 \text{ g kg}^{-1} \text{ C}$ ) are also found (SENAI/FIEMG, 2014).

## 4.2 Experimental

### 4.2.1 Sampling and sample preparation

The soil sampling and analyses were undertaken according to the procedure adopted by the State Program Soils of Minas (*Solos de Minas*) following the State Environmental Agency - FEAM (2013) protocols and in agreement with international practice (USEPA, 1992). The sampling was undertaken in four geological units and four classes of soils comprising areas of gold mineralization and areas representing the region's background (Figure 4.1). The collection of forty-nine samples was carried out in June-July 2014 with an excavator and a stainless-steel sampler to make composite samples. The surface soil samples (0-20 cm) were transferred to clean polypropylene bags, identified and stored at room temperature until further processing. Composite samples from soils were collected through the entire study area to have a comprehensive sampling distribution. Twenty samples were tested for bioaccessibility (fraction <250 $\mu$ m). Based on As concentrations, the samples fell into two groups: thirteen samples with the high As concentrations (approximately 100 - 4000 mg kg<sup>-1</sup>), hereafter labelled "high As" (H-As), and seven "low As" samples below 100 mg kg<sup>-1</sup> As (L-As).

The bulk samples were oven-dried at 40°C for 12 hours until they reached a constant weight, then disaggregated, split into sub-samples and sieved at 2 mm. Some sub-samples were finely-ground (<44  $\mu$ m) for chemical analyses and particle characterization by TEM. Others sub-samples were ground (<250  $\mu$ m) for particle characterization by SEM-MLA.

### 4.2.2 Chemical concentrations using Method 3051a (USEPA 2007)

The concentration of arsenic in soil samples was determined following digestion with *Aqua regia* using a microwave-assisted (Ethos, Milestone, USA) digestion procedure (USEPA, 2007). An amount of 200 $\pm$ 0.1 mg of ground < 44  $\mu$ m samples (in triplicate), 3 mL of HNO<sub>3</sub> (65% P.A., Química Moderna, Brazil) and 9 mL HCl (37%, ACS P.A., Química Moderna, Brazil) were weighed into Teflon digestion vessels (50 mL) and digested as described in Table IV.1

Table IV.1: Microwave digestion conditions.

Step	Time (min)	Temperature (°C)	Power (W)
Ramp	5.5	RT <sup>1</sup> – 175	1500
Hold	4.5	175	1500
Cooling	30	175 – 80	-
Total run	40		-

Pressure:  $9.2 \times 10^5 \text{ N/m}^2$  - 1. RT: room temperature

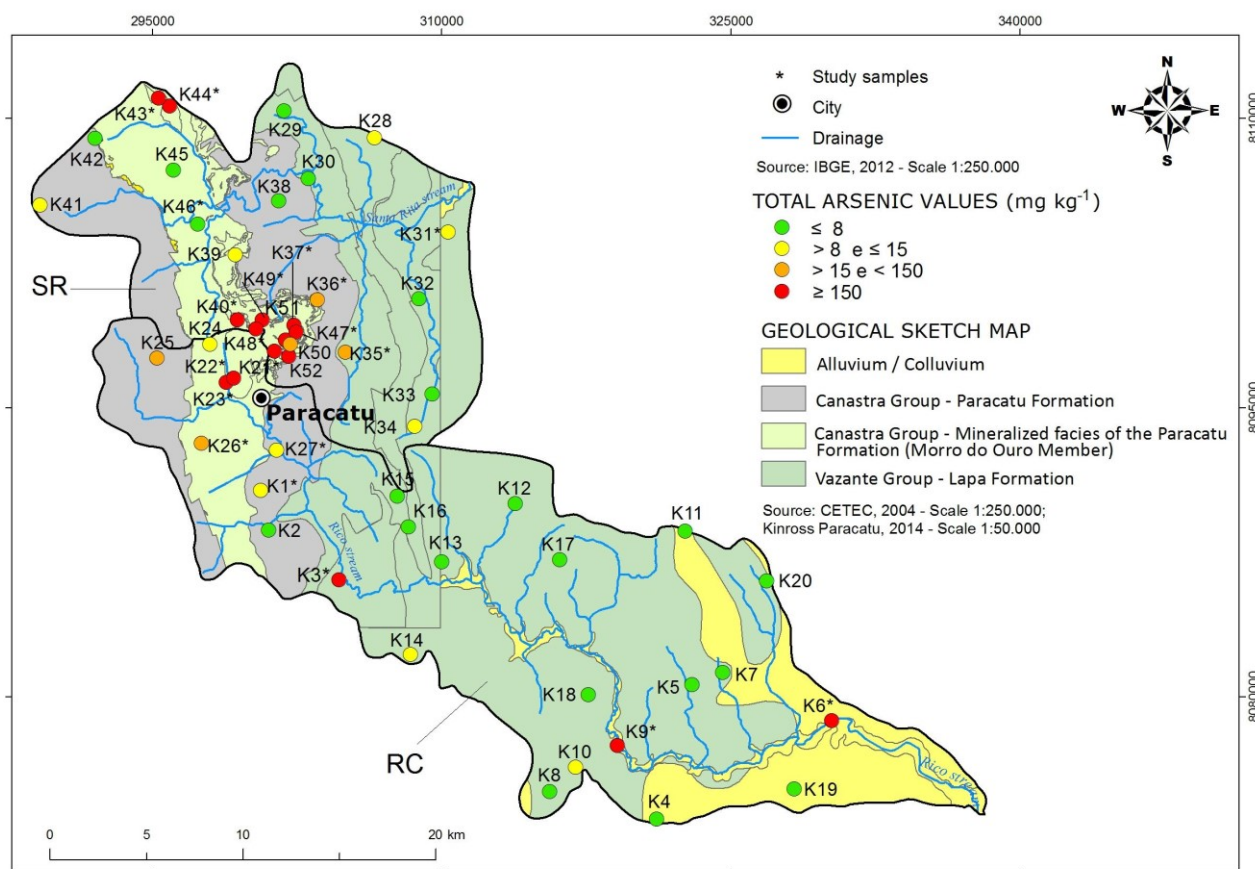


Figure 4.1. Sampling location, Paracatu, MG, Brazil, showing the complete set of samples and the selected samples (\*) for this study. Santa Rita (SR) and Rico creek (RC) watersheds are also shown.

On the following day and after reaching room temperature ( $\sim 25^{\circ}\text{C}$ ), in a fume hood, the extracted solutions were transferred to Falcon<sup>TM</sup> tubes and made up to 50 mL with deionized (Milli-Q Integral 5) water. The vessels were washed at least three times with deionized water to ensure the complete recovery of the extracted solution. The resultant solutions were stored at  $4^{\circ}\text{C}$  until further analysis. Arsenic was analyzed by a Perkin Elmer (Norwalk, Connecticut, USA model Optima 7300DV) inductively coupled plasma optical emission spectrometry (ICP-OES), according to the conditions indicated in [Table IV.2](#).

Table IV.2: Instrumental conditions (ICP-OES)

<i>Parameter</i>	<i>Condition</i>
Radiofrequency (W)	1300
Internal Spike	Lu $1 \text{ mg kg}^{-1}$
Nebulizer	Gemcone high flow at $0.60 \text{ L min}^{-1}$
Alumina injector (mm)	2.0
Plasma flow ( $\text{L min}^{-1}$ )	15
Auxiliary gas ( $\text{L min}^{-1}$ )	0.2
Sample flow ( $\text{mL min}^{-1}$ )	1.30
Wash between samples (s)	30
$\lambda$ (nm)	As 193.7 radial

As quality assurance and quality control, two standard reference materials (NIST SRM 2710a, National Institute of Standards and Technology, Washington, DC) and CCRMP-Till 3, CANMET Mining and Mineral Sciences Laboratories-NCR, Ontario, Canada) were analyzed together with each batch of 10 samples (see Tab.A.I.2). Lutetium ( $1 \text{ mg L}^{-1}$ , UltraScientific, N. Kingstown, USA) was used as an internal standard element to monitor matrix effects and sensitivity drifts of the ICP-OES instrument. Duplicates and analytical blanks were analyzed as well. The certified materials used for quality control were selected based on the As level and matrix similarities with the samples. The good quality of the analytical procedure is demonstrated by As recovery ranging from 84 to 101%. All blank extractions for all digestion types returned values below the method detection limits ( $\text{DL} < 0.2 \text{ mg L}^{-1}$ ).

### 4.2.3 Oral bioaccessibility

The arsenic bioaccessible fraction was determined using the standard operating procedure adopted by the United States Environmental Protection Agency – USEPA (USEPA, 2012), which consists of a simple extraction with a glycine solution in an acid environment to simulate the gastric phase. Prior to the test, the < 2 mm soil samples were sieved to < 250 µm.

In summary, a 0.4 mol L<sup>-1</sup> glycine (99%, Sigma-Aldrich, Missouri, USA) solution was prepared and acidified with HCl (37%, Química Moderna, Brazil) to reach pH 1.50 ± 0.05 simulating a gastric intestinal solution (“stomach phase”) and heated to 37°C. A 30 mL aliquot of this solution was added to an amount of 0.3 g of soil sample placed in a 120 mL high-density polypropylene (HDPE) vial (Fisherbrand, USA) and left under constant horizontal agitation (200 ± 2 rpm) at 37 ± 2 °C (Innova 44 incubator, New Brunswick scientific) for one hour. After 1 h, the HDPE vials were removed from the incubator and the pH of the suspension was measured. After confirming that both the pH (1.5 ± 0.5) and the time criteria (total elapsed time less than 1 hour and 30 minutes) were met, the extract was centrifuged (Rotofix 32A, Hettich, Germany) at 3000 rpm for 10 min. A 20 mL aliquot of the supernatant fluid was then filtered through a 0.45 µm cellulose acetate membrane with Swinnex<sup>TM</sup> holder filter (25 mm diameter) and stored at 4 ± 2°C for one week until analysis by hydride generation inductively coupled plasma optical emission spectroscopy (HG-ICPOES, Optima 7300DV, Perkin-Elmer, USA). Pre-reductant solution (1 mL 5% w.v<sup>-1</sup> KI / 5% w.v<sup>-1</sup> ascorbic acid and 2 mL 50% v.v<sup>-1</sup> HCl) was added to the undigested samples, and made up to 10 mL with deionized water. After 45 minutes at room temperature (~ 25°C) for reaction, the samples were analyzed. In a flow-injection mode, reductant (0.65% w.v<sup>-1</sup> NaBH<sub>4</sub>- 0.2 mol L<sup>-1</sup> NaOH) and samples were mixed in a sample valve. The calibration curve ranged from 2.5 to 50 µg L<sup>-1</sup>. A blank and a synthetic sample of 10 µg L<sup>-1</sup> As were analyzed every ten samples as a quality control parameter. The recovery of synthetic samples (n = 20) was within 95±11%.

A batch of analyses was composed by samples in triplicate, a blank consisting of a glycine solution at pH 1.5 and a reference soil material (NIST 2710a). No statistical differences were observed between samples analyzed by ICP-OES and ICPMS. Table IV.3 provides additional information on the experimental conditions selected for the analysis.



Subsamples of  $0.15 \pm 0.01$ g of the pulverized material were mixed with  $0.30 \pm 0.01$ g of COM-CAT™ and analyzed in duplicate for total sulfur (S-total) and total carbon (C-total) using a LECO SC632 furnace instrument. Six reference materials (LECO – ore standards (502-320 411B, 502-318/1009, 502-319/ 1014), CANMET- RTS-3a, kzk-1 and MP-1b) were analyzed as quality assurance and quality control and the recoveries ranged from 98 to 109% for further data see [Table A.1.2](#).

Table IV.3. Instrumental conditions (HG-ICP-OES)

<i>Parameter</i>	<i>Condition</i>
Radiofrequency (W)	1450
Nebulizer	Gemcone high flow at $0.80 \text{ L min}^{-1}$
Alumina injector (mm)	2.0
Plasma flow ( $\text{L min}^{-1}$ )	17
Auxiliary gas ( $\text{L min}^{-1}$ )	0.3
Pump flow ( $\text{mL min}^{-1}$ )	1.00
Wash between samples (s)	30
Reductant ( $\text{NaBH}_4/\text{NaOH}$ )	$0.65\% (\text{w v}^{-1}) - 0.2 \text{ mol L}^{-1}$
Reaction time (min)	45 at room temperature
$\lambda$ (nm)	As 193.7 radial
DL ( $\mu\text{g kg}^{-1}$ , n=7)	1.5
QL ( $\mu\text{g kg}^{-1}$ , n=7)	5.6

#### 4.2.4 Electron Microscopy analyses

Six samples representing different soil classes were selected for arsenic-bearing phase characterization and quantitative mineralogy based on single particle using a FEI Quanta 650 Field Emission Gun Scanning Electron Microscope (FEG-SEM) equipped with two Bruker Quantax X-Flash 5010 energy dispersion X-ray (EDX) detectors and FEI's MLA suite 3.1.1.283 for data acquisition and process. In this study, the grain-based X-ray mapping (GXMAP) measurement mode was applied for identification. In this measurement mode, a series of backscattered electron (BSE) images is collected. Identification of mineral grains by MLA is based on BSE image segmentation and collection of EDX-spectra of the particles and grains identified in BSE-imaging mode. Collected EDX-spectra are then classified using a pre-defined list of mineral spectra collected by the user ([Gu, 2003](#)). A summary of the main instrumental parameters is given in [Table IV.5](#). The method

has a resolution of grain size down to 0.1 – 0.2  $\mu\text{m}$  (Gu, 2003). Prior to the analyses the selected (< 2 mm and > 2 mm) samples were ground in an agate mortar with pestle and sieved through a 250  $\mu\text{m}$  screen to create a uniform particle size material and a statistically representative number of particles. Two of these samples, identified as K03 and K06, were already below 250  $\mu\text{m}$ . Samples were embedded in epoxy following the standard MLA sample preparation procedure. The resulting polished sections were prepared in a 25 x 25 mm polypropylene mounting cup roughed and polished using a grinder/polisher (MiniMet 1000, Buehler, USA) system and finally coated with a conductive carbon film.

For the TEM analyses each powder sample was dispersed in Milli-Q water in Eppendorf tubes and sonicated in ultrasound bath for three minutes. A drop of each suspension was placed on carbon coated Cu-TEM grids (300 mesh) and left drying in a desiccator for at least 1 day. The analysis was performed using High Resolution TEM (HRTEM), Scanning TEM (STEM), EDX spectroscopy and Electron Energy-Loss Spectroscopy (EELS) using a FEI FEG-TEM Tecnai F20 (200 kV). The analyses were performed in the Centre for Microscopy and Microanalysis of The University of Queensland, Australia.

Table IV.4. SEM/MLA mainly instrumental parameters

<i>SEM Parameters</i>		<i>MLA Parameters</i>	
Voltage (kV)	25	Scan speed (a.u.)	16
Working distance (mm)	11	Resolution (a.u.)	1000x1000
Spot size* (a.u.)	5.1	Pixel size ( $\mu\text{m}/\text{px}$ )	1.49
Horizontal field width ( $\mu\text{m}$ )	600	Acq. time (ms)	12
Brightness (a.u.)	93.77	GXMAP BSE trigger (a.u.)	20-255
Contrast (a.u.)	19.40	Minimum grain size (px)	4
BSE Calibration	Au 245	GXMAP X-ray step (px)	6

SEM, scanning electron microscopy; MLA, mineral liberation analyzer; BSE, backscattered electron.

\*Spot size of 5.1 equates to a ca. 10 nm beam diameter.

## 4.3 Results and discussion

### 4.3.1 Bioaccessible Arsenic in the soil samples

Table IV.5 shows the median, mean, minimum and maximum chemical concentrations for the three size fractions investigated ( $> 2$  mm,  $< 2$  mm and  $< 250$   $\mu\text{m}$ ). The size fraction cutoffs were chosen based on national guidelines and USEPA methods (2012) for soil classification ( $< 2$  mm) and bioaccessibility test ( $< 250$   $\mu\text{m}$ ), respectively. Figure 4.2 shows the chemical As concentrations in the three fractions ( $> 2$  mm,  $n= 2$ ;  $< 2$  mm and  $< 250$   $\mu\text{m}$ ,  $n= 3$ ) of H-As samples. The results (Figure 4.2 and Table IV.5) show relatively high As concentrations in the coarse fraction ( $> 2$  mm), ranging from 1407 to 8036  $\text{mg kg}^{-1}$ . For the finer fractions ( $< 2$  mm and  $< 250$   $\mu\text{m}$ ), the ranges are 250-6354  $\text{mg kg}^{-1}$  and 211 - 4304  $\text{mg kg}^{-1}$ , respectively, indicating a decrease in the As concentration with decreasing particle size. The chemical analysis of the individual samples is shown in Table IV.6. The arsenic enrichment in the coarser fractions is likely associated with the iron oxides enrichment, which will be discussed further.

Table IV.5. Median, mean and range of chemical As concentration ( $\text{mg kg}^{-1}$ ) in different size fractions of the select soil samples and quality control results. For each sample, analyses were carried out in triplicate.

	High As concentration (n=13)			Low As concentration (n=7)	
	Bulk	$> 2\text{mm}$	$< 2$ mm	$< 250$ $\mu\text{m}$	$< 250$ $\mu\text{m}$
Median	1947	4014	806	443	17
Mean	2317	4494	1252	735	22
Range	177-6825	1407-8036	250-6354	211-4304	8-47
SRM NIST 2710a (n=7)		Measured			1557 $\pm$ 88
		Certified value			1540
		Recovery (%)			101
RM Till-3 (n=10)		Measured			70 $\pm$ 22
		Certified value			84
		Recovery (%)			83

Table IV.6. Chemical As content in different particle sizes of the soil samples (mean±SD, n=3)

Samples	As (mg kg <sup>-1</sup> )		
	> 2 mm	< 2 mm	< 250 µm
K03	*	411±62	464±64
K06	*	392±45	405±3
K09	*	250±8	325±5
K21	2802±16	1560±204	841±28
K22	3852±65	1738±102	575±83
K23	8036±934	6354±468	4304±286
K37	4984±17	930 ±109	494±46
K40	5832±140	690 ±30	443±14
K43	*	262 ±25	211±39
K44	1396±16	614 ±42	459±15
K47	3927±122	916 ±200	379±33
K48	7456±180	1355 ±161	324±29
K49	2153±132	806 ±115	332±36
K43	*	262 ±25	211±39
Range	207–8036	112-6354	40-4304
Median	2478	748	443
Mean	2998	1171	735
SRM NIST 2710a (n=7)		Measured Certified value	1557±88 1540
RM Till-3 (n=10)		Measured Certified value	70±22 84

\*no fraction > 2mm.

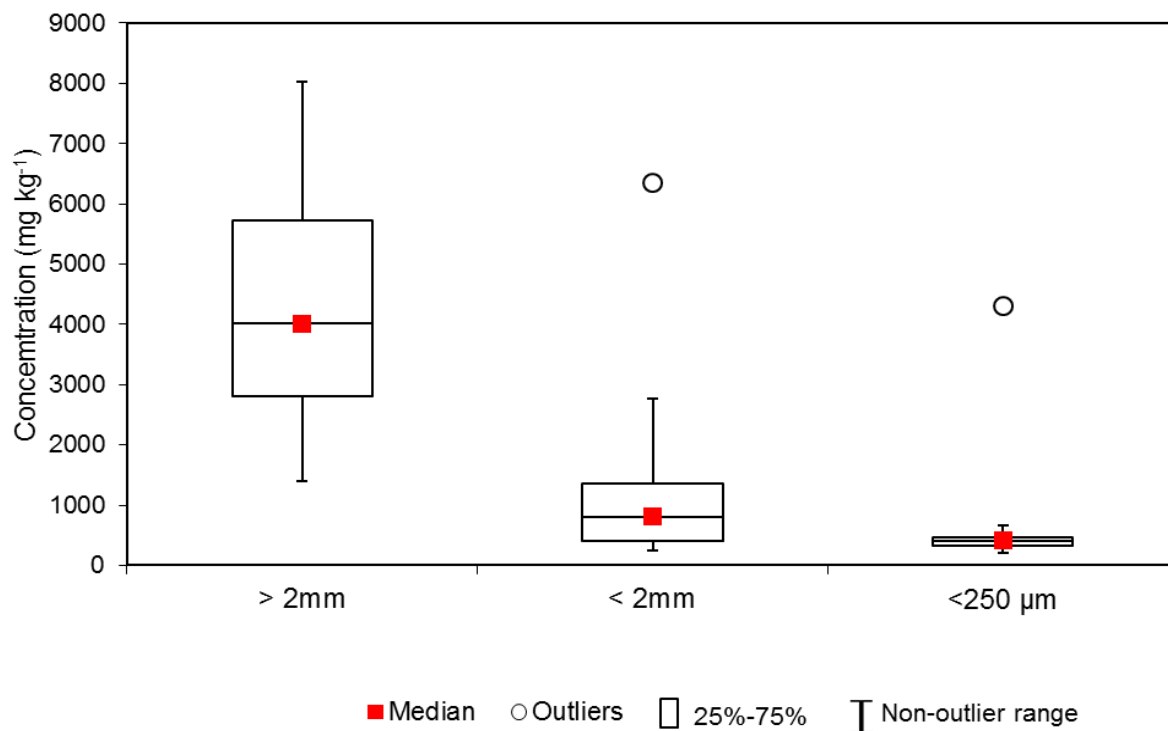


Figure 4.2. Concentrations (expressed in mg kg<sup>-1</sup>) of chemical As in the three fractions of the high arsenic samples. Square dots (in red) represent the median; circle dots represent the outliers, the box indicates the range 25–75% of the distribution and the whiskers represent minimum and maximum. Analyses carried out in duplicate for the >2 mm fraction and in triplicate for the others.

The H-As samples (Table IV.5 and IV.6) show As concentrations significantly higher than the investigation values (Anonymous, 2009) for arsenic in soils (fraction < 2 mm) in agricultural (35 mg kg<sup>-1</sup>) and residential (55 mg kg<sup>-1</sup>) areas according to Brazilian national criteria. The L-As samples (Table IV.5) present As concentrations below the investigation values for residential areas, and with the exception of sample K36 (47 mg kg<sup>-1</sup>), for agricultural areas as well. The investigation value is defined as the concentration of a given substance in soil or in groundwater above which there are potential direct or indirect risks to human health, considering a scenario of standardized exposure (Anonymous, 2009). The high As concentrations shown in Table IV.1 are in agreement with the results available in the literature for soil samples collected in gold mining regions in the state of Minas Gerais (Ono et al., 2012; Mello et al., 2006) and in other parts of the world, such as Australia (81 to 2270 mg kg<sup>-1</sup>, Juhasz et al., 2015), England (3.8 to 848 mg kg<sup>-1</sup>, Palumbo-Roe et al., 2015), the United States (app. 10 to 3500 mg kg<sup>-1</sup>, Gonzales et al., 2014) and China (110 – 802 mg kg<sup>-1</sup>, Yin et al., 2016). The As concentrations found in the study site are similar to those reported for mineralized areas worldwide and are significantly higher than the background values reported in the literature for non-mineralized areas, which are in the range of 0.2 to 40 mg kg<sup>-1</sup>, according to WHO (2000).

Regarding the soil type (Table IV.6), Leptosols generally show the highest As concentrations, whereas the Ferralsol and Fluvisol samples have the lowest As levels. Sample K23 is classified as an outlier according the Grubbs' Test (G-test) (ISO 5725, 1994) as it lies at an abnormal distance (>25%) from the mean (Figure 4.2).

Incidental soil ingestion is the main pathway for As exposure from soils. The < 250 µm fraction is regarded as the particle size fraction that is likely to stick to hands and hence could result in exposure via hand-to-mouth. Physiologically based extraction test methods have been widely adopted for the estimation of bioavailability, have been validated against *in vivo* models (Ng et al., 2015, Juhasz et al., 2007; 2009; 2009b) and are accepted by USEPA (2007).

The bioaccessible As concentrations are shown in Table IV.7 for the H-As and L-As samples. Also shown in Table IV.7 is the mean bioaccessible concentration (440 mg kg<sup>-1</sup>) for NIST SRM 2710a, which corresponds to 30 ± 5% % BAC and therefore agrees with previously reported BAC of 28 ± 17% (Koch et al., 2007). The bioaccessible As for the H-As samples varied from 0.86 mg kg<sup>-1</sup> to 22 mg kg<sup>-1</sup> with a mean of 7.53 mg kg<sup>-1</sup> and a

median value of  $4.60 \text{ mg kg}^{-1}$ . The As BAC ranged from 0.3% to 5.0%, with a mean of 1.4% and a median of 0.9%. The relatively large difference between the median and mean values is due to the presence of an outlier (sample K23), and therefore the median values are taken as being more representative. For the L-As samples, BAC varied from 0.2 to  $0.7 \text{ mg kg}^{-1}$  with mean and median values of  $0.4 \text{ mg kg}^{-1}$ . The As BAC ranged from 0.9% to 6.6%, with a mean of 2.7% and a median of 2.4% (Table IV.7).

The low As BAC for the H-As and L-As samples (means of 1.4% and 2.7%, respectively) found here is consistent with similar findings of other study (means of 2.2%) conducted in the same region (Ono et al., 2012; Ng et al., 2014). The bioaccessible As ( $4.6 \text{ mg kg}^{-1}$ ) is within the local guidelines and indicates that the metalloid is firmly held in the matrix. The arsenic bearing phases and the main features of this association are discussed below.

#### 4.3. 2 Arsenic-bearing phases

Table IV.8 shows the main mineral phases in the soil samples according to the analyses carried out by MLA (see Tab.A.V.1). The main phases (here defined as  $> 2 \text{ wt.}\%$ ) are quartz ( $\text{SiO}_2$ ), mica/clay minerals, microcline ( $\text{KAlSi}_3\text{O}_8$ ), goethite and hematite and other non-identified nanoaggregates of Fe-(hydr)oxides, which are in agreement with the features of these classes of soils and the XRD analysis (see Appendix. II). The MLA tool allows for quantitative single particle analysis of a large number of grains. The total number of particles analyzed in each sample ranged from 27,244 (K23  $< 2 \text{ mm}$ ) to 79,330 (K03), which can provide good statistics as discussed by Delbem et al. (2015). The variation in particle counts is simply due to the choice of the analysis parameters: by selecting a fixed scanning time (2 hours), a larger number of particles was analyzed in the samples with finer particle size distribution (e.g., K03) and therefore a larger number of particles per unit area of the polished section. Large variations in the content of Fe-(hydr)oxides from approx. 1% (K06) to approx. 45% (K23  $> 2 \text{ mm}$  and  $< 2 \text{ mm}$ ) and K48  $(> 2 \text{ mm})$ ) were observed (Tab. IV.8). In general, the concentration of arsenic increased with the increase of the concentration of Fe-(hydr)oxides. In most samples, the total Fe-(hydr)oxides content (with and without As) varied also with particle size (e.g., sample K48 shows 44% and 11% for  $> 2 \text{ mm}$  and  $< 2 \text{ mm}$ , respectively). This higher Fe-(hydr)oxides content may explain the As-enrichment in the coarse fractions (Figure 4.2).

Table IV.7. Bioaccessible arsenic in the < 250  $\mu\text{m}$  soil samples and in the certified material (Mean $\pm$ SD; n=4).

Samples	[As] ( $\text{mg kg}^{-1}$ )	Bioaccessible As ( $\text{mg kg}^{-1}$ )	As bioaccessibility (%)
<i>High As samples (H-As)</i>			
K03	464 $\pm$ 64	1.9 $\pm$ 0.1	0.41 $\pm$ 0.03
K06	405 $\pm$ 3	1.21 $\pm$ 0.01	0.30 $\pm$ 0.00
K09	325 $\pm$ 5	1.8 $\pm$ 0.1	0.57 $\pm$ 0.03
K21	841 $\pm$ 28	19.47 $\pm$ 0.03	2.31 $\pm$ 0.00
K22	575 $\pm$ 83	1.9 $\pm$ 0.4	0.33 $\pm$ 0.10
K23	4304 $\pm$ 286	17 $\pm$ 1	0.39 $\pm$ 0.03
K37	494 $\pm$ 6	8.2 $\pm$ 0.6	1.67 $\pm$ 0.10
K40	443 $\pm$ 14	22 $\pm$ 4	5.01 $\pm$ 1.00
K43	211 $\pm$ 39	0.86 $\pm$ 0.04	0.41 $\pm$ 0.02
K44	459 $\pm$ 15	4.3 $\pm$ 0.9	0.94 $\pm$ 0.20
K47	379 $\pm$ 33	9.3 $\pm$ 2.9	2.45 $\pm$ 0.80
K48	324 $\pm$ 29	4.6 $\pm$ 0.1	1.42 $\pm$ 0.05
K49	332 $\pm$ 36	5.4 $\pm$ 1.3	1.62 $\pm$ 0.40
Mean	735	7.53	1.4
Median	443	4.60	0.9
Min.	211	0.86	0.3
Max.	4304	22	5.0
<i>Low As samples (L-As)</i>			
K01	8	0.505 $\pm$ 0.004	6.55 $\pm$ 0.06
K26	22	0.30 $\pm$ 0.02	1.40 $\pm$ 0.05
K27	28	0.69 $\pm$ 0.05	2.45 $\pm$ 0.15
K31	16	0.420 $\pm$ 0.004	2.70 $\pm$ 0.02
K35	17	0.56 $\pm$ 0.06	3.25 $\pm$ 0.32
K36	47	0.42 $\pm$ 0.01	0.89 $\pm$ 0.02
K46	13	0.22 $\pm$ 0.02	1.66 $\pm$ 0.18
Mean	22	0.44	2.7
Median	17	0.42	2.4
Min.	8	0.22	0.9
Max.	47	0.69	6.5
SRM NIST 2710a			
Indicative value	1540	-	28 $\pm$ 17*
Measured (n=4)	1461 $\pm$ 41	440 $\pm$ 74	30 $\pm$ 5

\* reported by the literature



Table IV.8. Major mineral phases (wt%) in soil samples

Phases	Samples							
	K03	K06	K21	K22	K23		K48	
	(<2mm)	(<2mm)	(<2mm)	(<2mm)	(>2mm)	(<2mm)	(>2mm)	(<2mm)
Fe Oxides/Hydroxides-(no As)	1.7	0.7	1.4	30.5	23.2	23.9	22.6	6.7
Fe Oxides/Hydroxides-As	0.6	0.2	4.1	8.5	20.9	21.1	21.3	4.4
Quartz	21.6	6.2	49.1	20.5	27.0	28.9	26.6	28.2
Ilmenite	----	----	2.7	----	----	3.8	----	4.2
Mica/Clay Minerals	67.8	84.1	36.9	35.8	27.2	20.7	27.6	50.7
Microcline	4.3	6.3	3.0	2.6	----	----	----	4.4
Others ([Wt and Area] <2%)	4.0	2.5	2.9	2.0	1.6	1.5	1.9	1.4
Total	100.0	100.0	100.0	100.0	100.0	100.0	100.0	100.0
Total particle number	79330	73857	41831	36123	32282	27244	33864	59477

Table IV.9 shows selected mineral phases (< 2 wt.%) related directly or indirectly to the presence of As in the sample. Arsenopyrite (FeAsS) and scorodite (FeAsO<sub>4</sub>.2H<sub>2</sub>O) are the main arsenic phases in the local sulfide and oxidized ore bodies, respectively. In contrast, arsenic in the soil samples is found mainly in association with Fe-(hydr)oxides, as well as with rare ferric arsenates, likely scorodite, and arsenopyrite. The presence of As in pyrite is not detected (detection limit of app. 0.1 wt%), though pyrite (FeS<sub>2</sub>) is also a potential As carrier (Campbell and Nordstrom, 2014). The relatively low number of pyrite particles (ranging from 8 to 300) and arsenopyrite (ranging from 0 to 7) is consistent with the low bulk sulfur concentration (median value of 130 mg kg<sup>-1</sup>, range of < 100 to 288 mg kg<sup>-1</sup>), and indicates that the overall contribution of As-bearing sulfides and arsenates from the mineralized lithologies to the bulk soil chemistry is negligible.

Table IV.9. Number of particles for selected phases

Phases	Samples							
	K03	K06	K21	K22	K23		K48	
	(<2mm)	(<2mm)	(<2mm)	(<2mm)	(>2mm)	(<2mm)	(>2mm)	(<2mm)
Fe (hydr)oxides	2765	1880	1453	11483	13654	11268	12914	3161
Fe (hydr)oxides-As	738	396	2901	4776	11822	9459	11702	1968
Pyrite	80	37	287	232	300	102	54	8
Arsenopyrite	0	7	4	0	0	0	0	0
Scorodite	0	9	1	0	2	2	0	0
Total particle number	79330	73857	41831	36123	32282	27244	33864	59477

Figure 4.3 shows BSE-SEM images of polished sections prepared from the soil samples. The chemical composition provided by energy dispersive spectroscopy - EDS of the different phases is also indicated. Figures 4.3a and 4.3b show typical mineral associations found in the soil samples: hematite, quartz, muscovite and the intergrowth of phyllosilicate lamellae with Fe-(hydr)oxides (goethite and hematite). Figures 4.3c and 4.3d depict As-bearing, botryoidal goethite and hematite, respectively, both with typical concentric growth layers that are usually indicative of phase transformation. Fe-(hydr)oxides, which make up the bulk of the soil (Table IV.8), are the main As reservoir in the soil samples. The intergrowth of phyllosilicates with the Fe-(hydr)oxides should be noted. The low As BAC (Table IV.7) is consistent with As association with these phases, as they are chemically stable under surficial environmental conditions.

Figure 4.4 shows typical TEM images of the As-bearing Fe-(hydr)oxides phases. A nanometer-scale map of chemical composition and the spatial distribution of Al, Fe, O and As are provided by STEM-EDS (Fig. 4.4i-j). The EDS maps of Fe-(hydr)oxides aggregates suggest that Al and As are dispersed within the structure of the Fe-(hydr)oxide along with O and Fe. The distribution of As suggests that the metalloid is incorporated in the Fe-(hydr)oxides aggregates. Freitas et al. (2015) investigated As-enriched Fe-Al-oxisols after their use as liners in disposal facilities of sulfide tailings. The samples were analyzed by HRTEM, Nano-Beam Electron Diffraction (NBD), EDS and EELS. The results demonstrated that As was present in oriented aggregates formed by crystalline nanoparticles of Fe-(hydr)oxides. The same pattern was found in the samples described in this study. It is important to observe that in the present investigation, the samples were collected in sites with no evidence of anthropogenic activities or input from external arsenic sources.

The aggregates shown in Figures 4.4a and 4.4g were further investigated by HRTEM analysis. The interplanar distances ( $d$ ) were measured by selected area electron diffraction (SAD) and Fast Fourier Transform (FFT) of the HRTEM image (insets of Figs. 4.4b and 4.4h). The  $d$ -spaces of goethite reflections (010) and (-401) were measured (inset in Figure 4.4a). For Figure 4.4g, the distances of 0.25 nm, 0.27 nm and 0.36 nm correspond to the  $d_{hkl}$  of hematite reflections (110), (104) and (102), respectively (Figure 4.4h). Based on these  $d_{hkl}$  spaces, the aggregates were identified as goethite and hematite, respectively. The TEM results demonstrate that the Fe-(hydr)oxides nanoaggregates diffract as a single crystal, as expected for crystals formed by oriented-aggregation crystal growth.

Previous work (Ono et al., 2015) suggested, according to bulk-XANES spectra, Micro-XANES and  $\mu$ -SXRF analyses, that As occurs mostly in poorly crystalline ferric arsenate with minor arsenopyrite. The low As Bac was ascribed to the ferric arsenate, though the less crystalline phase is expected to be relatively soluble (Krause and Ettl, 1989). We argue that the low As BAC is a result of As association with crystalline nanoparticles of Fe-(hydr)oxides aggregates. The intergrowth of the Fe-(hydr)oxides with the phyllosilicates adds additional constraint to arsenic release/mobilization as these mineral phases are expected to remain stable. Arsenic is therefore expected to remain immobilized under a wide range of environmental conditions and therefore pose low risk to human health.

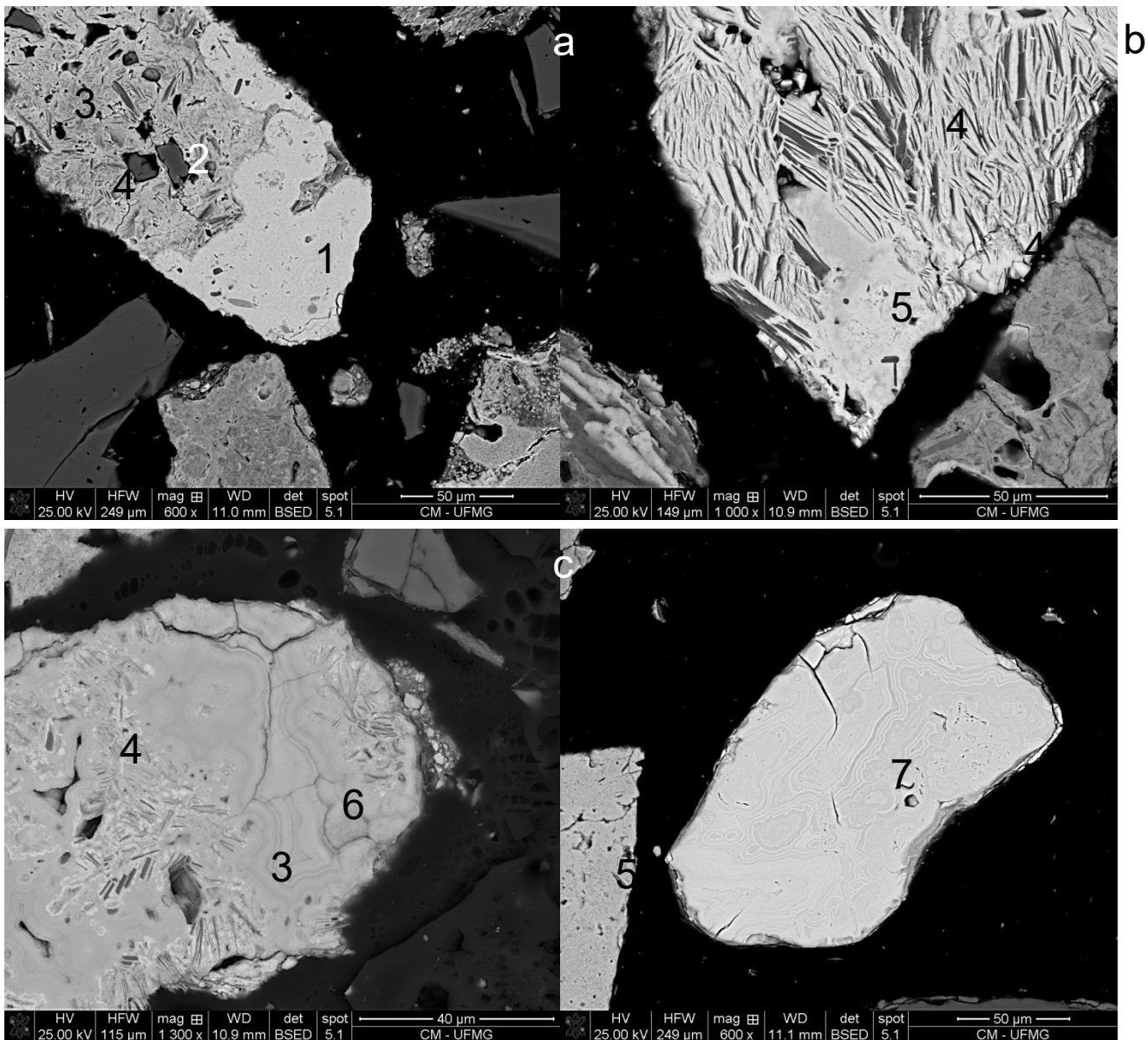


Figure 4.3 SEM micrographs of typical soil samples

**(a)** (1) Hematite (66.5% Fe, 30.6% O, 1.5% Al, 1.4% As), (2) Quartz, (3) Muscovite; (highlighted by the arrow); **(b)** (4) Muscovite within the Fe-(hydr)oxide matrix (1.8% As) and (5) Goethite (62.4% Fe, 34.2% O, 1.5% Al, 1.0% As, 0.1% Si, 0.8% P); **(c)** (3) Muscovite, (4) Fe-(hydr)oxide matrix (1.1% As); (6) Botryoidal goethite (62.9% Fe, 31.9% O, 2.3% Al, 2.9% As); **(d)** (5) Goethite (62.9% Fe, 31.9% O, 2.4% Al, 2.9% As) and (7) Botryoidal hematite (67.0% Fe, 27.8% O, 1.5% Al, 0.6% As, 0.4% Si).

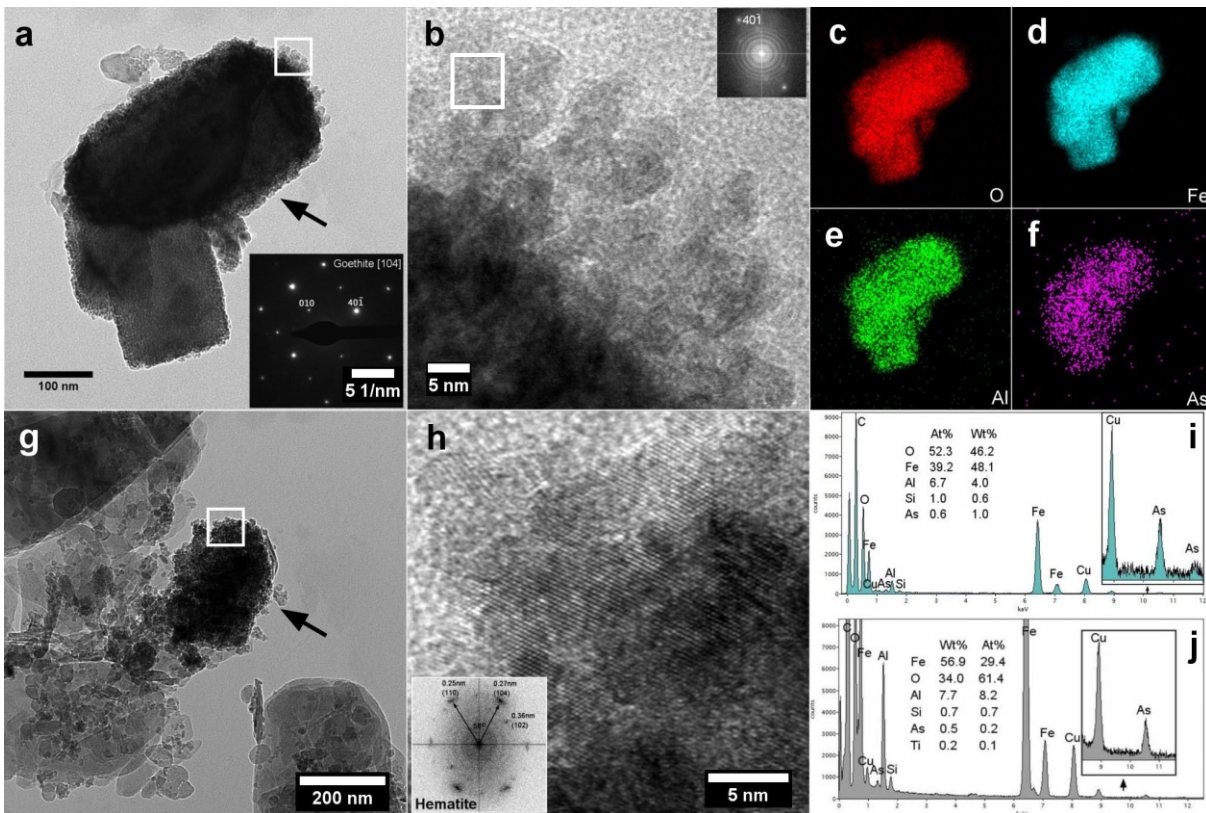


Figure 4.4 (a) Bright Field TEM image of an oriented aggregate of goethite nanoparticles in sample K21 (< 2mm) and the selected area electron diffraction pattern (inset); (b) HRTEM image of the area inside the white square in (a) with the Fast Fourier transform (FFT) of goethite; (c-f) EDS maps of oxygen, iron, aluminum and arsenic of the goethite particle shown in (a); (g) Bright Field TEM image of sample K48 (> 2mm) showing oriented aggregates of hematite nanoparticles pointed by the arrow; (h) HRTEM image of the area inside the white square in (g) with FFT; (i and j) EDS spectra of the goethite and hematite, respectively pointed in the insets (a) and (g). Copper signal originated from the sample grid.

### 4.3.3 HRA and Environmental Implications

The arsenic intake from unintentional ingestion of H-As and L-As soils by adults and children are presented in Table IV.10 considering three scenarios (A1, A2 and A3). The first one (A1) refers to the median value of BAC for the H-As samples, the second (A2) refers to the maximum BAC As value for the H-As samples and the third (A3) refers to the median value for the L-As soil. The assessment of As exposure was based on the ingestion of 50 mg of soil per day and a body weight of 70 kg for adults, and the ingestion of 100 mg of soil per day and a body weight of 16 kg for children, in line with local regulations (Ministry of Health, 2010). The assessment of exposure was based on the product of exposure factors being equal to 1 (worst-case scenario). Using this very conservative approach, a continuous exposure implies soil ingestion 365 days per year.

Table IV.10. Arsenic intake from soil, water and food ingestion and predicted cancer risk

Pathway	iAs ingestion ( $\mu\text{g per kg b.w.day}$ )		Predict Cancer Risk	% Intake adult (A1)	% Intake adult (A2)
	Adult	Child			
A1 - H-As soils (median As BAC $4.6 \text{ mg kg}^{-1}$ )	0.0033	0.0288	$4.9\text{E-}06$	1.7	
A2 - H-As soils (max As BAC $22 \text{ mg kg}^{-1}$ )	0.0157	0.1375	$2.4\text{E-}05$		7.5
A3 - L-As soils (median BAC As $0.42 \text{ mg kg}^{-1}$ )	0.0003	0.0026	$4.5\text{E-}07$		
B - Food *	0.188	0.094	$2.8\text{E-}04$	95.3	89.6
C - Water ( $0.21 \mu\text{g L}^{-1}$ )*	0.006	0.013	$9.0\text{E-}06$	3.0	2.9
Total (A1, B, C)	0.1973	0.1359	$3.0\text{E-}04$		
Total (A2, B, C)	0.2097	0.2446	$3.1\text{E-}04$		
Total (A3, B, C)	0.1943	0.1099	$2.9\text{E-}04$		
Water ( $10 \mu\text{g L}^{-1}$ )	0.286	0.625	$4.30\text{E-}04$		

\*(Ciminelli et al., 2017)

Risk assessment calculations were carried out by comparing the total As intake to Benchmark Dose Lower Confidence Limit (BMDL) and linear dose relationship for the As Cancer Slope Factors (CSF) for oral ingestion set at 1.5 per  $\text{mg kg}^{-1} \text{ b.w. day}^{-1}$  (USEPA, 1995). In Table IV.10, we illustrate the relative risk in different scenarios of soil ingestion using CSF. The essence of this exercise is to calculate the dietary intake of arsenic and to compare the results to those of the provisional guideline value of  $10 \mu\text{g L}^{-1}$  in drinking water (WHO, 2011). It can be noted that when the CSF approach is considered, the soil ingestion in all three scenarios (A1, A2, A3) is one to three orders of magnitude lower ( $2.4 \times 10^{-5}$  and  $4.7 \times 10^{-7}$ , respectively) than the risk ( $4.30 \times 10^{-4}$ ) associated with the ingestion of  $10 \mu\text{g As L}^{-1}$  water. Brazil defines the tolerable risk for carcinogenic substances to human health as the probability of one additional case of cancer in an exposed population of 100,000 individuals ( $1 \times 10^{-5}$ ). It is worthy to note that even in the most conservative, unlikely scenario (A2) of maximum As BAC and continuous exposure, the calculated risk associated with soil ingestion is lower than that prescribed by both the Brazilian legislation and WHO for drinking water.

There is an ongoing debate related to the use of CSF and benchmark dose lower limit (BMDL). The derivation of BMDL does not assume that arsenic-induced cancers are non-threshold as the IRIS (Integrated Risk Information System) cancer slope factor does. The inorganic arsenic lower limit on the benchmark dose (BMDL<sub>0.5</sub>) for a 0.5% increased incidence of lung cancer was calculated to be  $3 \mu\text{g kg}^{-1} \text{ b.w. per day}$  with a margin of exposure (MOE) of approximately 10 (range:  $2\text{--}7 \mu\text{g kg}^{-1} \text{ b.w. per day}$  with MOE of 30 to 1) using a range of assumptions to estimate total dietary exposure to inorganic arsenic from drinking water and food (JECFA, 2011). There is significant evidence from international studies confirming that the BMDL approach adopted by WHO and JECFA (2011) is more realistic and appropriate than the US EPA linear dose relationship approach for setting the As Cancer Slope Factors (CSF) for oral ingestion and inhalation respectively for risk assessment calculations (USEPA, 1995).

The combined risks as well as the contribution of each source of exposure are also calculated for the combined intake of soil, food and water (Table IV.10). The data for food and water were taken from a recent publication of our group (Ciminelli et al., 2017) applied to the study region. When water and food intake are taken into consideration, the total intake increases from  $0.0033 \mu\text{g kg}^{-1} \text{ b.w. day}^{-1}$  (soil only in scenario A1) to  $0.1973 \mu\text{g.kg}^{-1} \text{ b.w.day}^{-1}$  (soil + water + food) and from  $0.0157 \mu\text{g kg}^{-1} \text{ b.w. day}^{-1}$  (soil only in scenario A2) to  $0.2097 \mu\text{g kg}^{-1} \text{ b.w.day}^{-1}$ , with food being the main source of exposure. Under these

scenarios, the calculated risks are of the same order of magnitude compared to that of drinking  $10 \mu\text{g As L}^{-1}$  water. However, the contributions of soil to the total daily As intake remain very low (1.7% for A1 and 7.5% for A2).

The As exposure from soil only or from combined soil, food and water intake is less than 10% of  $\text{BMDL}_{0.5}$ , and therefore we argue that the associated risk to human health for the local population can consider being low. This conclusion is further supported by the fact that  $\text{BMDL}_{0.5}$  of  $3 \mu\text{gkg}^{-1}$  b.w. per day (that is, more than an order of magnitude higher than that calculated under the worst-case scenario for the combined soil, food and water intake) has a safety factor of 10 (MOE), which is derived from an epidemiology study conducted on a population exposed to high levels of arsenic and whose nutritional status might have been compromised (JECFA, 2011).

#### 4.4 Conclusions

Soil samples collected in a gold mining district in Minas Gerais were investigated to establish their As content, the mineralogy of the As-bearing particles and the potential risk to human health posed by their ingestion. The median arsenic concentration in the high arsenic (H-As) bulk samples was  $1947 \text{ mg kg}^{-1}$ . The bioaccessible As in the H-As samples ranged from  $0.86 \text{ mg kg}^{-1}$  to  $22 \text{ mg kg}^{-1}$  with a mean of  $7.53 \text{ mg kg}^{-1}$  and a median value of  $4.60 \text{ mg kg}^{-1}$ . The As BAC ranged from 0.3% to 5.0%, with a mean of 1.4% and a median of 0.9%. For the low arsenic samples (L-As), bioaccessible As varied between 0.22 and  $0.69 \text{ mg kg}^{-1}$  with mean of  $0.44 \text{ mg L}^{-1}$  and median value of  $0.42 \text{ mg kg}^{-1}$ . The As BAC ranged from 0.9% to 6.5%, with a mean of 2.7% and a median of 2.4%.

Large variations in the content of Fe-(hydr)oxides (from approx. 1% to 45%) was observed. In general, the concentration of arsenic increased with the increase of the Fe-(hydr)oxides content. This observation was consistent with the As-enrichment in the coarse particle size fractions. Arsenic was mainly found in iron (hydr)oxides in fine association with phyllosilicates. Only a few arsenopyrite (e.g., 7 out of approximately 74,000 particles) and scorodite particles (e.g., 9 out of approximately 74,000 particles) were identified. Arsenic was fixed in the oriented aggregates of crystalline Fe-(hydr-)oxides nanoparticles. The calculated As exposure from soil only, or from a combined soil, food and water intake, was less than 10% of the Benchmark Dose Lower Limit -  $\text{BMDL}_{0.5}$ . Therefore, the risk to human health for the local population from the ingestion of these



soils is considered to be low. The form of arsenic in association with the iron (hydr)oxides nanoparticles further substantiates the stability data of As-bearing phases and the low potential risk to human health.

## 5. CONCLUSIONS

Concentrations of arsenic up to  $6354 \text{ mg kg}^{-1}$  in soil samples ( $< 2\text{mm}$ ) were detected in soil samples collected in a region close to a mining site where gold is found in association with arsenopyrite. The samples constituents are mainly silicates (quartz and muscovite) according to X-ray diffraction (XRD) analyses. Hematite and goethite are the Fe-(hydr)oxides identified by XRD, Raman, and scanning (SEM) and transmission electron microscopy (TEM) analyses. The Raman spectra of these minerals presented features suggesting the presence of substitution atoms or contaminant species. The phase transformation of goethite to hematite is also indicated. The increase in BET specific surface areas showed a good correlation with the aluminum soluble in *Aqua regia*. Among the minor constituents of environmental concern identified by Inductively coupled plasma optical emission spectroscopy, only As showed concentrations significantly higher (median of  $748.0 \text{ mg kg}^{-1}$ , including high As concentration and low As concentration soils in fraction  $< 2\text{mm}$ ) than the guideline values established by the local legislation for As concentration in soils. According to the chemical analysis, an As-enrichment in the coarse fractions associated to Fe-enrichment was observed. For high As concentration soils, the mean bioaccessible As is  $7.5 \text{ mg kg}^{-1}$  (median of  $4.6 \text{ mg kg}^{-1}$ ); percent As bioaccessible has a mean value of 1.4% (median of 0.9%).

Quantitative, single particle identification of As-bearing phases by the Mineral Liberation Analyser showed that arsenic is mainly found in iron (hydr)oxides–phyllosilicates mixture. Few arsenopyrite (e.g. 7 out of approx. 74,000 particles) and scorodite particles (e.g., 9 out of approx. 74,000) were identified. Arsenic was shown to be trapped in oriented aggregates of crystalline Fe-(hydr)oxides nanoparticles by TEM, in a pattern that supports the large difference between As concentration and the bioaccessible arsenic. The unambiguously and precise identification of As association with crystalline nanoparticles of Fe-(hydr)oxides supports the low As bioaccessibility reported here. Furthermore, the observed intergrowth of the Fe-(hydr)oxides with mica (muscovite mainly) adds additional constrain to As release/mobilization, as both group of minerals are insoluble in the extraction solution and stable under broad environmental conditions.

## 6. REFERENCES

- Alam, M.S., Wu, Y. & Cheng, T. (2014) **Silicate minerals as a source of arsenic contamination in groundwater**. *Water, air, and soil pollution*, vol. 225, no. 11.
- Andrade, R.P., Figueiredo, B.R., Mello, J.W.V., Santos, J.C.Z. & Zandonadi, L.U. (2008) **Control of geochemical mobility of arsenic by liming in materials subjected to acid mine drainage**. *Journal of Soils and Sediments*, vol. 8, pp.123–129.
- Andrade, R.P.A; Mello, J.W.V.; W, C.C.; Silva, J.B.B. & Figueiredo, B.R. (2012) **Evaluation of arsenic availability in sulfidic materials from gold mining areas in Brazil**. *Water, Air and Soil Pollution*, vol. 223, pp. 4679-4686.
- Anonymous (2009) **CONAMA 420/2009** - CONAMA – CONSELHO NACIONAL DO MEIO AMBIENTE – Resolution no. 420/2009, of December 28, 2009. Provides criteria and guiding values of soil quality for the presence of chemical substances and establishes guidelines for the environmental management of areas contaminated by these substances as a result of anthropic activities. Brasilia DF (*in portuguese*).
- ATSDR (Agency for Toxic Substances and Disease Registry) (2007). **Public Health Statement for Arsenic**. **Toxic Substances Portal - Arsenic U. S. Department of Health and Human Services**, Public Health Service. Atlanta, GA. <http://www.atsdr.cdc.gov/phs/phs.asp?id=18&tid=3>, (accessed 11.14.16).
- Bagla, P. & Kaiser, J. (1996) **India's spreading health crisis draws global arsenic experts**. *Science*, vol. 274, no. 5285, pp. 174-175.
- Bradham, K.D., Scheckel, K.G., Nelson, C.M., Seales, P.E., Lee, G.E., Hughes, M.F., Miller, B.W., Yeow, A., Gilmore, T., Serda, S.M., Harper, S. & Thomas, D.J. (2011) **Relative bioavailability and bioaccessibility and speciation of arsenic in contaminated soils**. *Environmental health perspectives*, vol. 119, no. 11, pp. 1629-1634.
- Brown, G., Foster, A.L., Ostergren, J. D.(1999). **Mineral surfaces and Bioavailability of heavy metals: a molecular-scale perspective**. *Proc. Natl. Acad. Sci. USA*. 96, pp.3388-3395.
- Caetano, M.L., Ciminelli, V.S.T., Rocha, S.D.F. Spitale, M.C.& Caldeira, C.L. (2009). **Batch and Continuous Precipitation of Scorodite from Diluted Industrial Solutions**. *Hydrometallurgy*, vol. 95, pp. 44-52.

- Campbell, K.M. & Nordstrom, D.K. (2014). **Arsenic speciation and sorption in natural environments**. Reviews in Mineralogy & Geochemistry, vol., 79, pp. 185-216.
- Ciminelli, V.S.T. (2014). **Arsenic in mining: sources and stability** In: 5th International Congress on Arsenic in the Environment - As 2014, Buenos Aires. One Century of the Discovery of Arsenicosis in Latin America (1914-2014). London: Taylor & Francis Group, pp. 3-7.
- Ciminelli, V.S.T., Gasparon, M., Ng, J.C., Silva, G.C. & Caldeira, C.L. (2017) **Dietary arsenic exposure in Brazil: The contribution of rice and beans**. Chemosphere, vol. 168, pp. 996-1003.
- Cullen, W.R. & Reimer, K.J. (1989). **Arsenic speciation in the environment**. Chemical reviews, vol. 89, no. 4, pp. 713-764.
- Das, S. & Hendry, M.J. (2011). **Application of Raman spectroscopy to identify iron minerals commonly found in mine wastes**. Chemical Geology, vol. 290, no. 3-4, pp. 101-108.
- De Miguel, E.; Mingot, J.; Chacón, E. & Charlesworth, S. (2012) **The relationship between soil geochemistry and the bioaccessibility of trace elements in playground soil**. Environmental Geochemistry Health, vol. 34, pp.77-687.
- De Vicq, R., Matschullat, J., Leite, M.G.P., Nalini Junior, H.A. & Mendonça, F.P.C. (2015) **Iron Quadrangle stream sediments, Brazil: geochemical maps and reference values**. Environmental Earth Sciences, vol. 74, no. 5, pp. 4407-4417.
- Delbem, I.D; Galéry, R.; Brandão, P.R.G.& Peres, A.E.C. (2015) **Semi-automated iron ore characterisation based on optical microscope analysis: Quartz/resin classification**. Minerals Engineering, vol. 82, pp. 2-13.
- Deschamps, E., Ciminelli, V.S.T., Frank, L.F.T., Matschullat, J., Raue, B. & Schmidt, H., (2002). **Soil and sediment geochemistry of the Iron Quadrangle, Brazil: the case of arsenic**. Journal Soils Sediments, vol. 2, pp. 216–222.
- Dionísio, A.G.G., Gonzalez, M.H. & Nobrega, J.A. (2011). **Determination of arsenic in samples of the productive chain of broilers by atomic absorption spectrometry with graphite furnace (in portuguese)**. Quim. Nova, vol. 34, no 1, pp.49-52.
- Duarte, G., Ciminelli, V.S.T., Dantas, M.S.S., Duarte, H.A., Vasconcelos, I.F., Oliveira, A.F. & Osseo-Asare, K. (2012). **As(III) immobilization on gibbsite: Investigation of the complexation mechanism by combining EXAFS**

- analyses and DFT calculations.** *Geochimica et Cosmochimica Acta*, vol. 83, pp. 205-216.
- Fandrich, R.; Gu, Y.; Burrows, D.; Moeller, K. (2007) **Modern SEM-based mineral liberation analysis.** *International Journal of Mineral Processing*, vol.84, pp. 310 – 320.
- Faria, D.L.A., Venâncio Silva, S. & De Oliveira, M.T. (1997). **Raman microspectroscopy of some iron oxides and oxyhydroxides.** *Journal of Raman Spectroscopy*, vol. 28, no. 11, pp. 873-878.
- FEAM (2013) **Manual of soil collection for reference values of quality in the state of Minas Gerais.** (*in portuguese*) 19 p.
- Flanagan, S.V., Johnston, R.B. & Zheng, Y. (2012) **Arsenic in tube well water in Bangladesh: Health and economic impacts and implications for arsenic mitigation.** *Bulletin of the World Health Organization*, vol. 90, n. 11, pp. 839-846.
- Foster, A.L., Brown, Jr. G.E., Tingle, T.N., Parks, G.A. (1998) **Quantitative As speciation in mine tailings using X-ray absorption spectroscopy.** *American Mineralogist*, vol. 83, pp.553-568.
- Freitas, E.T.F., Montoro, L.A., Gasparon, M. & Ciminelli, V.S.T. (2015) **Natural attenuation of arsenic in the environment by immobilization in nanostructured hematite.** *Chemosphere*, vol. 138, pp. 340–347.
- Gasparon, M.; Delbem, I.D.; Elmes, M & Ciminelli, V.S.T (2016) **Detection and analysis of arsenic-bearing particles in atmospheric dust using Mineral Liberation Analysis in Arsenic Research and Global Sustainability: Proceedings of the Sixth International Congress on Arsenic in the Environment (As2016), June 19-23, 2016, Stockholm, Sweden, pp. 217-218.**
- Gialanella, S., Girardi, F., Ischia, G., Lonardelli, I., Mattarelli, M. & Montagna, M. (2010) **On the goethite to hematite phase transformation.** *Journal of Thermal Analysis and Calorimetry*, vol. 102, no. 3, pp. 867-873.
- Gonzales, P., Felix, O., Alexander, C., Lutz, E., Ela, W. & Eduardo Sáez, A. (2014) **Laboratory dust generation and size-dependent characterization of metal and metalloid-contaminated mine tailings deposits.** *Journal of Hazardous Materials*, vol. 280, pp. 619-626.
- Gu, Y. (2003). **Automated scanning electron microscope based mineral liberation analysis.** *Journal of Minerals and Materials Characterization and Engineering*, vol. 2, pp. 33-41.

- IARC (International Agency for Research on Cancer), (2012). **Monographs on the Evaluation of Carcinogenic Risks to Humans**. IARC Monographs, Volume 100 (C). International Agency for Research on Cancer, Lyon, France.
- ISO 5725 (1994) **Precision of test methods**.
- IUPAC (2014) **Compendium of chemical terminology – Gold book**. Compiled by McNaught, A.D. & Wilkinson, A. Version 2.3.3, 1622 p.
- Jamieson, H.E., Walker, S.R.; Parsons, M.B. (2015). **Mineralogical characterization of mine waste**. Applied Geochemistry, vol. 57, pp. 85-105.
- JECFA (Joint FAO/WHO Expert Committee on Food Additives) (2011). **Evaluation of Certain Contaminants in Food**. The seventy-second report, WHO, pp. 1-115.
- Juhasz, A. L., E. Smith, J. Weber, R. Naidu, M. Rees, A. Rofe, T. Kuchel & L. Sansom (2009). **Assessment of four commonly employed in vitro arsenic bioaccessibility assays for predicting in vivo arsenic bioavailability in contaminated Soils**. Environmental Science and Technology, vol. 43, pp. 9487-9494.
- Juhasz, A. L., Smith, E. Weber, J., Rees, M., Rofe, A., Kuchel, T., Sansom, L. & Naidu, R. (2007). **In vitro assessment of arsenic bioaccessibility in contaminated (anthropogenic and geogenic) soils**. Chemosphere, vol., 69, pp.69-78.
- Juhasz, A.L., Herde, P., Herde, C., Boland, J. & Smith, E. (2015). **Predicting Arsenic Relative Bioavailability Using Multiple *in-vitro* Assays: Validation of in Vivo-in Vitro Correlations**. Environmental Science and Technology, vol. 49, no. 18, pp. 11167-11175.
- Kim, E.J.; Yoo, J.C; Baek, K. (2014) **Arsenic speciation and bioaccessibility in arsenic-contaminated soils: sequential extraction and mineralogical investigation**. Environmental Pollution, vol.186, pp. 29-35.
- Kinross (2017). Available in [http://www.kinross.com.br/paracatu.php?id\\_category=11](http://www.kinross.com.br/paracatu.php?id_category=11). accessed 15.01.17.
- Koch, I.; Sylvester, S.; M.Lai, V.W.; Owen, A.; Reimer, K.J. & Cullen, W.R. (2007) **Bioaccessibility and excretion of arsenic in Niu Huang Jie Du Pian pills**. Toxicology and Applied Pharmacology, vol. 222, pp. 357 – 364.
- Krause, E. and Ettl, V. A. (1989). **Solubility and stabilities of ferric arsenate compounds**. Hydrometallurgy, 22, 311-337.

- Kumar, S. (1997). **Widescale arsenic poisoning found in South Asia**. The Lancet, vol. 349, pp. 1378.
- Ladeira, A.C.Q.; Ciminelli, V.S.T; Alves, M.C.M. & Duarte, H.A. (2001). **Mechanism of anion retention from EXAFS and Density Functional Calculations: Arsenic (V) adsorbed on Gibbsite**. Geochim. and Cosmochim. Acta, vol. 65, no 8, pp. 1211-1217.
- Ladeira, A.C.Q.; Ciminelli, V.S.T; Alves, M.C.M. & Duarte, H.A. (2001). **Mechanism of anion retention from EXAFS and Density Functional Calculations: Arsenic (V) adsorbed on Gibbsite**. Geochim. and Cosmochim. Acta, vol. 65, no 8, pp. 1211-1217.
- Landrot, G., Tappero, R., Webb, S.M. & Sparks, D.L. (2012). **Arsenic and chromium speciation in an urban contaminated soil**. Chemosphere, vol. 88, pp. 1196–120.
- Lehninger, A.L.; Nelson, D.L.; Cox, M.M. (1995) **Principles of biochemistry**. 2<sup>nd</sup> Edition, 839p.
- Liu, H., Chen, T., Zou, X., Qing, C. & Frost, R.L. (2013). **Effect of Al content on the structure of Al-substituted goethite: A micro-Raman spectroscopic study**. Journal of Raman Spectroscopy, vol. 44, no. 11, pp. 1609-1614.
- Lowell, S., Shields, J.E., Thomas, M.A. & Thommes, M. (2004) **Characterization of Porous Solids and Powders: Surface Area, Pore Size and Density**. Springer Science, 339 p.
- Mandal, B.K.; Suzuki, K.T. (2002) **Arsenic round the world: a review**. Talanta, vol. 58, pp. 201-235.
- Massey, M. J.; Baier, U.; Merlin, R. and Weber, W. H. (1990). **Effects of pressure and isotopic substitution on the Raman spectrum of alpha-Fe<sub>2</sub>O<sub>3</sub>: Identification of two-magnon scattering**. Physical Review B, vol. 41, pp. 7822-7827.
- Matschullat, J. (2000) **Arsenic in the geosphere – a review**. The science of the total environment, vol. 249, pp. 297-312.
- Mello, J.W.V.; Roy, W.R.; Talbott, J.L.; Scott, J.; Stucki, J.W. (2006) **Mineralogy and arsenic mobility in arsenic-rich Brazilian soils and sediments**. Journal of Soils and Sediments, vol.6, pp.9–19.
- Meunier, L.; Walker, S.R.; Wragg, J.; Parsons, M.B.; Koch, I.; Jamieson, H.E. & Reimer, K.J. (2010) **Effects of soils composition and mineralogy on the bioaccessibility of arsenic from tailings and soil in gold mine districts of**

**Nova Scotia.** Environmental Science & Technology, v.44, no, 7, pp. 2667-2674.

**Ministry of Health (2010).** Guidelines for Evaluation of Risks to Human Health from Exposure to Chemical Contaminants (*in portuguese*). Available in <[http://www.saude.rs.gov.br/upload/1347884770\\_Avaliacao%20de%20Risco%20-%20Diretrizes.pdf](http://www.saude.rs.gov.br/upload/1347884770_Avaliacao%20de%20Risco%20-%20Diretrizes.pdf)>, accessed 17.02.17.

Monsanto (2017). Available in <<http://www.monsanto.com/global/br/noticias/pages/monsanto-lanca-primeiro-livro-de-projeto-nacional.aspx>>, accessed 15.01.17.

Müller, K., Ciminelli, V.S.T., Dantas, M.S.S. & Willscher, S. (2010). **A comparative study of As(III) and As(V) in aqueous solutions and adsorbed on iron oxyhydroxides by Raman spectroscopy.** Water research, vol. 44, no. 19, pp. 5660-5672.

Naidu, R., Channey, R., McConnell, S., Johnston, N., Semple, K.T., McGrath, S., Dries, V., Nathanail, P., Harmsen, J., Pruszinski, A., MacMillan, J. & Palanisami, T. (2015) **Towards bioavailability-based soil criteria: past, present and future perspectives.** Environmental Science and Pollution Research, vol. 22, no. 12, pp. 8779-8785.

Navarro, M.C.; Pérez-Sirvent, C.; Martínez-Sánchez, Vidal, J. & Marimón, J. (2006) **Lead, cadmium and arsenic bioavailability in the abandoned mine site of Cabezo Rajao (Murcia, SE Spain).** Chemosphere, vol. 63, pp. 484-489.

Ng, J.C., Gasparon, M., Silva, G.C. & Ciminelli, V.S.T. (2014) **Health risk assessment of arsenic near a gold mine in Brazil - One Century of the Discovery of Arsenicosis in Latin America (1914-2014): As 2014 - Proceedings of the 5th International Congress on Arsenic in the Environment**, pp. 607.

Ng, J.C., Juhasz, A.L., Smith, E. & Naidu, R. (2010). Contaminant bioavailability and bioaccessibility: Part 1. Scientific and Technical Review. CRC CARE Technical Report 14.CRC for Contamination Assessment and Remediation of the Environment, Adelaide, Australia.74 p.

Ng, J.C.; Juhasz, A.; Smith, E. & Naidu, R. (2015) **Assessing the bioavailability and bioaccessibility of metals and metalloids.** Environmental Science and Pollution Research, vol. 12, pp. 8802-8825.

Ng., J.C.; Wang, J.; SHRAIM, A. (2003) **A global health problem caused by arsenic from natural sources.** Chemosphere, vol. 52, pp. 1353-1359.



- Nickson, R., McArthur, J., Burgess, W., Matin Ahmed, K., Ravenscroft, P. & Rahman, M. (1998). **Arsenic poisoning of Bangladesh groundwater**. *Nature*, vol. 395, no. 6700, pp. 338.
- Nordstrom, D.K. (2002) **Worldwide occurrences of arsenic in ground water**. *Science*, vol.296, pp. 2143-2145.
- Ono, F.B., Tappero, R., Sparks, D. & Guilherme, L.R.G. (2015) **Investigation of arsenic species in tailings and windblown dust from a gold mining area**. *Environmental Science and Pollution Research*, vol. 23, no. 1, pp. 638-647.
- Ono, F.B.; Guilherme, L.R.G.; Penido, E.S.; Carvalho, G.S.; Hale,B.; Toujaguez,R. & Bundschuh, J. (2012) **Arsenic bioaccessibility in a gold mining area: a health risk assessment for children**. *Environmental Geochemistry Health*, vol.34, pp. 457-465.
- Palumbo-Roe, B., Wragg, J. & Cave, M. (2015) **Linking selective chemical extraction of iron oxyhydroxides to arsenic bioaccessibility in soil**. *Environmental Pollution*, vol. 207, pp. 256-265.
- Paye, H.S., de Mello, J.W.V. & de Melo, S.B. (2012). **Multivariate analysis methods for the establishment of background levels of trace elements in soils of Brazil**. *Revista Brasileira de Ciencia do Solo*, vol. 36, no. 3, pp. 1031-1041.
- Redwan, M., Rammlmair, D. & Meima, J.A. (2012). **Application of mineral liberation analysis in studying micro-sedimentological structures within sulfide mine tailings and their effect on hardpan formation**, *Science of the Total Environment*, vol. 414, pp. 480-493.
- Reimann, C., Matschullat, J., Birke, M. & Salminen, R. (2009). **Arsenic distribution in the environment: The effects of scale**. *Applied Geochemistry*, vol. 24, no. 7, pp. 1147-1167.
- Rezende, P.S.; Costa, L.M. & Windmöller, C.C. (2015) **Arsenic mobility in sediments from Paracatu river basin, MG, Brazil**. *Archives of Environmental Contamination and Toxicology*, vol. 68, pp. 588-602.
- Riveros, P.A., Dutrizac, J.E.& Spencer, P. (2001). **Arsenic disposal practices in the metallurgical industry**. *Canadian Metallurgical Quarterly*, vol. 40, no. 4, pp.395-420.
- Ruby, M.V.; Schoof, R.; Brattin, W.; Goldade, M.; Post, G.; Harnois, M.; Mosby, D.E.; Casteel, S.W.; Berti, W.; Carpenter, M.; Edwards, D.; Cragin, D & Chappell, W. (1999) **Advances in evaluating the oral bioavailability of inorganics in soil for use in human health risk assessment**. *Environmental Science & Technology*, vol.33, nº, 21, pp. 3697-3705.

- SBRC (2001) **Standard operating procedure: *in vitro* method for determination of lead and arsenic bioaccessibility.** Solubility/bioavailability research consortium, 19p.
- SENAI/FIEMG -Serviço Nacional de Aprendizagem Industrial (2014). **Assessment of Soil Quality in the Ribeirão Santa Rita and Córrego Rico watershed (*in portuguese*).** 125 p. (report)
- Serrano, S., Gomez-Gonzalez, M.A., O'Day, P.A., Laborda, F., Bolea, E. & Garrido, F. (2015) **Arsenic speciation in the dispersible colloidal fraction of soils from a mine-impacted creek.** Journal of hazardous materials, vol. 286, pp. 30-40.
- Silva, J., Mello, J. W. V.; Gasparon, M.; Abrahão, W.A.P.; Ciminelli, V.S.T. & Jong, T. (2010). **The role of Al- Goethites on arsenate mobility.** Water Research (Oxford), vol. 2, pp. 10-16.
- Silvetti, M.; Castaldi, P.; Holm, P.E.; Deiana, S.; Lombi, E. (2014) **Leachability, bioaccessibility and plant availability of trace elements in contaminated soils treated with industrial by-products and subjected to oxidative/reductive conditions.** Geoderma, vol. 214-215, pp. 204-212.
- Smedley, P.L. & Kinniburgh, D.G. (2002) **A review of the source, behaviour and distribution of arsenic in natural waters.** Applied Geochemistry, vol. 17, pp. 517-568.
- Smith, E., Weber, J. & Juhasz, A.L. (2009). **Arsenic distribution and bioaccessibility across particle fractions in historically soils.** Environmental Geochemistry and Health, vol 31, pp.85-92.
- Sowers, T.D., Harrington, J.M., Polizzotto, M.L. & Duckworth, O.W. (2017) **Sorption of arsenic to biogenic iron(oxyhydr)oxides produced in circumneutral environments.** Geochimica et Cosmochimica Acta, vol. 198, pp. 194-207.
- Suryanarayana, C. & Norton, M.G. (1998) **X-Ray Diffraction – Pratical Approach.** New York, Springer, Science 275 p.
- Sylvester, P.J. (2012). **Use of the Mineral Liberation Analyzer (MLA) for mineralogical studies of sediments and sedimentary rocks.** Mineral. Assoc. Can. Short Course, vol. 42, pp. 1-16.
- Toujaguez, R., Ono, F.B., Martins, V., Cabrera, P.P., Blanco, A.V., Bundschuh, J. & Guilherme, L.R.G. (2013). **Arsenic bioaccessibility in gold mine tailings of Delita, Cuba.** Journal of hazardous materials, vol. 262, pp. 1004-1013.

- USEPA - United States Environmental Protection Agency (2013) **Regional Screening Table - User's Guide (May 2013) Mid-Atlantic Risk Assessment** [www.epa.gov/reg3hwmd/risk/human/rb-concentration\\_table/usersguide.htm](http://www.epa.gov/reg3hwmd/risk/human/rb-concentration_table/usersguide.htm), accessed 17.02.17
- USEPA (1992). **Preparation of soil sampling protocols: sampling techniques and strategies.** 169 p.
- USEPA (1992). **Preparation of soil sampling protocols: sampling techniques and strategies.** 169p.
- USEPA (1995). **Integrated Risk Information System (IRIS) National Center for Environmental Assessment.** Arsenic, inorganic (CASRN-7440-38-2), Available in [https://cfpub.epa.gov/ncea/iris/iris\\_documents/documents/subst/0278\\_summary.pdf](https://cfpub.epa.gov/ncea/iris/iris_documents/documents/subst/0278_summary.pdf), (accessed 02.17. 17).
- [/iris\\_documents/documents/subst/0278\\_summary.pdf](https://cfpub.epa.gov/ncea/iris/iris_documents/documents/subst/0278_summary.pdf), (accessed 02.17. 17).
- USEPA (1996) **Soil Screening Guidance: User's Guide.** 89p.
- USEPA (2007a) **Microwave assisted acid digestion of sediments, sludges, soils and oils - Method 3051a.** Revision 1,30p.
- USEPA (2007b). **Estimation of relative bioavailability of lead in soil and soil-like materials using in vivo and in vitro methods.** USEPA OSWER 9285.7-77, Office of Solid Waste and Emergency Response U.S. Environmental Protection Agency, Washington, DC 20460.
- USEPA (2012a) **Standard operating procedure: *in vitro* method for determination of lead and arsenic bioaccessibility.** 16p.
- USEPA (2012b) **Validation of an *in vitro* bioaccessibility test method for estimation of bioavailability of arsenic from soil and sediment.** Final Report, ESTCP Project ER-200916, 277p.
- Vallejuelo, S.F., Madariaga, J.M., Gredilla, A., da Boit, K., Sampaio, C.H., Teixeira, E.C., Silva, L.F.O., Silva, L.F.O. & Silva, L.F.O. (2017) **Nanominerals and potentially hazardous elements from coal cleaning rejects of abandoned mines: Environmental impact and risk assessment.** Chemosphere, vol. 169, pp. 725-733.
- Veen, E.M., Lottermoser, B.G., Parbhakar-Fox, A., Fox, N. & Hunt, J. (2016) **A new test for plant bioaccessibility in sulphidic wastes and soils: A case study from the Wheal Maid historic tailings repository in Cornwall, UK.** Science of the Total Environment, vol 563-564, pp. 835-844.

- VMetais (2017). Available in <<http://www.vmetais.com.br/pt-BR/Negocios/Zinco/Paginas/UnidadesProdutivas.aspx>, accessed 15.01.17.
- Wester, R.C.; Huix.; Barbadillo, S.; Maibach, H.; Lowney, Y.W.; Schoof, R.A.; Holm, S.E. & Ruby, M.V. (2004) ***In Vivo* percutaneous absorption of arsenic from water and CCA-Treated wood Residue**. Toxicological sciences, vol. 79, pp. 287-295.
- WHO (2000) **Air Quality Guidelines for Europe**. Second Edition, 273 p.
- WHO (2011) **Arsenic in drinking-water – Background document for development of WHO guidelines for drinking-water quality**. Rev 1, 24 p.
- Williams, D.B. & Carter, C.B. (2009) **Transmission electron microscopy: A textbook for materials science**, 760 p.
- Xia Q., Peng, C., Lamb, D. & Ng, J.C. (2017). **Interaction effects of As, Cd and Pb on their respective bioaccessibility with time in co-contaminated soils assessed by the Unified BARGE Method**. Environmental Science and Pollution Research, vol 24, pp. 5585-5594.
- Xia Q., Peng, C., Lamb, D., Mallavarapu, M., Naidu, R. & Ng, J.C. (2016). **Bioaccessibility of arsenic and cadmium assessed for in vitro bioaccessibility in spiked soils and their interaction during the Unified BARGE Method (UBM) extraction**. Chemosphere, vol 147, pp 444-450.
- Yin, N., Du, H., Zhang, Z., Cai, X., Li, Z., Sun, G. & Cui, Y. (2016). **Variability of arsenic bioaccessibility and metabolism in soils by human gut microbiota using different in vitro methods combined with SHIME**. Science of the Total Environment, vol. 566-567, pp. 1670-1677.

**APPENDIX I – Quality control and quality assured**

**Table A.I.1.** Quality control results for the reference materials NIST 2710a and CANMET-Till-3

Samples	Al (%)	Fe (%)	As	Cd	Co	Cr	Cu (mg kg <sup>-1</sup> )	Ni	Pb	Zn
SRM NIST 2710 a										
Measured (n=7)	1.6±0.4	3.8±0.3	1556.9±88.2	10.1±1.4	6.8±5.4	14.1±2.4	3238.8±223.1	6.9±1.6	5143.9±392.1	3596.4±304.0
Certified values	5.95	4.32	1540	12.3	5.99	----	3420	----	5520	4180
Recovery (%)	26	88	101	82	114	----	95	----	93	86
CANMET Till- 3										
Measured (n=10)	1.3±0.2	2.2±0.2	70.2±22.4	<0.02	13.8±2.8	65.6±10.9	19.3±2.3	33.8±6.5	18.7±5.8	37.3±5.0
Certified values	1.20	2.10	84	<0.35	14.8	64.7	16.5	26.5	23	42.7
Recovery (%)	108	105	84	-----	93	101	117	127	81	87

**Table A.I.2:** Quality control results for the reference materials analyzed by LECO (n=4)

Samples	Measured (%)		Certified values (%)		Recovery (%)	
	S	C	S	C	S	C
LECO standards						
502-318	lot					
1009		3.25	0.36	3.22	0.36	101
502-319	lot					
1014		1.65	1.93	1.66	1.96	100
502-320	lot					
411B		4.2	4.13	4.07	4.19	103
CANMET materials						
kzk-1		0.79	0.93	0.8	0.95	99
MP-1b		15.07	<0.1	13.79	0.028	109
RTS-3a		10.45	<0.1	9.59	0.04	109

Detection limit (DL): C <0.1% and S <0.01%.

**APPENDIX. II - XRD Pattern of soil samples (< 2mm)**

**Table AII.1** XRD Pattern of soil samples (< 2mm) - Subtitles

Mineral Phase	Symbol	ICDD card	Chemical formula
Quartz	Q	88-2302	SiO <sub>2</sub>
Muscovite	M	07-0042	(K,Na)(Al,Mg,Fe) <sub>2</sub> (Si <sub>3.1</sub> Al <sub>0.9</sub> )O <sub>10</sub> (OH) <sub>2</sub>
Kaolinite	K	80-0886	Al <sub>2</sub> Si <sub>2</sub> O <sub>5</sub> (OH) <sub>4</sub>
Feldspar	F	41-1486	(Na,Ca)Al(Si,Al) <sub>3</sub> O <sub>8</sub>
Goethite	Gt	81-0463	FeOOH
Hematite	Hm	87-1166	Fe <sub>2</sub> O <sub>3</sub>
Pyroxene	P	86-0005	(Mg <sub>0.944</sub> Fe <sub>0.056</sub> )(Ca <sub>0.844</sub> Na <sub>0.156</sub> Fe <sub>0.014</sub> )(Si <sub>2</sub> O <sub>6</sub> )
Gibbsite	Gb	74-1775	Al(OH) <sub>3</sub>

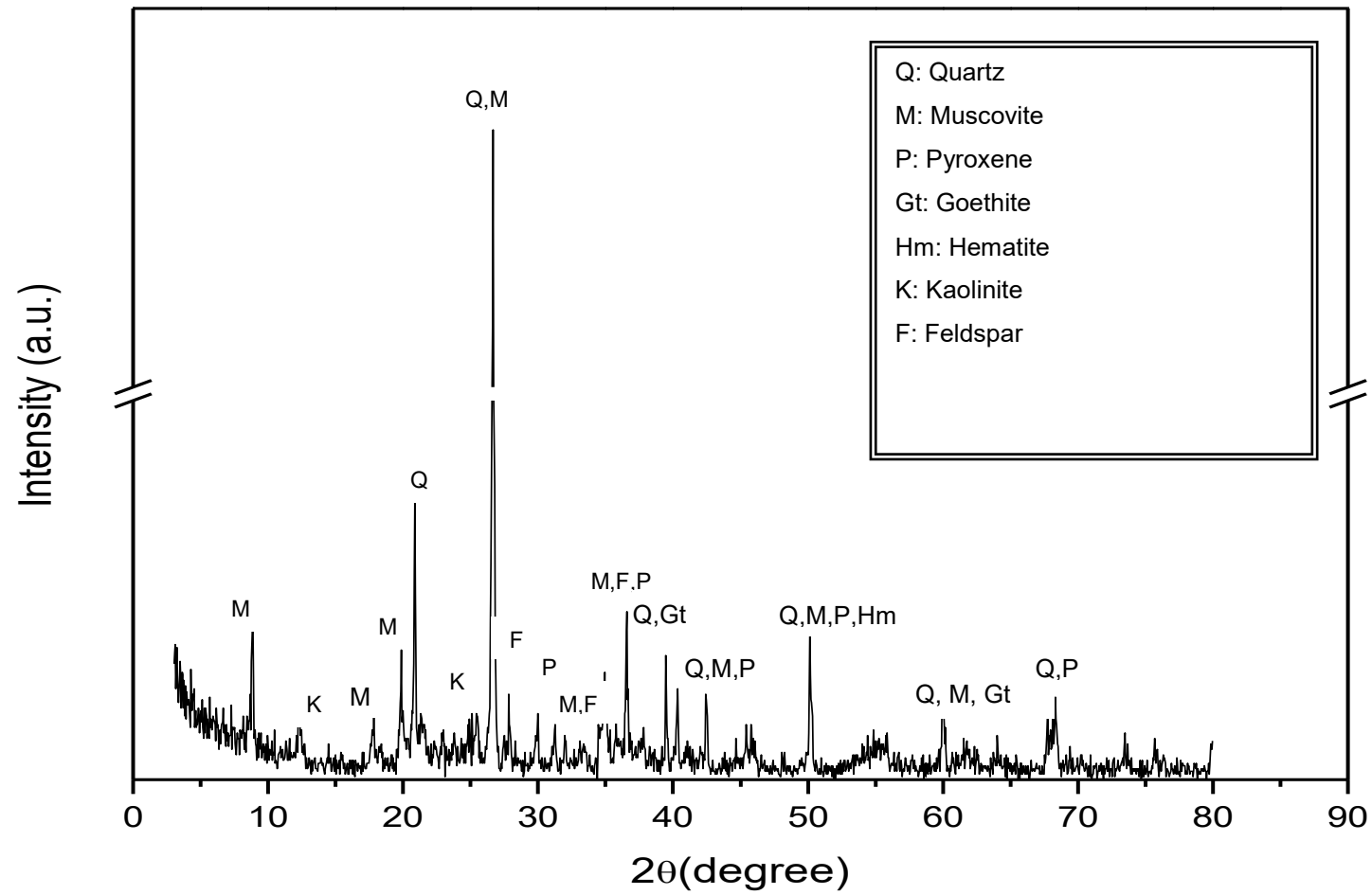


Figure AII.1: Powder X-ray diffraction patterns for soil sample K03 (< 2mm).



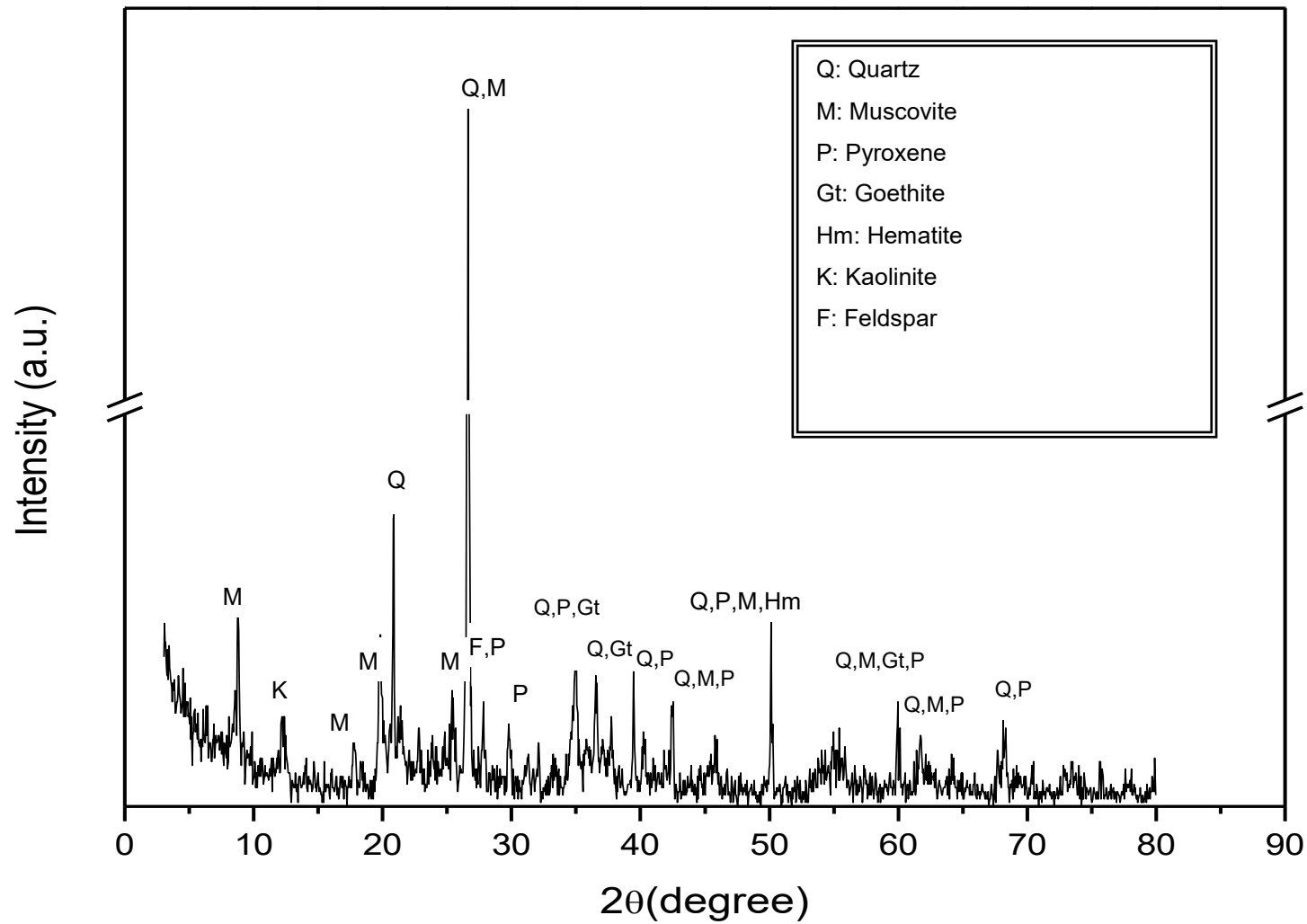


Figure AII.2: Powder X-ray diffraction patterns for soil sample K06 (< 2mm).

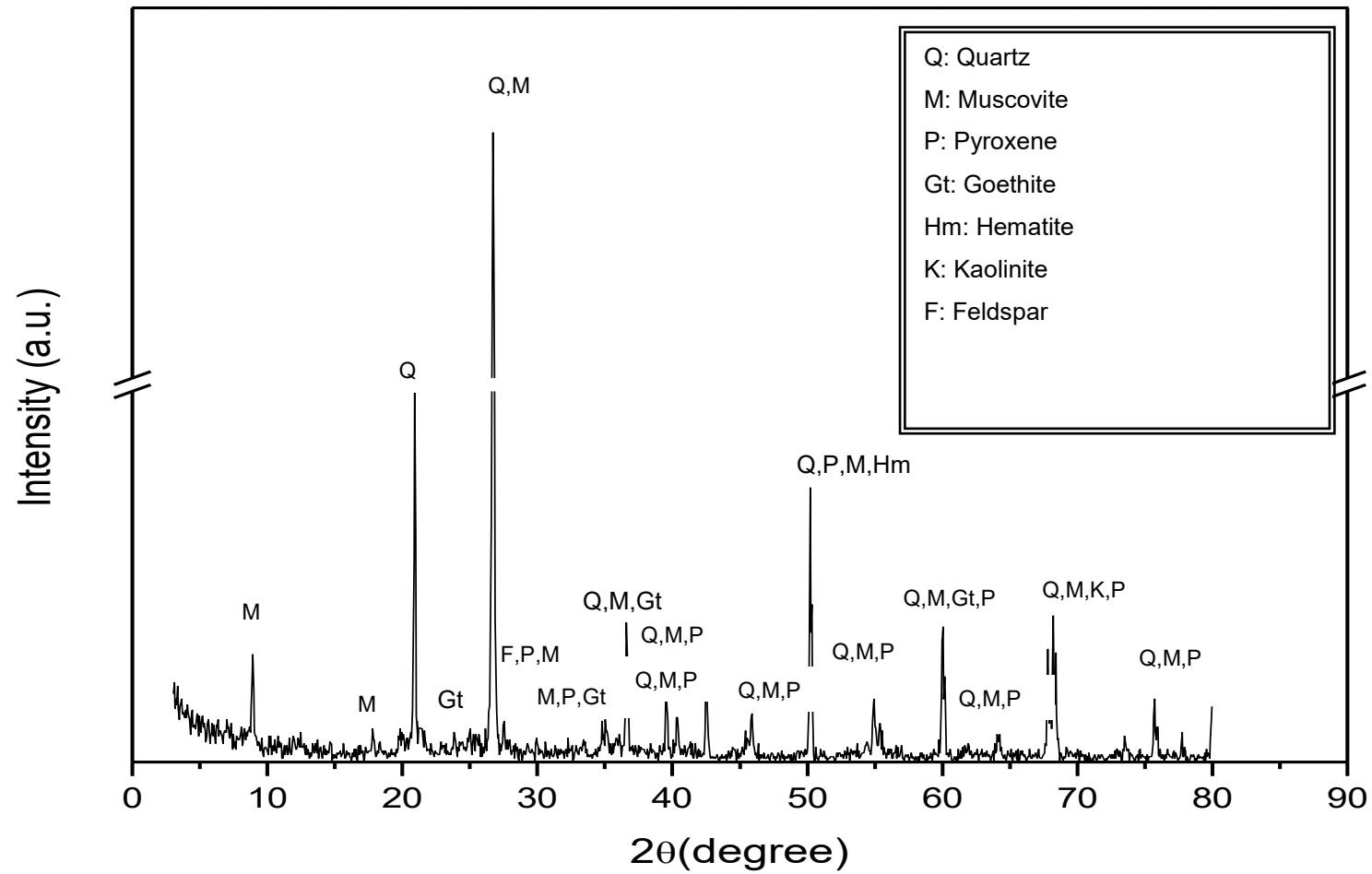


Figure AII.3: Powder X-ray diffraction patterns for soil sample K09 (< 2mm).

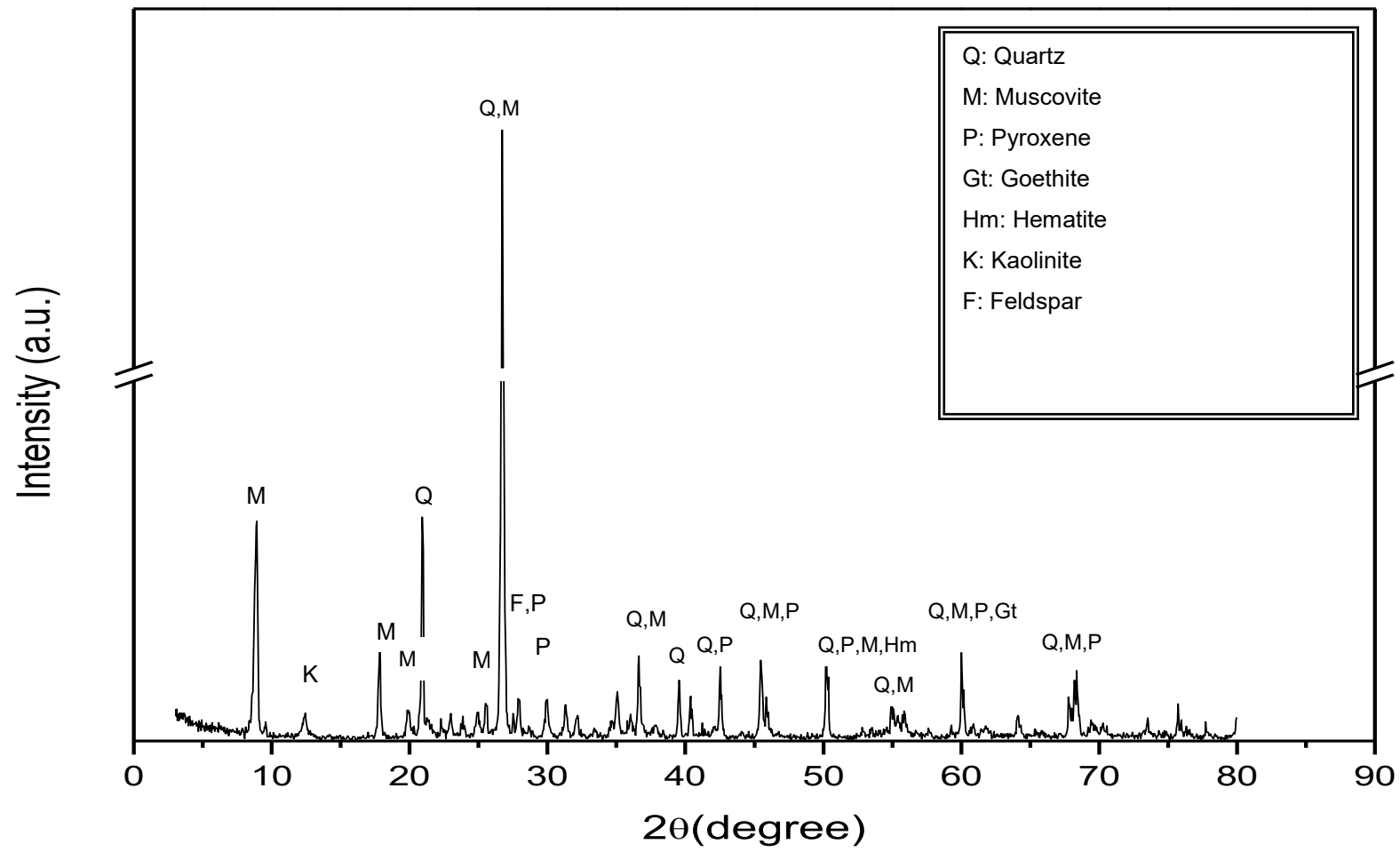


Figure A.II.4: Powder X-ray diffraction patterns for soil sample K21 (< 2mm).

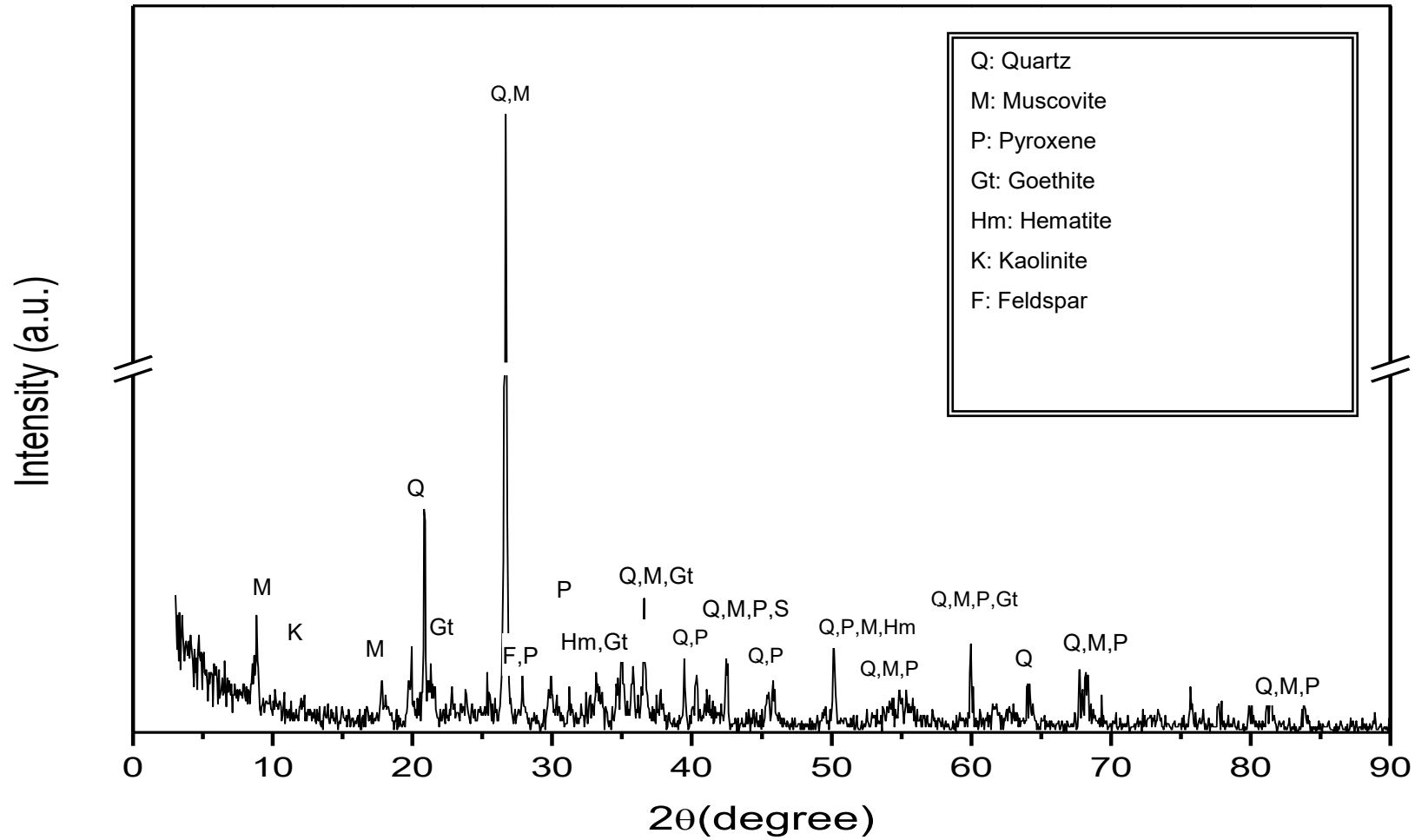


Figure A.II.5: Powder X-ray diffraction patterns for soil samples K22 (< 2mm).

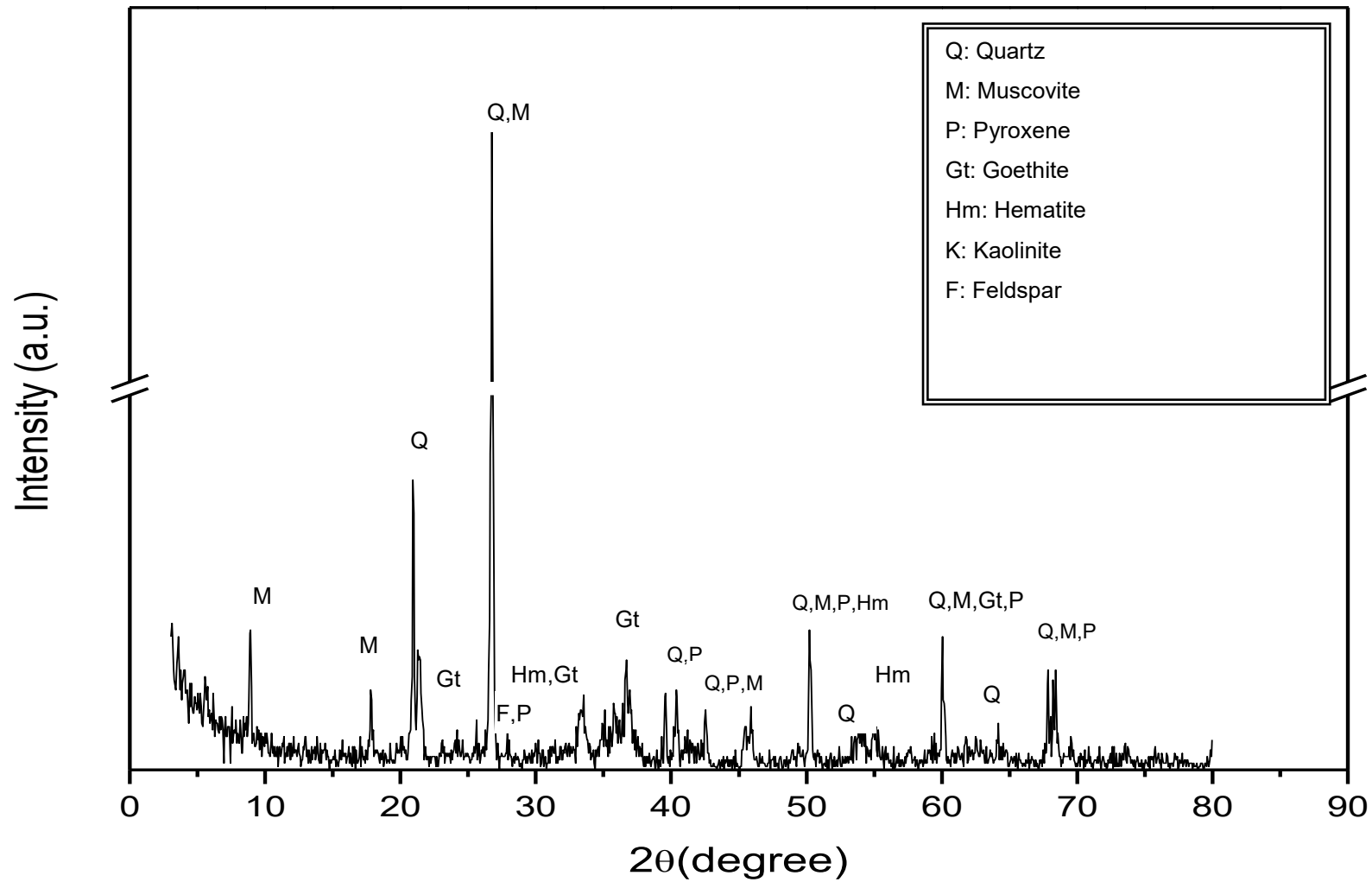


Figure A.II.6: Powder X-ray diffraction patterns for soil sample K23 (< 2mm).

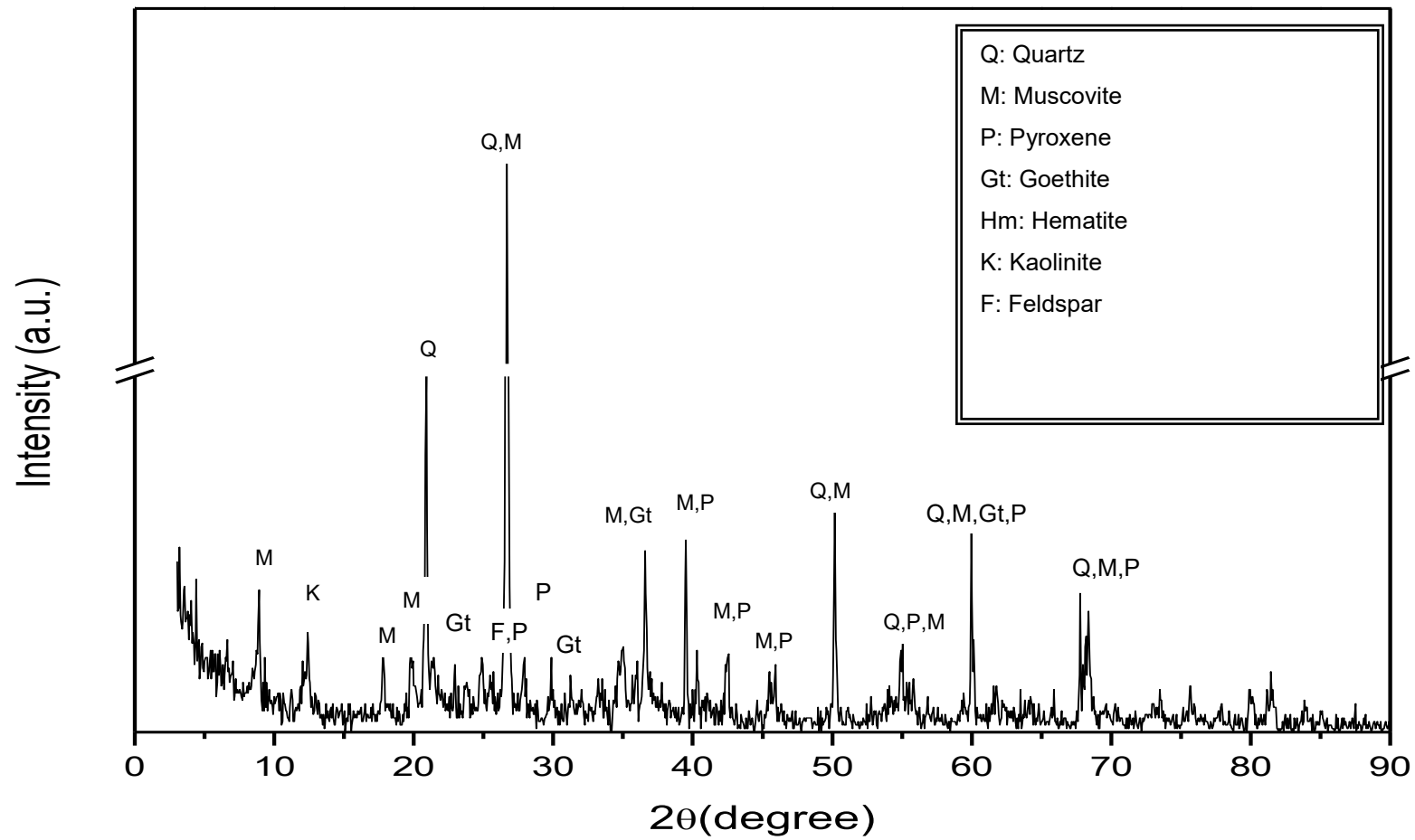


Figure A.II.7: Powder X-ray diffraction patterns for soil sample K36 (<2 mm).

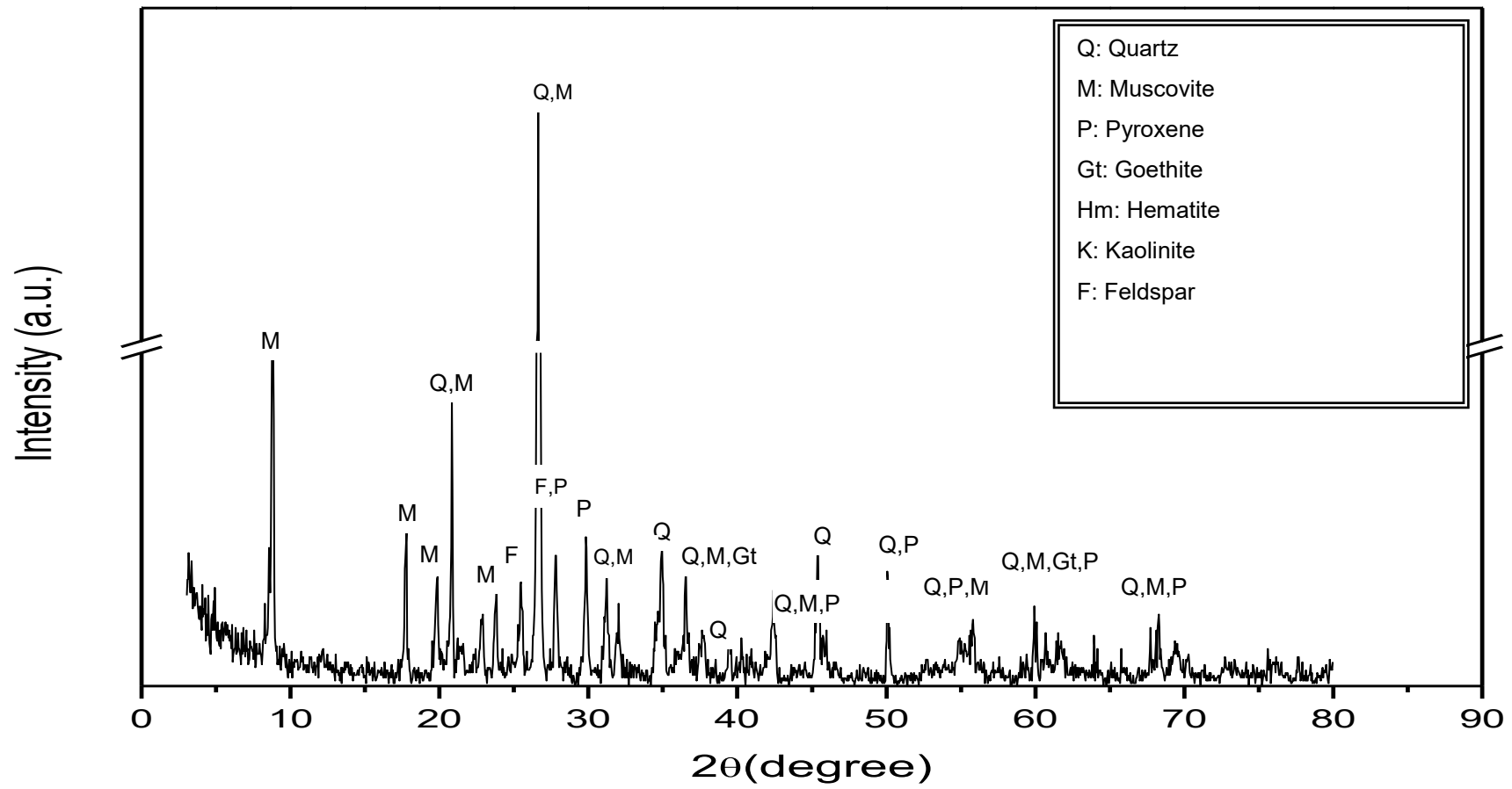


Figure A.II.8: Powder X-ray diffraction patterns for soil sample K37 (<2mm).

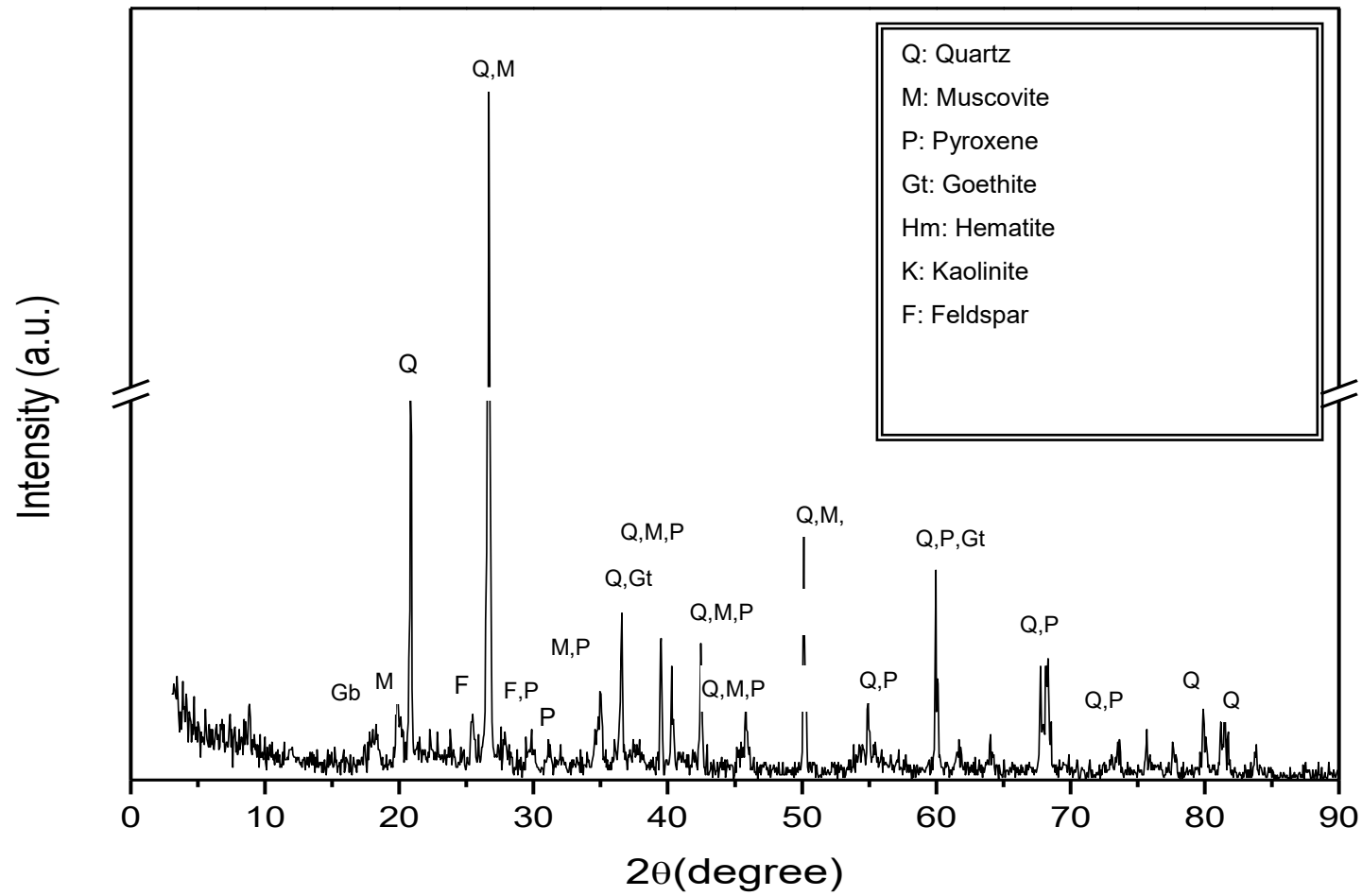


Figure A.II.9: Powder X-ray diffraction patterns for soil sample K40 (<2mm).



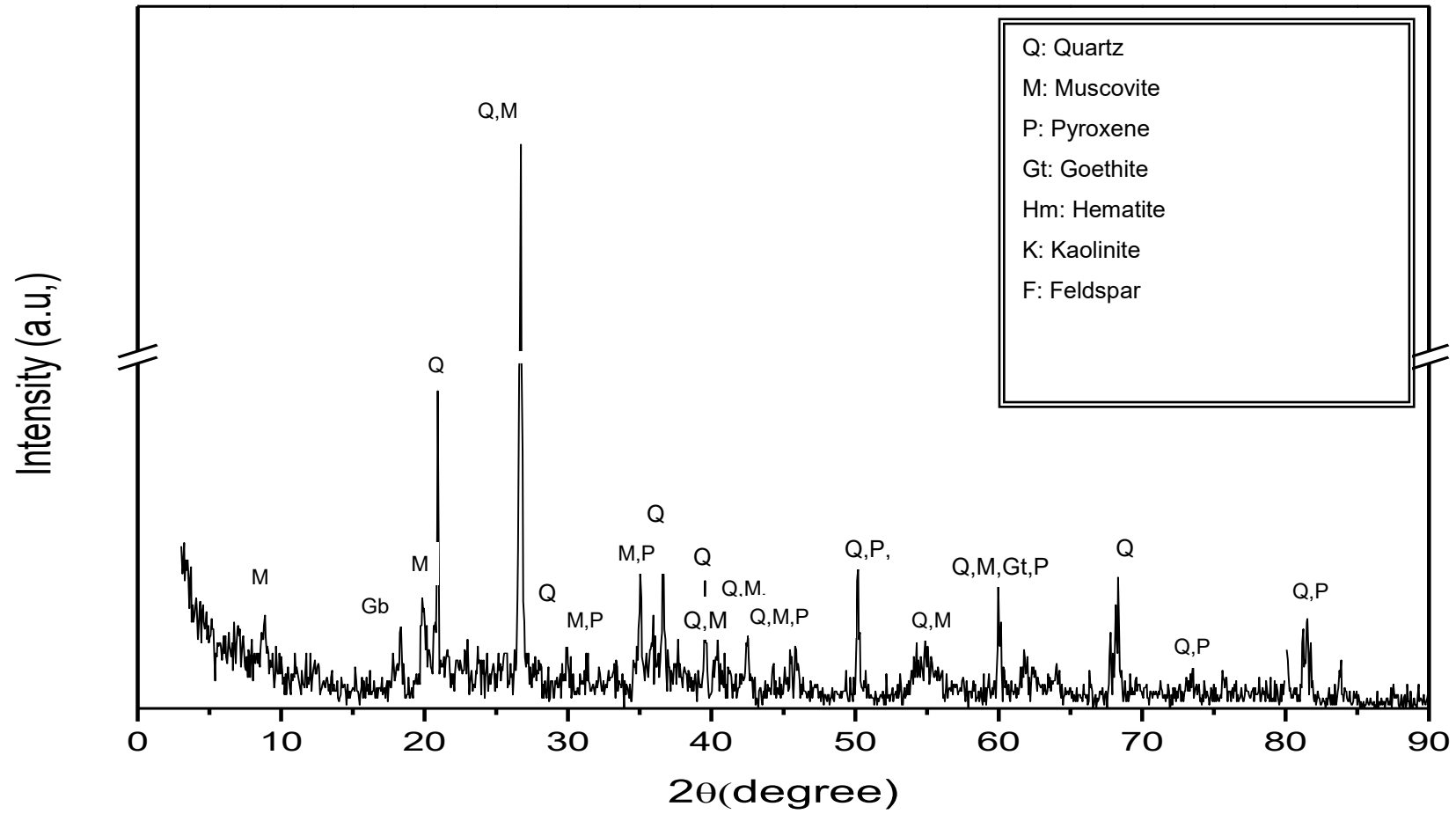


Figure A.II.10: Powder X-ray diffraction patterns for soil sample K43 (<2 mm).

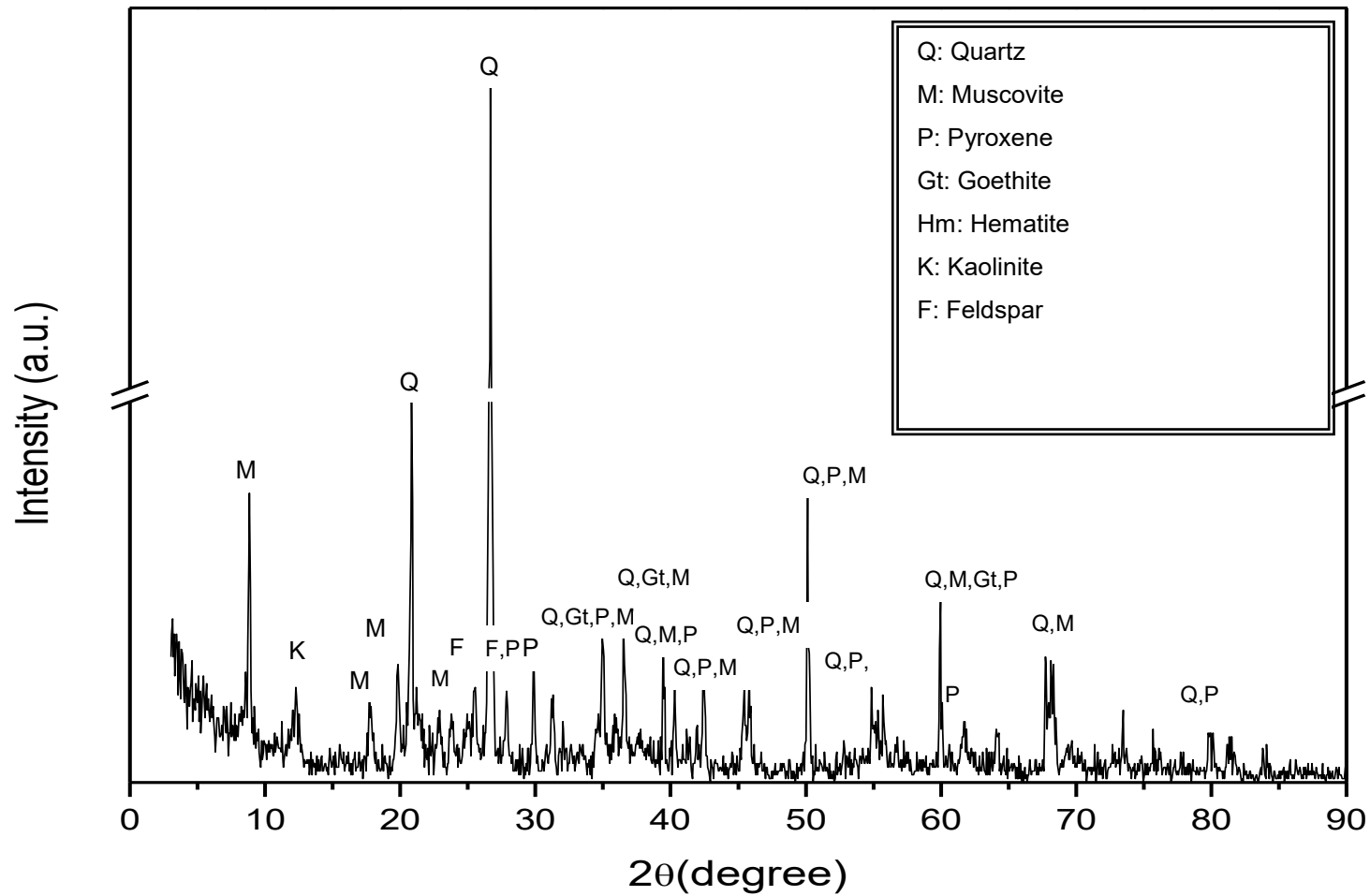


Figure A.II.11: Powder X-ray diffraction patterns for soil sample K44 (<2mm).

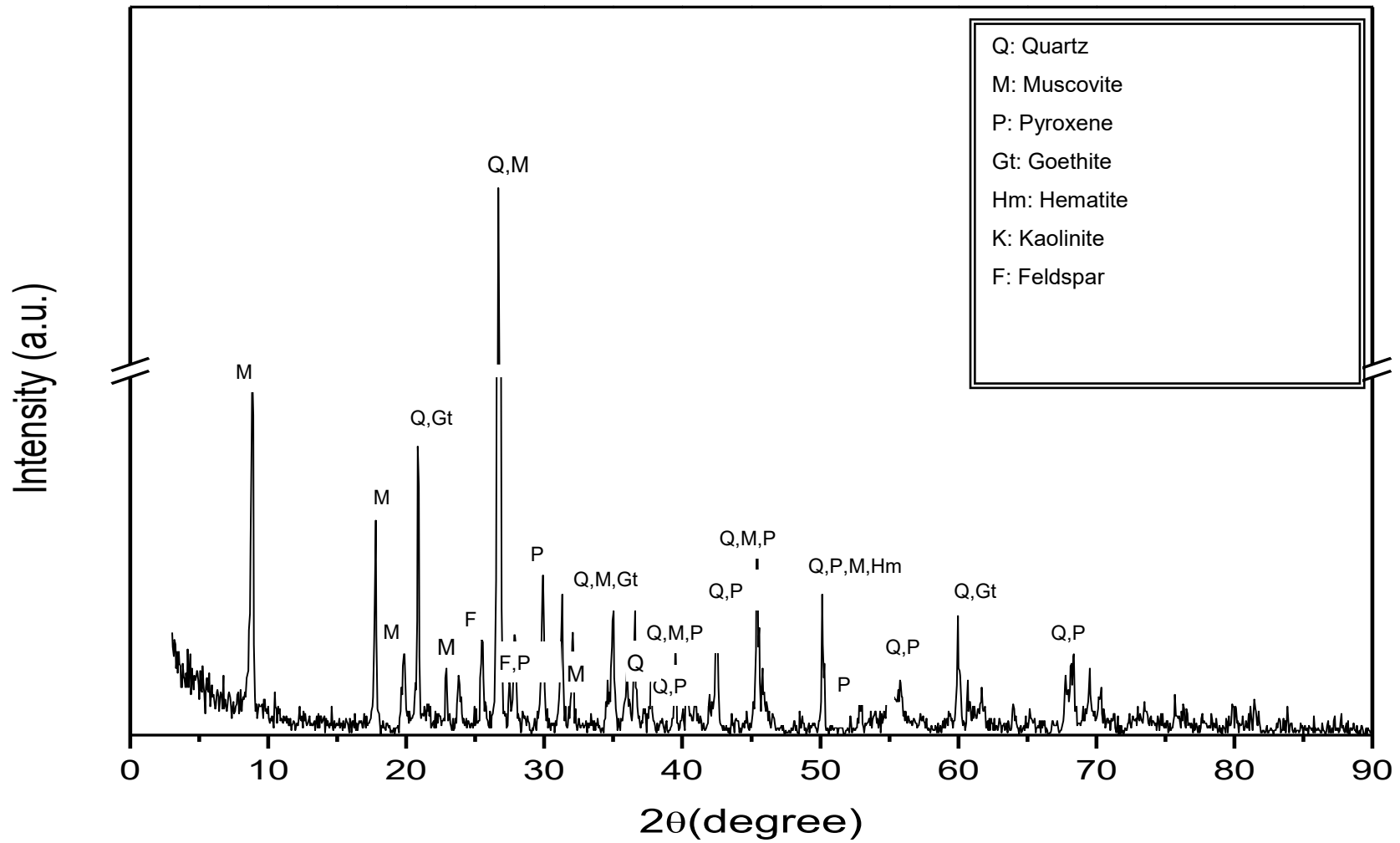


Figure A.II.12: Powder X-ray diffraction patterns for soil sample K47 (< 2mm).

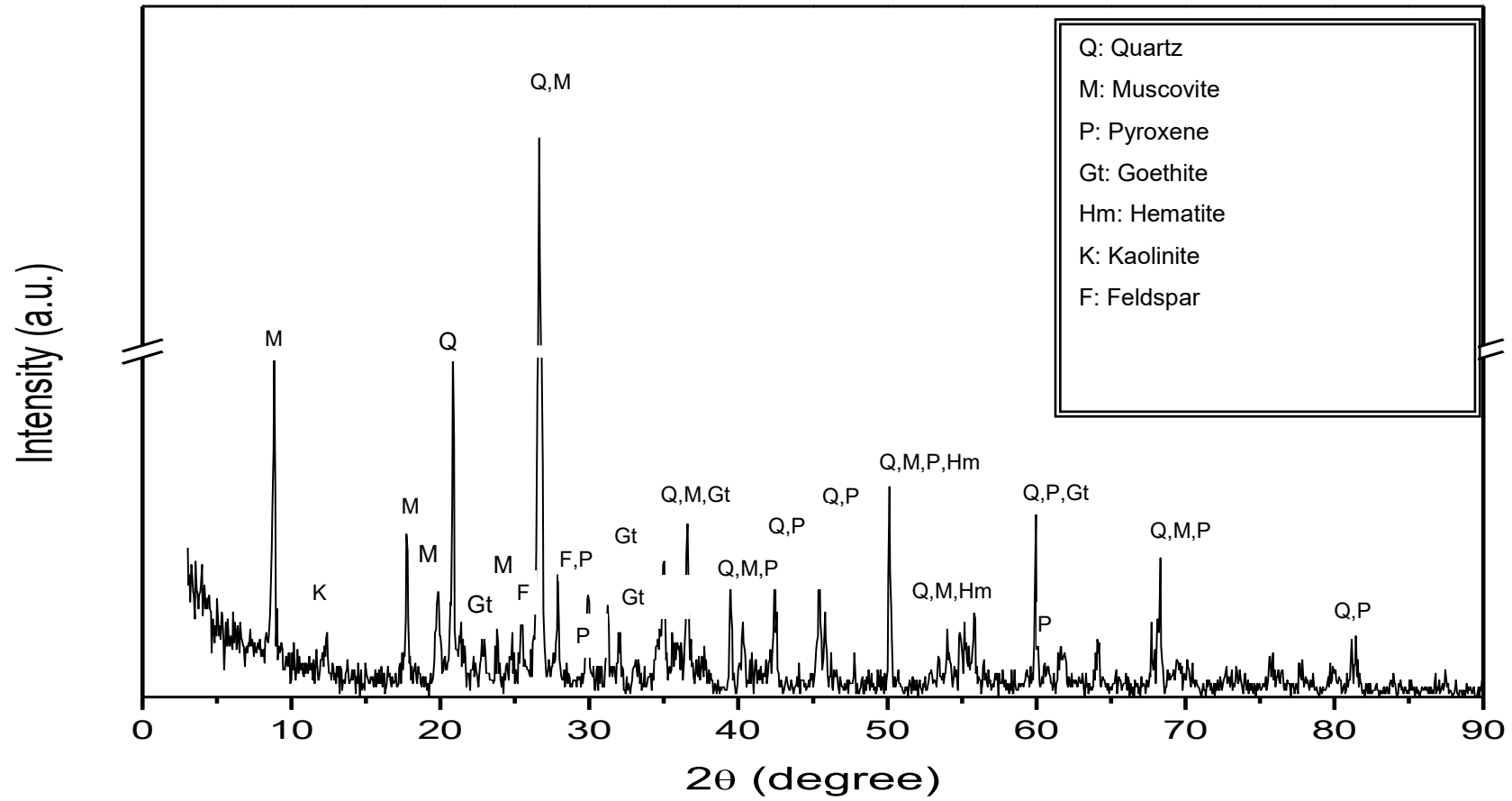


Figure A.II.13: Powder X-ray diffraction patterns for soil sample K48 (<2 mm).

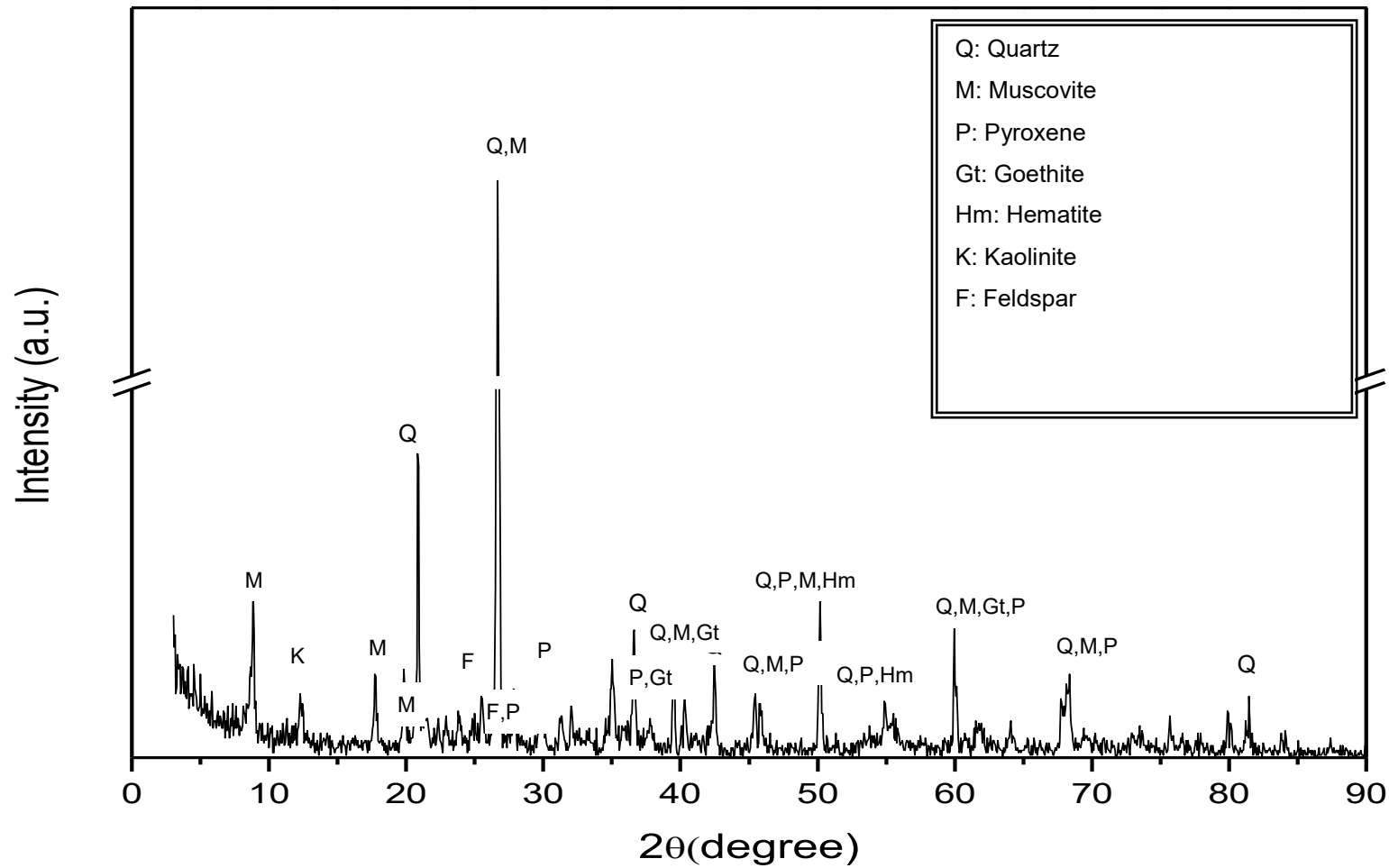


Figure A.II.14: Powder X-ray diffraction patterns for soil sample K49 (< 2mm).

### APPENDIX III. EDXRF

Table A.III.1. Major elements expressed as oxides by EDXRF (> 2mm)

Samples (>2mm)	Na <sub>2</sub> O	MgO	Al <sub>2</sub> O <sub>3</sub>	SiO <sub>2</sub>	K <sub>2</sub> O	CaO	TiO <sub>2</sub>	Fe <sub>2</sub> O <sub>3</sub>
%								
<b>Neossolo Flúvico Alterado</b>								
K23	0.00	0.80	15.78	33.65	3.03	0.09	0.63	44.56
<b>Nessolo Litólico</b>								
K21	0.00	0.42	17.20	66.63	4.58	0.12	0.65	9.90
K22	0.74	0.40	11.42	37.75	2.13	0.07	0.55	46.20
K36	0.29	0.28	11.10	68.31	2.15	0.07	0.39	17.39
K37	0.00	0.69	20.97	48.60	5.87	0.14	0.90	21.89
K40	0.00	0.57	11.10	53.59	1.39	0.10	0.52	31.44
K44	0.18	0.47	19.85	56.58	4.16	0.11	0.70	17.74
K47	0.00	0.69	22.08	57.06	6.43	0.16	0.70	12.27
K48	0.00	0.53	14.02	40.23	2.74	0.10	0.74	40.42
K49	0.58	0.42	14.60	57.41	2.98	0.08	0.56	23.03
SRM 2710a	NIST							
Measured	1.00	1.03	14.38	68.74	3.81	1.91	0.73	8.11
Certified value	1.20	1.22	11.24	66.53	5.23	1.35	0.52	6.18
Recovery (%)	83	85	128	103	73	142	140	131

Table A.III.2. Major elements expressed as oxides by EDXRF (&lt; 2mm)

Samples (< 2mm)	Na <sub>2</sub> O	MgO	Al <sub>2</sub> O <sub>3</sub>	SiO <sub>2</sub>	K <sub>2</sub> O %	CaO	TiO <sub>2</sub>	Fe <sub>2</sub> O <sub>3</sub>
<b>Neossolo Flúvico</b>								
K03	0.31	0.55	25.68	55.13	4.3	0.48	1.77	11.69
K06	0.15	0.62	26.97	52.06	5.07	0.27	1.53	13.24
K09	0.00	0.41	17.66	65.51	2.75	0.31	3.68	9.63
<b>Neossolo Flúvico Alterado</b>								
K23	0.00	0.67	12.64	45.89	2.29	0.06	1.27	36.02
<b>Nessolo Litólico</b>								
K21	0.15	0.52	20.29	65.08	5.54	0.17	1.97	6.02
K22	0.15	0.56	20.1	48.84	4.38	0.16	1.41	24.10
K36	0.0	0.5	20.63	57.47	4.06	0.14	1.8	15.37
K37	0.21	0.68	27.08	55.33	8.47	0.24	1.52	6.31
K40	0.10	0.56	23.76	62.91	3.95	0.47	1.72	6.37
K44	0.62	0.66	24.89	55.58	5.35	0.14	1.42	11.22
K47	0.11	0.8	25.7	58.5	8.54	0.25	1.42	4.54
K48	0.05	0.56	23.54	56.03	5.9	0.24	1.81	11.64
K49	0.48	0.47	22.41	59.54	4.95	0.14	2.28	9.59
<b>Latossolo Vermelho</b>								
K43	0.00	0.44	30.61	49.09	4.58	0.15	1.79	13.26
SRM NIST 2710a								
Measured	1.00	1.03	14.38	68.74	3.81	1.91	0.73	8.11
Certified value	1.20	1.22	11.24	66.53	5.23	1.35	0.52	6.18
Recovery (%)	83	85	128	103	73	142	140	131

Table A.III.3. Major elements expressed as oxides by EDXRF (&lt;250µm)

Samples (<250µm)	Na <sub>2</sub> O	MgO	Al <sub>2</sub> O <sub>3</sub>	SiO <sub>2</sub>	K <sub>2</sub> O %	CaO	TiO <sub>2</sub>	Fe <sub>2</sub> O <sub>3</sub>
<b>Neossolo Flúvico</b>								
K03	0.00	0.54	25.82	54.77	4.34	0.51	1.85	12.06
K06	0.00	0.52	27.36	52.88	4.94	0.29	1.48	12.43
K09	0.00	0.36	13.99	69.92	2.19	0.24	4.31	8.92
<b>Neossolo Flúvico Alterado</b>								
K23	0.00	0.50	12.18	46.77	2.00	0.07	6.62	31.06
<b>Nessolo Litólico</b>								
K21	0.35	0.55	21.45	65.31	5.92	0.18	2.16	3.94
K22	0.72	0.68	21.00	59.64	4.85	0.20	2.42	10.38
K36	0.25	0.59	19.61	62.04	3.91	0.14	2.37	11.06
K37	0.01	0.72	27.55	56.32	8.67	0.25	1.63	4.75
K40	0.00	0.54	26.45	59.83	4.85	0.63	2.07	5.51
K44	0.37	0.59	23.93	57.90	5.41	0.14	2.13	9.44
K47	0.02	0.81	26.08	59.04	8.67	0.24	1.58	3.48
K48	0.53	0.61	25.27	58.90	6.66	0.22	2.06	5.67
K49	0.56	0.49	23.25	61.00	5.28	0.17	2.60	6.58
<b>Latossolo Vermelho</b>								
K43	0.00	0.46	31.01	49.98	4.37	0.12	2.15	11.85
SRM 2710a	NIST							
Measured	1.00	1.03	14.38	68.74	3.81	1.91	0.73	8.11
Certified value	1.2	1.22	11.24	66.53	5.23	1.35	0.52	6.18
Recovery (%)	83	85	128	103	73	142	140	131



### APPENDIX IV – Pseudo total content – chemical analysis

**Table IV.1:** Pseudo total content of Al, Fe, As, Cd, Co, Cr, Cu, Mo, Ni, Pb and Zn for the soil samples (n=2, >2 mm)

Sample	Al (%)	Fe (%)	As (mg.kg <sup>-1</sup> )	Cd (mg.kg <sup>-1</sup> )	Co (mg.kg <sup>-1</sup> )	Cr (mg.kg <sup>-1</sup> )	Cu (mg.kg <sup>-1</sup> )	Ni (mg.kg <sup>-1</sup> )	Pb (mg.kg <sup>-1</sup> )	Zn (mg.kg <sup>-1</sup> )
<b>Neossolo Flúvico Alterado</b>										
K23	2.44±0.15	26.06±3.01	8036±934	6.9±1.1	7.7±0.6	168±16	75±11	14.1±0.3	75±12	70±9
<b>Nossolo Litólico</b>										
K21	0.557±0.027	6.00±0.17	2802±16	1.631±0.003	1.50±0.05	59±4	57±8	3.6±0.2	113±2	24±3
K22	2.13±0.14	27.53±2.43	3852±65	6.6±0.1	17.6±0.5	103±5	57±4	33±2	70.7±0.1	109±11
K36	0.88±0.03	9.47±0.48	207±16	2.3±0.2	37±3	117±18	45±3	15.5±0.1	145±20	40±2
K37	1.54±0.61	13.06±0.60	4984±17	2.8±1.3	6.1±2.3	64.4±0.5	61±4	10.6±0.6	185±2	95±4
K40	2.44±0.15	16.89±1.40	5832±140	3.2±1.0	4.8±2.3	128±2	26.6±0.1	4.2±0.1	63±9	31±6
K44	1.08±0.48	12.81±0.75	1396±16	1.8±1.6	18±3	41.21±0.05	35±16	14.29±0.03	64±5	94±6
K47	1.02±0.26	8.06±0.27	3927±122	1.5±1.0	4±3	41.7±0.3	52±8	1.2±0.2	171±17	26±3
K48	2.47±0.07	23.8±0.9	7456±180	6.3±0.1	14±1	139±10	52±1	23.8±1.4	71±1	130±14
K49	1.04±0.14	16.82±1.05	2153±132	4.0±0.2	15±1	42±5	90±10	33±1	21±1	174±13

**Table IV.2.** Pseudo total content of Al, Fe, As, Cd, Co, Cr, Cu, Mo, Ni, Pb and Zn for the soil samples (n=3, < 250 µm)

Samples (< 250 µm)	Al	Fe	As	Cd	Co	Cr	Cu	Ni	Pb	Zn
	(%)		(mg kg <sup>-1</sup> )							
<b>Neossolo Flúvico</b>										
K03	2.9±0.9	5.39±0.02	464±64	1.7±0.2	10±2	41±10	73±7	19±6	19±6	67±17
K06	3.2±0.4	6.1±0.2	405±3	1.9±0.1	11±1	49±3	59±4	20±2	46±5	68±24
K09	1.6±0.3	4.7±0.4	325±5	1.4±0.4	13±2	43±2	42±4	15±3	40±2	80±12
<b>Neossolo Flúvico Alterado</b>										
K23	1.8±0.2	16±1	4304±286	4.82±0.04	10±2	104±8	89±10	25±4	115±31	78±11
<b>Neossolo Litólico</b>										
K21	0.47±0.09	1.60±0.04	841±28	0.6±0.1	1.4±0.3	14±2	36±3	12±7	120±14	15±1
K22	2.5±0.6	5.4±0.3	575±83	1.6±0.4	5±1	27±5	50±3	24±2	44±15	46±19
K36	1.4±0.2	4.7±0.4	40±6	1.445±0.007	10±1	33±3	61±4	16±1	43±1	42±3
K37	0.46±0.07	1.42±0.07	494±6	0.49±0.07	0.57±0.04	7±2	28±3	2.67±0.02	84±6	15±2
K40	3.7±0.5	1.8±0.2	443±14	0.6±0.2	1.4±0.5	30±3	54±4	20±9	41±7	38±4
K44	0.93±0.05	3.8±0.2	459±15	1.2±0.1	3.224±0.003	14±1	35±4	7±1	32±5	38±1
K47	0.33±0.02	0.77±0.05	379±33	0.25±0.04	0.5 ±0.1	6±1	19±1	10±2	30±4	9±3
K48	0.76±0.07	1.7±0.1	324±29	0.5±0.2	0.7±0.2	8±2	16±1	1.6±0.1	8±2	9±2
K49	0.75±0.04	2.3±0.1	332±36	0.61±0.02	1.9 ±0.2	14±3	43±5	5±1	12±2	27±1
<b>Latossolo Vermelho</b>										
K43	4.9±0.3	5.0±0.2	211±39	1.9±0.5	3.224±0.003	35±4	46±6	<0.003	79±50	53±13

## Appendix V MLA results

Table A .V.1: Mineral phases identified by MLA

Mineral	Wt%	Area%	Area (mm)	Particle Count	Grain Count	Wt%	Area%	Area (mm)	Particle Count	Grain Count
K03 (< 2mm ,100% wt%)						K06 (< 2mm ,100% wt%)				
Unknown	0.0	0.7	32	2802	3197	0.0	0.5	13323	13	2322
Low_Counts	0.0	0.2	10	1071	1080	0.0	0.2	6315	6	962
No_XRay	0.0	0.0	1	941	943	0.0	0.0	405	0	628
Fe Oxides/Hydroxides	1.7	1.3	56	2765	8419	0.7	0.5	13945	14	4048
Fe Oxides/Hydroxides-As	0.6	0.4	19	738	2718	0.1	0.1	2871	3	905
Quartz	21.6	22.9	1018	14050	16234	6.2	6.6	176709	177	9984
Anatase/Rutile	0.8	0.6	27	878	1091	0.3	0.2	6251	6	630
Monazite-(La)	0.0	0.0	0	10	10	0.0	0.0	91	0	13
Ilmenite	1.7	1.0	44	512	620	0.2	0.1	3047	3	279
Pyrite	0.0	0.0	1	80	82	0.0	0.0	203	0	37
Arsenopyrite	0.0	0.0	0	0	0	0.0	0.0	41	0	7
Scorodite	0.0	0.0	0	0	0	0.0	0.0	54	0	9
Tourmaline	1.4	1.3	57	1578	2312	1.8	1.7	46949	47	3892
Mica/Clay Minerals	67.8	66.8	2970	63175	74485	84.1	83.0	2233168	2233	63110
Zircon	0.1	0.1	3	290	294	0.2	0.1	2467	2	441
Microcline	4.3	4.7	207	9323	14749	6.3	6.9	184353	184	19748
Total	100.0	100.0	4445	79330	126234	100.0	100.0	2690193	2690	107015

Table A .V.1: Mineral phases identified by MLA (cont.)

Mineral	K21 (< 2mm, 57% wt%)					K22 (< 2mm, 24% wt%)				
	Wt%	Area%	Area (mm)	Particle Count	Grain Count	Wt%	Area%	Area (mm)	Particle Count	Grain Count
Unknown	0.0	1.5	3858	3858	5376	0.0	0.8	263	1935	2823
Low_Counts	0.0	0.0	76	76	79	0.0	0.0	6	95	95
No_XRay	0.0	0.0	1728	1728	1732	0.0	0.0	9	1677	1686
Fe Oxides/Hydroxides	1.4	1.0	1453	1453	7153	30.5	24.7	8649	11483	42951
Fe Oxides/Hydroxides-As	4.1	3.0	2901	2901	14684	8.5	6.9	2420	4776	26616
Quartz	49.1	51.7	15555	15555	19542	20.5	24.1	8429	8197	17250
Anatase/Rutile	1.6	1.1	1215	1215	2756	0.2	0.2	68	317	435
Monazite-(La)	0.6	0.3	168	168	192	0.4	0.3	91	28	30
Ilmenite	2.7	1.6	1047	1047	2328	1.0	0.7	237	512	742
Pyrite	0.1	0.1	287	287	348	0.1	0.1	18	232	270
Arsenopyrite	0.0	0.0	4	4	4	0.0	0.0	0	0	0
Scorodite	0.0	0.0	1	1	1	0.0	0.0	0	0	0
Tourmaline	0.5	0.5	750	750	1177	0.2	0.2	61	549	694
Mica/Clay Minerals	36.9	36.0	23867	23867	60593	35.8	39.0	13646	28094	213230
Zircon	0.0	0.0	101	101	115	0.1	0.0	14	178	190
Microcline	3.0	3.2	4654	4654	9447	2.6	3.1	1083	4722	13265
Total	100.0	100.0	41831	41831	125527	100.0	100.0	34993	36123	320277

Table A .V.1: Mineral phases identified by MLA (cont.)

Mineral	K23 (> 2mm, 28% wt%)					K23 (< 2mm, 72% wt%)				
	Wt%	Area%	Area (mm)	Particle Count	Grain Count	Wt%	Area%	Area (mm)	Particle Count	Grain Count
Unknown	0.0	0.4	145	1274	1662	0.0	0.4	166	966	1403
Low_Counts	0.0	0.0	5	82	82	0.0	0.0	9	132	135
No_XRay	0.0	0.0	8	1564	1568	0.0	0.0	6	1176	1179
Fe Oxides/Hydroxides	23.2	19.0	7638	13654	78743	24.0	20.0	8288	11268	68125
Fe Oxides/Hydroxides-As	20.9	17.2	6906	11822	75841	21.1	17.6	7312	9459	65533
Quartz	27.0	32.1	12898	4367	5270	28.9	34.9	14488	4759	5895
Anatase/Rutile	0.1	0.1	43	182	243	0.4	0.3	140	419	774
Monazite-(La)	0.0	0.0	2	25	26	0.6	0.3	141	95	104
Ilmenite	0.9	0.6	228	541	762	3.8	2.5	1050	930	1265
Pyrite	0.1	0.1	23	300	346	0.0	0.0	7	102	108
Arsenopyrite	0.0	0.0	0	0	0	0.0	0.0	0	0	0
Scorodite	0.0	0.0	1	2	6	0.0	0.0	0	2	2
Tourmaline	0.3	0.4	145	403	649	0.3	0.3	144	477	724
Mica/Clay Minerals	27.2	30.1	12082	25717	377553	20.7	23.2	9638	20725	371293
Zircon	0.0	0.0	12	153	171	0.0	0.0	11	153	163
Microcline	0.1	0.2	68	254	533	0.2	0.2	82	421	782
Total	100.0	100.0	40203	32282	543455	100.0	100.0	41481	27244	517485

Table A.V.1 Mineral phases identified by MLA (cont.)

Mineral	K48 (> 2mm, 70% wt%)					K48 (< 2mm, 30% wt%)				
	Wt%	Area%	Area (mm)	Particle Count	Grain Count	Wt%	Area%	Area (mm)	Particle Count	Grain Count
Unknown	0.0	0.2	97	723	964	0.0	0.4	166	966	1403
Low_Counts	0.0	0.0	10	181	186	0.0	0.0	9	132	135
No_XRay	0.0	0.0	9	1606	1610	0.0	0.0	6	1176	1179
Fe Oxides/Hydroxides	22.6	18.5	7188	12914	91331	24.0	20.0	8288	11268	68125
Fe Oxides/Hydroxides-As	21.3	17.5	6777	11702	80494	21.1	17.6	7312	9459	65533
Quartz	26.6	31.7	12281	4813	5751	28.9	34.9	14488	4759	5895
Anatase/Rutile	0.1	0.1	29	78	144	0.4	0.3	140	419	774
Monazite-(La)	0.0	0.0	3	40	43	0.6	0.3	141	95	104
Ilmenite	1.1	0.7	281	513	776	3.8	2.5	1050	930	1265
Pyrite	0.0	0.0	4	54	56	0.0	0.0	7	102	108
Arsenopyrite	0.0	0.0	0	0	0	0.0	0.0	0	0	0
Scorodite	0.0	0.0	0	0	0	0.0	0.0	0	2	2
Tourmaline	0.4	0.4	165	523	739	0.3	0.3	144	477	724
Mica/Clay Minerals	27.7	30.5	11849	27471	419160	20.7	23.2	9638	20725	371293
Zircon	0.1	0.0	16	198	209	0.0	0.0	11	153	163
Microcline	0.2	0.2	88	783	1028	0.2	0.2	82	421	782
Total	100.0	100.0	38797	33864	602491	100.0	100.0	41481	27244	517485